Flavour Changing Neutral Current Processes of B and K Mesons from Lattice QCD

Chi-Jen David Lin

Doctor of Philosophy

The University of Edinburgh

1998

Abstract

Flavour Changing Neutral Current (FCNC) processes are essential for pinning down free parameters in the Standard Model and for probing possible new physics beyond it. In this work, we compute the non-perturbative strong-interaction effects on a collection of FCNC processes using Lattice QCD. The processes examined are

- $B^0_{(s)}$–$\bar{B}^0_{(s)}$ mixing, from which one can extract the magnitude of the Cabibbo-Kobayashi-Maskawa (CKM) matrix element V_{td};
- K^0–$\bar{K}^0$ mixing, which yields a constraint on the summit of the (db) unitarity triangle;
- the $\Delta I = 3/2$, electromagnetic-penguin contributions to $K \to \pi\pi$ decays which enter the calculation of the CP-violation parameter ϵ'.

Lattice simulations are performed with the mean-field-improved clover action on a $16^3 \times 48$ lattice at $\beta = 6.0$ and a $24^3 \times 48$ lattice at $\beta = 6.2$. 498 gauge configurations are used at $\beta = 6.0$ and 188 gauge configurations are used at $\beta = 6.2$.

Matrix elements and the bag parameter of the $B^0_{(s)}$–$\bar{B}^0_{(s)}$ mixing processes are simulated in the charm-mass region, and extrapolated to the beauty-mass region using Heavy Quark Effective Theory. Decay constants of D_s, D, B_s and B mesons and the ratios f_{B_s}/f_B and f_{D_s}/f_D are also calculated.

Ratios of the relevant matrix elements of Kaon processes are computed for several initial and final meson momenta and for six light-meson masses ranging from approximately 435 MeV to 815 MeV. Fits of these ratios to the mass and recoil behaviours predicted by Chiral Perturbation Theory are then used to extract the relevant bag parameters.

Declaration

This thesis has been composed by me and presents work carried out as a member of the UKQCD collaboration. The results presented in Chapter three and four were carried out in collaboration with Laurent Lellouch. The correlation functions for matrix elements of generic four-fermion operators with pseudo-scalar-meson external states were generated by the UKQCD collaboration. The code which processes these correlation functions to obtain the matrix elements of the four-fermion operators presented in this work was written by me. The codes which perform the bootstrap analyses of the relevant correlation functions and the extrapolations of the matrix elements with respect to quark masses were developed by me, with the help from Laurent Lellouch.

The materials in Chapter three and four can be found in

- Laurent Lellouch and C.-J. David Lin, for the UKQCD collaboration, in the procceedings of LATTICE98, hep-lat/9809018.
- Laurent Lellouch and C.-J. David Lin, for the UKQCD collaboration, in the procceedings of LATTICE98, hep-lat/9809142.

C.-J. David Lin.

Acknowledgements

I am indebted to Laurent Lellouch, who has been guiding me through my PhD work, and has been so patient to answer all the questions (including the silly ones) I have asked. Of course I have to thank him for driving me to the MacDonald in Marseille for many times and offering me a nice fondue in Annecy.

Constant supports from my parents are the most crucial for me to finish my PhD study. I would also like to thank my supervisors Brian Pendleton and Ken Bowler, and Richard Kenway, for their kind help through the three years and three months I spent in Edinburgh, such that I could learn a lot of things.

A very pleasant thing during my time in Edinburgh is to share a Banana Office with two nice people, Chris Maynard and Bálint Joó [1, 2].

Edinburgh is twenty-hour away from Taipei by plane (including a few hours of waiting time in Schipol airport in Amsterdam), but the warmth from people in EDQCD and other friends (Chen, Jinn, Jonathan, Julie, May-Fang, May-Shine, Olga and Victor) here has made it as good as home. Emails from Chi-Mao, Chun-Pei and Gi-Shin in Taiwan have offered me a lot of information from home.

My PhD project is partially funded by the CVCP through the Overseas Research Student Award. Travel grants from the Department of Physics and Astronomy, the University of Edinburgh and a short-term fellowship from CERN are acknowledged. I also appreciate the hospitalities of Centre de Physique Théorique, CNRS Marseille and the Theory Division of CERN during the progress of this work.

I would like to thank Chao-Liang Wu and Ai-Li Shiau who brought their daughter to Edinburgh when they decided to pursue their PhD degrees in the University of Edinburgh [3, 4]. Of course, I have to thank their daughter, Pensée, who has spent a lot of time, although being very busy with her work [5] , to make my stay in Edinburgh worth!

Contents

Chapter 1

Flavour Physics

One of the highlights of current particle physics is the better understanding of the Standard Model that will be gained through extensive confrontation of the theory with experiment. Amongst the experimental progress during the past few years, two areas are particularly relevant to this work:

1. The discovery of the top quark and the determination of its mass.

2. The improved measurement of CKM matrix elements which govern the mixing of quark flavours.

In the next few years, there will be even more relevant experimental progress. The construction of the B factories (KEK and SLAC) will enable extensive tests of the Standard Model's scenario for flavour mixing and CP violation. The NA48 (CERN) and KTEV (Fermilab) experiments will further constrain the parameters describing the CP violation in kaon systems. Significant theoretical advances have been made in understanding the strong-interaction effects on the weak interactions of quarks. This understanding is necessary for relating fundamental parameters of the Standard Model, such as the CKM matrix elements, to phenomena observed in experiments, such as those to be undertaken in the B factories. Although we already have rather good estimates of these QCD effects at high energies through perturbation theory, predictions for the low-energy effects are made difficult by the fact that quarks are confined in hadrons and the standard perturbative approach breaks down. A precise quantitative description of these low energy effects remains one of the most challenging theoretical issues in understanding the Standard Model.

In this chapter, we give a brief outline of flavour physics, from which we can understand the structure of the electroweak Lagrangian and its implications. A detailed review of this field can be found in [6, 7].

1.1 The Standard Model

The Standard Model is a gauge theory with three generations of fermions and with the gauge group $SU(3)\times SU(2)_L\times U(1)_Y$ spontaneously broken to $SU(3)\times U(1)_Q$, where L, Y and Q stand for left hand, weak hyper charge and electric charge respectively. There are many good references on the formulation of the Standard Model [8, 9]. We will only give a brief review of the aspects of the Standard Model which are relevant to this work.

1.1.1 Basic Interactions

The Lagrangian for the electroweak interactions between fermions and gauge bosons can be written as

$$\mathcal{L}_I = \mathcal{L}_{CC} + \mathcal{L}_{NC}, \tag{1.1}$$

where $\mathcal{L}_{CC}$ and $\mathcal{L}_{NC}$ are the Lagrangians for the charged- and neutral-current weak interactions

$$\mathcal{L}_{CC} = \frac{g_2}{2\sqrt{2}}(J^+_\mu W^{+\mu} + J^-_\mu W^{-\mu}), \tag{1.2}$$

$$\mathcal{L}_{NC} = eJ^{em}_\mu A^\mu + \frac{g_2}{2\cos\theta_W} J^0_\mu Z^{0\mu}, \tag{1.3}$$

where e and g_2 are the QED and $SU(2)_L$ coupling constants, θ_W is the Weak Mixing angle. J^{em}_μ is the electromagnetic current, J^+_μ and J^-_μ are the weak charge currents and J^0_μ is the weak neutral current. The currents can be written as

$$J^+_\mu = (\bar{u}, \bar{c}, \bar{t})\, \gamma_\mu (1-\gamma_5) \hat{V}_{\rm CKM} \begin{pmatrix} d \\ s \\ b \end{pmatrix}, \tag{1.4}$$

$$J^-_\mu = \left(J^+_\mu\right)^\dagger, \tag{1.5}$$

$$J^{em}_\mu = \sum_f Q_f \bar{f} \gamma_\mu f, \tag{1.6}$$

$$J^0_\mu = \sum_f \bar{f} \gamma_\mu \left(c_V - c_A \gamma_5\right) f, \tag{1.7}$$

where $c_V = T^3_f - 2Q_f \sin^2\theta_W$ and $c_A = T^3_f$. Q_f and T^3_f denote the charge and the third component of the weak isospin of the left-handed fermion. The unitary matrix $\hat{V}_{\rm CKM}$ is the CKM matrix as explained in the next subsection.

1.1.2 The CKM Matrix

The CKM matrix [10, 11] relates the mass eigenstates to the weak-interaction eigenstates which are not the same in the Standard Model

$$\begin{pmatrix} d' \\ s' \\ b' \end{pmatrix} = \begin{pmatrix} V_{ud} & V_{us} & V_{ub} \\ V_{cd} & V_{cs} & V_{cb} \\ V_{td} & V_{ts} & V_{tb} \end{pmatrix} \begin{pmatrix} d \\ s \\ b \end{pmatrix}. \tag{1.8}$$

The elements in this matrix cannot be predicted by the Standard Model, they have to be determined by comparing the experimental data with theoretical calculations of some weak-interaction processes. The particle physics community has put a lot of effort into constraining these CKM matrix elements, because

1. As we can see from equation (1.4), the CKM matrix governs the strength of the couplings in the weak charged currents.

2. The complex phase in the CKM matrix plays an important role in understanding CP violation in the framework of the Standard Model.

3. The unitarity of the CKM matrix is strongly related to the strength of the Flavour Changing Neutral Currents, which reveal a lot of information about the quantum structure of the Standard Model and possible new physics. We will give a more detailed description of this point in the next subsection.

Currently, the main difficulty in pinning down the CKM matrix elements is *the control of the non-perturbative strong-interaction effects* in the theoretical calculation of the relevant weak-interaction processes.

In a three-generation model, the unitary CKM matrix has nine real parameters. However, five of these can be absorbed into the redefinition of the phases of the quark fields. Hence there are four parameters to be determined.

The standard parameterisation is given by

$$\hat{V}_{\mathrm{CKM}} = \begin{pmatrix} c_{12}c_{13} & s_{12}c_{13} & s_{13}e^{-i\delta} \\ -s_{12}c_{23} - c_{12}s_{23}s_{13}e^{-i\delta} & c_{12}c_{23} - s_{12}s_{23}s_{13}e^{-i\delta} & s_{23}c_{13} \\ s_{12}s_{23} - c_{12}c_{23}s_{13}e^{-i\delta} & -c_{12}s_{23} - s_{12}c_{23}s_{13}e^{-i\delta} & c_{23}c_{13} \end{pmatrix}, \tag{1.9}$$

where $c_{ij} = \cos\theta_{ij}$ and $s_{ij} = \sin\theta_{ij}$, and δ is the phase necessary for the implementation of CP violation in a CKM framework.

Another popular way to parameterise the CKM matrix is to approximate each element by expanding it in terms of a power series in $\lambda = |V_{us}| \approx 0.22$, as proposed by Wolfenstein [12]

$$\hat{V}_{\mathrm{CKM}} = \begin{pmatrix} 1 - \frac{\lambda^2}{2} & \lambda & A\lambda^3(\rho - i\eta) \\ -\lambda & 1 - \frac{\lambda^2}{2} & A\lambda^2 \\ A\lambda^3(1 - \rho - i\eta) & -A\lambda^2 & 1 \end{pmatrix} + \mathcal{O}(\lambda^4). \tag{1.10}$$

There is more than one way to include the higher-order terms in λ in the Wolfenstein parameterisation. The authors of [13, 14] propose an efficient parameterisation by defining the parameters (λ, A, ρ, η) as

$$\begin{aligned} s_{12} &= \lambda, \\ s_{23} &= A\lambda^2, \\ s_{13}e^{-i\delta} &= A\lambda^3(\rho - i\eta), \end{aligned} \tag{1.11}$$

to all orders in λ. This corresponds to a change of variables which exactly preserves unitarity when parameterising the CKM matrix by (λ, A, ρ, η). The Wolfenstein parameterisation can be reproduced by substituting this change of variables into equation (1.9) then expanding each element in terms of λ up to the leading order.

By adopting the Wolfenstein parameterisation, it is easier to understand the structure of the CKM matrix from a geometrical point of view. The unitarity of the CKM matrix implies various relations amongst its elements. A particularly interesting one, which contains the poorly constrained V_{ub} and V_{td}, is

$$V_{ud}V_{ub}^* + V_{cd}V_{cb}^* + V_{td}V_{tb}^* = 0. \tag{1.12}$$

Keeping the expansion of the CKM matrix elements up to $\mathcal{O}(\lambda^4)$, based on equation (1.11), we find

$$\begin{aligned} V_{ud}V_{ub}^* &= A\lambda^3\,(\bar\rho + i\bar\eta) + \mathcal{O}(\lambda^7), \\ V_{cd}V_{cb}^* &= -A\lambda^3 + \mathcal{O}(\lambda^7), \qquad (1.13) \\ V_{td}V_{tb}^* &= A\lambda^3\,(1-\bar\rho - i\bar\eta) + \mathcal{O}(\lambda^7), \end{aligned}$$

$$(1.14)$$

where $\bar\rho = \rho(1-\frac{\lambda^2}{2})$ and $\bar\eta = \eta(1-\frac{\lambda^2}{2})$. Therefore, after being rescaled by $A\lambda^3$, the unitarity relation (1.12) can be represented by the unitarity triangle in figure 1.1.

The parameters λ and A in equation (1.10) can be very accurately related to the CKM matrix elements $|V_{us}|$ and $|V_{cb}|$ through

$$V_{us} = \lambda + \mathcal{O}(\lambda^7), \tag{1.15}$$

$$V_{cb} = A\lambda^2 + \mathcal{O}(\lambda^8), \tag{1.16}$$

as $\mathcal{O}(\lambda^7) \sim \mathcal{O}(10^{-5})$. Therefore a complete description of the CKM matrix can be given by the unitarity triangle in figure 1.1 together with $|V_{us}|$ and $|V_{cb}|$. Furthermore, from the relations between the lengths CA and BA in figure 1.1 and the relevant CKM matrix elements

$$\sqrt{\bar\rho^2 + \bar\eta^2} = (1-\frac{\lambda^2}{2})\frac{1}{\lambda}\left|\frac{V_{ub}}{V_{cb}}\right|, \tag{1.17}$$

$$\sqrt{(1-\bar\rho)^2 + \bar\eta^2} = \frac{1}{\lambda}\left|\frac{V_{td}}{V_{cb}}\right|, \tag{1.18}$$

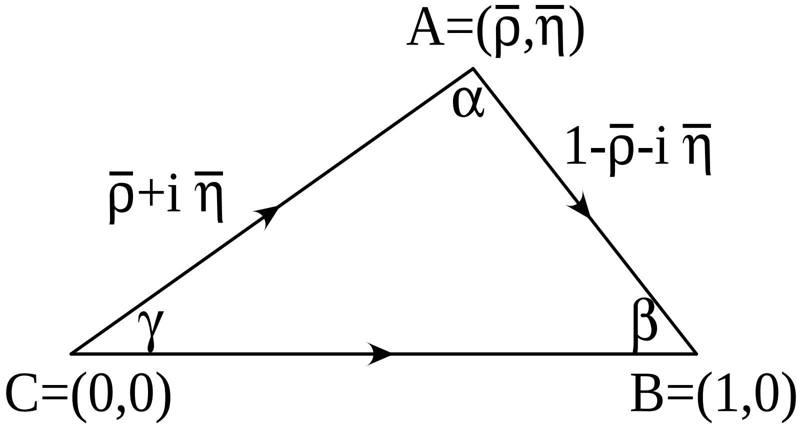

Figure 1.1: Unitarity triangle

it is clear that the measurements of four CP conserving processes which are sensitive to $|V_{us}|$, $|V_{ub}|$, $|V_{cb}|$ and $|V_{td}|$ can tell us whether η is zero or not. This in turn tells us if the CKM mechanism implements CP violation.

1.1.3 Flavour Changing Neutral Currents

Unitarity of the CKM matrix forbids the presence of Flavour Changing Neutral Currents (FCNC) at tree level via the GIM mechanism [15]. Although there is no FCNC basic vertex in the Standard Model, it is possible to construct effective FCNC vertices at one-loop or higher order with the help of the flavour-changing charged vertices involving $W^{\pm}$. Because these FCNC processes appear only at the one-loop level in the Standard Model, they are sensitive probes for new physics beyond the Standard Model. The fact they are zero at tree level means that new physical effects in these channels will not be obscured by a large Standard Model contribution and the fact that they appear only at one loop means that they are sensitive to any new particle which may be too massive to be produced directly, but which can contribute as a virtual particle in the loop. Therefore, from *high-precision* measurements of these low-energy FCNC processes, we might (or might not) see the signal from physics at higher energy scales.

Quantum loops in the Standard Model can generate FCNC effective vertices

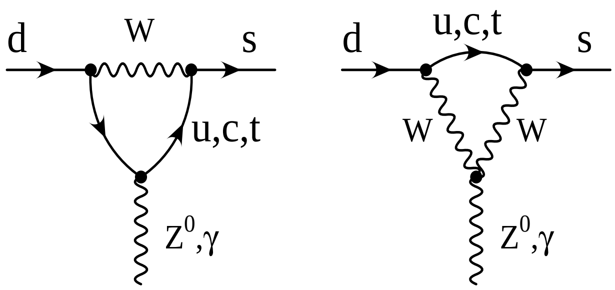

Figure 1.2: Electroweak penguin diagrams.

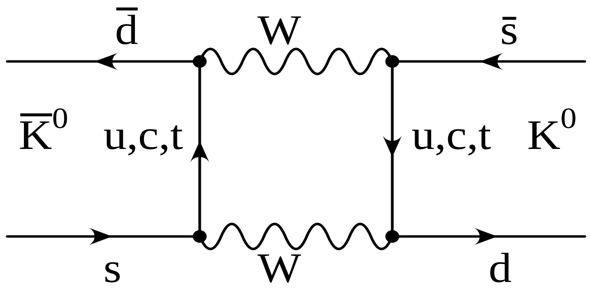

Figure 1.3: Box diagram for $K^0 - \bar{K}^0$ mixing.

through penguin diagrams or box diagrams, as in the examples shown in figures 1.2 and 1.3. These FCNC vertices vanish in the limit where the 'horizontal symmetry' amongst the three generations of fermions is valid, that is, where the relations $m_u = m_c = m_t$ and $m_d = m_s = m_b$ hold true. This is a consequence of the unitarity of the CKM matrix. For instance, in figures 1.2 and 1.3, the contribution of each quark in the loop is proportional to $V_{qd}V_{qs}^*$, where $q = u, c, t$. In the limit $m_u = m_c = m_t$, the unitarity relation

$$V_{ud}V_{us}^* + V_{cd}V_{cs}^* + V_{td}V_{ts}^* = 0 \tag{1.19}$$

implements the GIM mechanism. However, with a very heavy top quark, the horizontal symmetry amongst the up-type quarks is strongly broken. This is why the FCNC processes involving K and B mesons are sufficiently enhanced to be experimentally measurable, and therefore more interesting than other processes.

These one-loop FCNC effective vertices are constructed through the internal $W^\pm$ exchange, all penguin vertices contain a purely $V - A$ structure and all box vertices have the purely $(V-A)\otimes(V-A)$ structure. They have been extensively studied by Inami and Lim [16] in the $'$tHooft-Feynman gauge, where the Higgs bosons do not contribute at one-loop level. Inami and Lim show that these one-loop effective vertices depend on a set of basic universal functions of

$$x_i = \frac{m_i^2}{M_W^2}, \tag{1.20}$$

where $i = u, c, t$. These functions (called the Inami-Lim functions) and the CKM factors govern the strength of the vertex in question.

In this work, we will concentrate upon *the control of non-perturbative strong-interaction effects in some FCNC processes in B and K systems.* However, here we would like to mention two other aspects which are important in performing high-precision theoretical calculations for these processes.

- **Short-distance QCD effects**
  One-loop electroweak effective vertices can be systematically studied by using the operator product expansion which produces a low-energy effective theory. The matching between the effective theory and the full electroweak theory is most reliably done at the renormalisation scale of $\mathcal{O}(M_W)$. However, hadronic matrix elements are usually calculated at the renormalisation scale of a few GeV. Therefore, we need to have a reliable way to run between these two scales, and the most important task is to re-sum the scale-dependent logarithms arising from the short-distance QCD effects. Two-loop perturbative QCD results for most interesting weak processes have been obtained, which reach an accuracy of better than $\pm 1\%$. Reference [6] gives a good review of these results. We will come back to this issue in somewhat more detail in the next section, since it is closely related to the non-perturbative calculations we are focusing on.

- **Two-loop electroweak corrections**
  Although the one-loop effective FCNC vertices are already higher-order in terms of the weak coupling g_2 (for instance, the box diagram in figure 1.3 is of order g_2^4), the ambiguity arising from the choice of the scheme for defining g_2 at one-loop level gives about 5% error, as shown in [17]. Also,

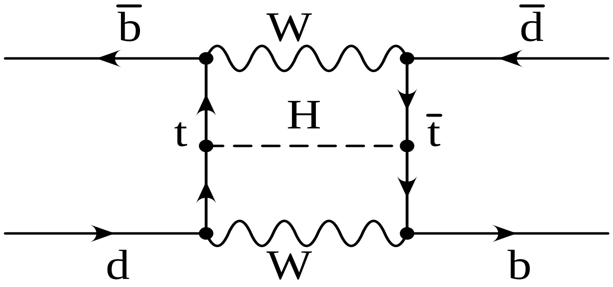

Figure 1.4: A two-loop electroweak correction to the box diagram of $B^0 - \bar{B}^0$ mixing, which might be large due to the heavy top quark.

because of the heavy top quark, the two-loop diagram in figure 1.4 might have a significant contribution, given the fact that the coupling of the Higgs particle to the top quark is proportional to $g_2 m_t / M_W$. There has not been much work done on this aspect. References [17, 18] give recent results for the effects of two-loop electroweak corrections upon $B^0 - \bar{B}^0$ mixing and $K \to \pi\nu\bar{\nu}$ decay.

1.2 Operator Product Expansion and Effective Weak Hamiltonian

Because of the asymptotic freedom of QCD and the difference between the weak-interaction energy scale which is of $\mathcal{O}(M_W)$ and the typical strong-interaction scale which is of $\mathcal{O}(1GeV)$, we can adopt the operator product expansion (OPE) and renormalisation group (RG) improved perturbation theory to obtain a low-energy effective theory describing the weak interaction of quarks. For any weak-interaction process, we can always construct a low-energy effective weak Hamiltonian which has the structure

$$\mathcal{H}_{\text{eff}} = \frac{G_F}{\sqrt{2}} \sum_i V_{\text{CKM}}^i C_i \left(\Phi^i; \mu\right) \mathcal{O}_i(\mu), \tag{1.21}$$

where V_{CKM}^i is the relevant CKM factor, μ some renormalisation scale, C_i the Wilson coefficient, $\mathcal{O}_i$ the relevant lowest-dimension local operators (We only keep the lowest-dimension operators). Φ^i contains the relevant Inami-Lim functions if we are dealing with a FCNC process. G_F is Fermi's coupling constant which is given by

$$\frac{G_F}{\sqrt{2}} = \frac{g_2^2}{8M_W^2}. \tag{1.22}$$

The OPE is an important tool in dealing with weak-interaction processes. For instance, it is very difficult to put the Standard Model on the lattice because of the problem of discretising the chiral fermions on the lattice and the high cost of any computation which can accommodate the heaviest and the lightest particles in the Standard Model.

1.2.1 OPE in the Pure Electroweak Sector

Let us disregard QCD effects and focus on the electroweak sector of the Standard Model for the moment. The basic idea here is to 'integrate out' the heavy weak bosons, and expand the non-local product of charged-current operators in a series of local operators dimension by dimension. Each term in this series is weighted by $(1/M_W^n)$ $(n \geq 0)$ and some effective coupling constant, the Wilson coefficient. In the low-energy limit, where the momentum (k) transfered through the propagating W boson is only a few GeV, we can safely neglect $\mathcal{O}(k^2/M_W^2)$ terms when expanding the W-boson propagator

$$\frac{1}{k^2 - M_W^2}, \tag{1.23}$$

in powers of k^2/M_W^2. In this case, it is sufficient to keep the leading terms of this series, *i.e.*, the lowest-dimension operators.

As a simple example, consider the decay of a kaon into two pions. We will use this process for illustration in this and the following two subsections. It is not difficult to generalise the treatment of this process to more complicated ones, *e.g.*, the FCNC processes.

Figure 1.5(a) shows the diagram of the leading-order quark-level operator for $K \to \pi\pi$ in the electroweak theory. The amplitude is given by

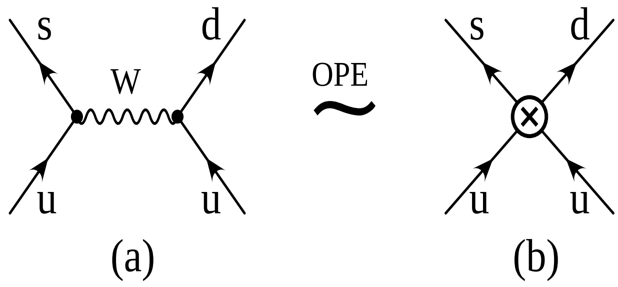

Figure 1.5: OPE for $K \to \pi\pi$ at the leading order

$$A = -\frac{G_F}{\sqrt{2}} V_{ud}^* V_{us} \frac{M_W^2}{k^2 - M_W^2} \langle \pi\pi | (\bar{d}u)_{V-A} (\bar{u}s)_{V-A} | K \rangle \quad (1.24)$$

$$= \frac{G_F}{\sqrt{2}} V_{ud}^* V_{us} \langle \pi\pi | (\bar{d}u)_{V-A} (\bar{u}s)_{V-A} | K \rangle + \mathcal{O}\left(\frac{k^2}{M_W^2}\right) \quad (1.25)$$

where

$$(\bar{d}u)_{V-A} = \bar{d}\gamma_\mu (1 - \gamma_5) u. \quad (1.26)$$

After implementing the OPE and neglecting the $\mathcal{O}(k^2/M_W^2)$ terms which correspond to higher-dimension operators, we obtain the operator in the effective theory

$$\mathcal{O}_1 = (\bar{d}_\alpha u_\alpha)_{V-A} (\bar{u}_\beta s_\beta)_{V-A}, \quad (1.27)$$

which generates the effective vertex given in figure 1.5(b). Here α and β denote the colour indices. In this example, the leading operator in the OPE is of dimension six, and the Wilson coefficient is unity.

A more formal treatment of OPE for this process which starts from the path-integral formalism can be found in [19]. In this approach, we perform the functional integration over the $W^\pm$ fields explicitly. This results in a non-local action for the quarks, which can be expanded in powers of $1/M_W^2$. This expansion then gives local operators.

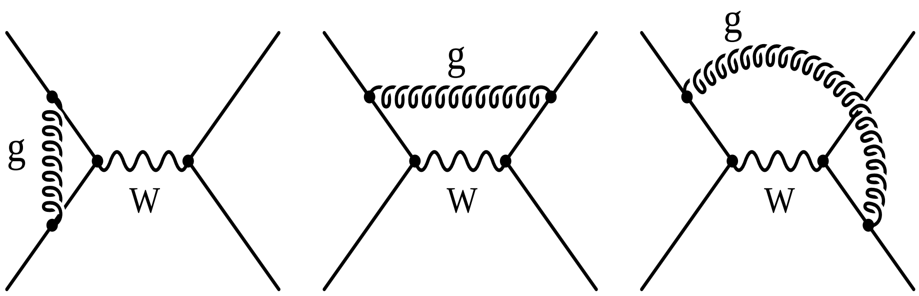

Figure 1.6: Diagrams for one-loop QCD effects upon $K \to \pi\pi$ in the full electroweak theory

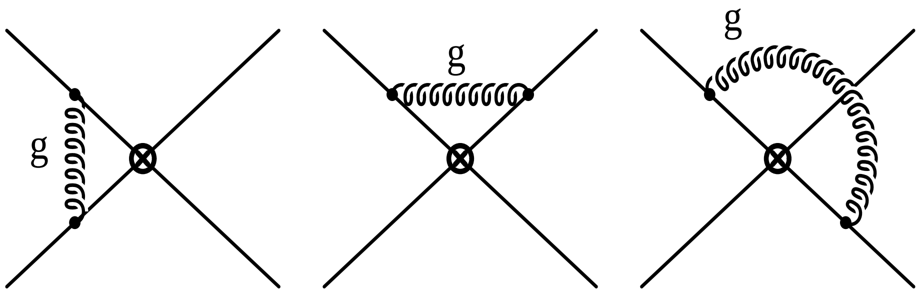

Figure 1.7: Diagrams for one-loop QCD effects upon $K \to \pi\pi$ in the low-energy effective theory

1.2.2 Factorisation of Short-distance and Long-distance QCD Effects

Now we take into account the QCD effects. Let's look at the example of $K \to \pi\pi$, as in the last subsection. Figures 1.6 and 1.7 show the diagrams for the one-loop QCD effects in the full electroweak theory and the low-energy effective theory respectively. Because of the colour structure of these diagrams and the algebraic relation

$$T^a_{\alpha\beta} T^a_{\gamma\delta} = \frac{-1}{2N} \delta_{\alpha\beta}\delta_{\gamma\delta} + \frac{1}{2}\delta_{\alpha\delta}\delta_{\gamma\beta} \tag{1.28}$$

where T^a are the generators of the $SU(N)$ group, there is another operator

$$\mathcal{O}_2 = (\bar{d}_\alpha u_\beta)_{V-A}(\bar{u}_\beta s_\alpha)_{V-A}, \tag{1.29}$$

which will mix with $\mathcal{O}_1$. The effective weak Hamiltonian is therefore of the form[1]

$$\mathcal{H}_{\text{eff}} = \frac{G_F}{\sqrt{2}} V_{ud}^* V_{us} \left(C_1(\mu)\mathcal{O}_1(\mu) + C_2(\mu)\mathcal{O}_2(\mu) \right). \tag{1.30}$$

The determination of the Wilson coefficients C_1 and C_2 can be done by matching the full electroweak theory onto the low-energy effective theory, that is, by requiring the transition amplitude A_{full} in the full electroweak theory to be reproduced by the one A_{eff} in the low-energy effective theory described by the effective Hamiltonian in equation (1.30)

$$A_{\text{full}} = A_{\text{eff}} = \frac{G_F}{\sqrt{2}} V_{ud}^* V_{us} \left(C_1(\mu)\langle\mathcal{O}_1(\mu)\rangle + C_2(\mu)\langle\mathcal{O}_2(\mu)\rangle \right). \tag{1.31}$$

The matching procedure involves the calculations of the amplitudes of the diagrams in figures 1.6 and 1.7. While the amplitudes in figure 1.6 (full theory) are ultra-violet finite, the ones in figure 1.7 (effective theory) are ultra-violet divergent, and therefore require renormalisation. This results in the fact that the amplitude A_{eff} depends on $\ln\left(\mu^2/(-p^2)\right)$ at $\mathcal{O}(\alpha_s)$, where μ is the renormalisation scale, and p is the off-shell external momentum which we have to keep in order to regulate the infra-red divergence. On the other hand, A_{full} depends on $\ln\left(M_W^2/(-p^2)\right)$ at the same order. We then find the Wilson coefficients are

$$\begin{aligned} C_1(\mu) &= 1 + \frac{3}{N}\frac{\alpha_s}{4\pi}\ln\frac{M_W^2}{\mu^2}, && (1.32) \\ C_2(\mu) &= -3\frac{\alpha_s}{4\pi}\ln\frac{M_W^2}{\mu^2}. && (1.33) \end{aligned}$$

There are two important observations at this point:

1. The Wilson coefficients do not contain any information about the long-distance QCD effects. As can be seen in equations (1.32) and (1.33), the external momentum p, which reveals the long-distance structure of A_{full} does not show up in the Wilson coefficients at all. This means we have factored out all the long-distance QCD effects which are now contained in the matrix

[1] For simplicity, we neglect penguin contributions at this moment. These contributions will be discussed in chapter 4

elements $\langle \mathcal{O}_1(\mu) \rangle$ and $\langle \mathcal{O}_2(\mu) \rangle$. This factorisation can be schematically seen as

$$\begin{aligned} \text{Full Amplitude} &= \text{Wilson Coeff} \times \text{Operator Matrix Element} \\ (1+\frac{\alpha_s}{4\pi}\Gamma\ln\frac{M_W^2}{-p^2}) &= (1+\frac{\alpha_s}{4\pi}\Gamma\ln\frac{M_W^2}{\mu^2})\cdot(1+\frac{\alpha_s}{4\pi}\Gamma\ln\frac{\mu^2}{-p^2}), \end{aligned} \tag{1.34}$$

where Γ is just the one-loop anomalous dimension. This can be represented as the splitting of the logarithms according to

$$\ln\frac{M_W^2}{-p^2} = \ln\frac{M_W^2}{\mu^2} + \ln\frac{\mu^2}{-p^2}, \tag{1.35}$$

which arises from the integration over some virtual loop momentum as

$$\int_{-p^2}^{M_W^2} \frac{dk^2}{k^2} = \int_{\mu^2}^{M_W^2} \frac{dk^2}{k^2} + \int_{-p^2}^{\mu^2} \frac{dk^2}{k^2}, \tag{1.36}$$

so it is clear that μ is the scale which separates the long-distance and the short-distance regions. *The operator matrix elements which contain the information from this region then have to be calculated non-perturbatively* because of confinement of QCD.

2. The Wilson coefficients do not depend upon the choice of the external states in the calculation of the amplitudes. This is obvious since they only represent the short-distance structure of the theory. The point is that we have to regularise the quark mass and the infra-red divergence in the same way in both the full theory and the effective theory.

To conclude this subsection, we stress that it is important to have the short-distance QCD information from the Wilson coefficients when performing the non-perturbative calculation of the matrix elements. This is because we need the Wilson coefficients to obtain the physical answer in the full theory, which does not depend upon μ. Also, for the purpose of making comparison with other non-perturbative calculations for the same matrix element, we might have to run it to other scales.

1.2.3 Renormalisation Group Analysis

Let's take a closer look at equations (1.32) and (1.33). When $\mu = \mathcal{O}(M_W)$, the scale-dependent one-loop correction to the Wilson coefficients is small. However, when $\mu = \mathcal{O}(1\text{GeV})$, which happens in most cases, $\alpha_s(\mu)$ is between 0.1 and 0.2. Therefore, we have

$$\alpha_s(\mu)\ln\frac{M_W^2}{\mu^2} = \mathcal{O}(1), \tag{1.37}$$

which gives a 100% correction at one loop. What is worse is that at all orders, we have the so-called leading logarithms

$$\alpha_s^n(\mu)\ln^n\frac{M_W^2}{\mu^2} = \mathcal{O}(1), \tag{1.38}$$

which completely spoil the convergence of the perturbation theory. Therefore, we need to find a way to re-sum them. This is best done by solving Renormalisation Group Equations (RGEs) for the Wilson coefficients. The resulting expansion is known as RG improved perturbation theory. In this expansion, the first order is represented by the sum of all the terms of the form $\alpha_s^n\ln^n\frac{M_W^2}{\mu^2}$, and the second order is represented by the sum of the next-to-leading logarithms, $\alpha_s^{n+1}\ln^n\frac{M_W^2}{\mu^2}$, which are numerically of $\mathcal{O}(\alpha_s)$.

From equations (1.30) and (1.31), we see that $\mathcal{O}_1$ and $\mathcal{O}_2$ are not multiplicatively renormalised, as they mix with each other under renormalisation through the one-loop diagrams in figure 1.7 and equation (1.28). That means that the renormalised operators $\mathcal{O}_1^{\rm r}$ and $\mathcal{O}_2^{\rm r}$ are related to the bare ones $\mathcal{O}_1^{\rm b}$ and $\mathcal{O}_2^{\rm b}$ through

$$\begin{pmatrix} \mathcal{O}_1^{\rm b} \\ \mathcal{O}_2^{\rm b} \end{pmatrix} = \hat{Z}(\mu) \begin{pmatrix} \mathcal{O}_1^{\rm r}(\mu) \\ \mathcal{O}_2^{\rm r}(\mu) \end{pmatrix}, \tag{1.39}$$

where μ is the renormalisation scale. $\mathcal{O}_1^{\rm b}$ and $\mathcal{O}_2^{\rm b}$ depend on the cut-off we introduce. $\hat{Z}(\mu)$ is a 2×2 mixing matrix, which can be written as

$$\hat{Z}(\mu) = \begin{pmatrix} 1+\frac{\alpha_s}{4\pi}Z_{11}(\mu) & \frac{\alpha_s}{4\pi}Z_{12}(\mu) \\ \frac{\alpha_s}{4\pi}Z_{21}(\mu) & 1+\frac{\alpha_s}{4\pi}Z_{22}(\mu) \end{pmatrix}, \tag{1.40}$$

where $Z_{ij}(\mu)$ all contain renormalisation-scale-dependent logarithms. This means, when we vary μ to run between different scales, we cannot run $\mathcal{O}_1^{\rm r}(\mu)$ and $\mathcal{O}_2^{\rm r}(\mu)$ separately.

In the example of $K \to \pi\pi$ decays, we can diagonalise the mixing matrix $\hat{Z}$,

$$\hat{Z} \xrightarrow{\text{diag}} \begin{pmatrix} Z_+(\mu) & 0 \\ 0 & Z_-(\mu) \end{pmatrix}, \tag{1.41}$$

where $Z_\pm$ are just the eigenvalues of $\hat{Z}$ and contain μ-dependent logarithms. The eigenbasis operators $\mathcal{O}_+$ and $\mathcal{O}_-$ are multiplicatively renormalised, and they are related to $\mathcal{O}_1$ and $\mathcal{O}_2$ in (1.31) through

$$\mathcal{O}_\pm = \frac{\mathcal{O}_1 \pm \mathcal{O}_2}{2}. \tag{1.42}$$

We now have

$$\mathcal{O}^{\text{b}}_\pm = Z_\pm \mathcal{O}^{\text{r}}_\pm, \tag{1.43}$$

and the corresponding Wilson coefficients for $\mathcal{O}_+$ and $\mathcal{O}_-$ are

$$C_\pm(\mu) = 1 + (\frac{3}{N} \mp 3)\frac{\alpha_s}{4\pi}\ln\frac{M_W^2}{\mu^2}. \tag{1.44}$$

We can run $\mathcal{O}^{\text{r}}_\pm(\mu)$ separately when varying the scale μ.

The RGEs for $C_\pm$ simply follow from the fact that the transition amplitude in the full electroweak theory does not depend upon μ at all. In a mass-independent renormalisation scheme, *e.g.*, $\overline{\text{MS}}$,

$$\frac{dC_\pm(\mu)}{d(\ln\mu)} = \gamma_\pm(g)C_\pm(\mu), \tag{1.45}$$

where g is the strong coupling constant and $\gamma_\pm$ is the anomalous dimension of the operator $\mathcal{O}_\pm$

$$\gamma_\pm(g) = \frac{1}{Z_\pm}\frac{dZ_\pm}{d(\ln\mu)}, \tag{1.46}$$

where $Z_\pm$ is the renormalisation constant of $\mathcal{O}_\pm$.

The solution of equation (1.45) is

$$C_\pm(\mu) = U_{c\pm}(\mu, M_W)C_\pm(M_W), \tag{1.47}$$

where $U_{c\pm}(\mu, M_W)$ is the scale-evolution function

$$U_{c\pm}(\mu, M_W) = \exp\left[\int_{g(M_W)}^{g(\mu)} dg' \frac{\gamma_\pm(g')}{\beta(g')}\right], \tag{1.48}$$

of the Wilson coefficients. $\beta(g)$ is the QCD β function

$$\beta(g) = -\beta_0 \frac{g^3}{16\pi^2} + \ldots, \tag{1.49}$$

$$\beta_0 = 11 - \frac{2}{3} n_f, \tag{1.50}$$

with n_f the number of flavours. It is straightforward to find the one-loop solution which sums up the leading logarithms

$$C_\pm(\mu) = \left[\frac{\alpha_s(\mu)}{\alpha_s(M_W)}\right]^{\frac{-\gamma_\pm^{(0)}}{2\beta_0}} = \left[1 + \beta_0 \frac{\alpha_s(\mu)}{4\pi} \ln \frac{M_W^2}{\mu^2}\right]^{\frac{-\gamma_\pm^{(0)}}{2\beta_0}}, \tag{1.51}$$

where $\gamma_\pm^{(0)}$ is the one-loop anomalous dimension in the expansion

$$\gamma_\pm = \gamma_\pm^{(0)} \frac{\alpha_s}{4\pi} + \gamma_\pm^{(1)} \frac{\alpha_s^2}{16\pi^2} + \ldots. \tag{1.52}$$

This is the Leading-Logarithm Approximation (LLA) of the Wilson coefficients. It actually implies

$$C_\pm(M_W) = 1 \tag{1.53}$$

$$U_{c\pm}(\mu, M_W) = \left[\frac{\alpha_s(\mu)}{\alpha_s(M_W)}\right]^{\frac{-\gamma_\pm^{(0)}}{2\beta_0}}, \tag{1.54}$$

which means a tree-level matching (at M_W) and a one-loop running (down to the scale μ).

Note that if we do not diagonalise $\hat{Z}$ in equation (1.40), then we have an 'anomalous dimension matrix', $\hat{\gamma}(g)$, from equation (1.46). In general, if there are n operators which mix under renormalisation, $\hat{\gamma}(g)$ is a $n \times n$ matrix, and the RGEs become a set of n coupled equations. This implies that when we evolve the scale, we cannot run the Wilson coefficients (or the operators) separately. Consider a set of n operators $\mathcal{O}_1, \mathcal{O}_2, \ldots, \mathcal{O}_n$ and corresponding Wilson coefficients

$$\vec{\mathcal{O}}^T = (\mathcal{O}_1 \mathcal{O}_2, \ldots, \mathcal{O}_n), \tag{1.55}$$

$$\vec{C}^T = (C_1, C_2, \ldots, C_n). \tag{1.56}$$

Label a renormalised quantity by a superscript 'r', and a bare quantity by a superscript 'b', we have

$$\vec{\mathcal{O}}^{\mathrm{b}} = \hat{Z} \vec{\mathcal{O}}^{\mathrm{r}}, \quad \vec{C}^{\mathrm{b}} = \left(\hat{Z}^{-1}\right)^T \vec{C}^{\mathrm{r}}, \tag{1.57}$$

where $\hat{Z}$ is the matrix which accounts for the renormalisation and mixing of these n operators. Defining the anomalous dimension matrix $\hat{\gamma}$ by

$$\hat{\gamma} = \hat{Z}^{-1}\frac{d\hat{Z}}{d\ln\mu}, \tag{1.58}$$

The RGEs of the Wilson coefficients can be written as

$$\frac{d\vec{C}}{d\ln\mu} = \hat{\gamma}^T\vec{C}, \tag{1.59}$$

where we have dropped the superscript 'r'. Solving these RGEs results in an $n \times n$ matrix which accounts for the scale evolution (between μ_1 and μ_2) of these Wilson coefficients

$$\hat{U}_c(\mu_1,\mu_2) = T_g\mathrm{exp}\left[\int_{g(\mu_2)}^{g(\mu_1)} dg'\frac{\hat{\gamma}^T(g')}{\beta(g')}\right], \tag{1.60}$$

where T_g means 'g-ordered'. The scale evolution of the Wilson coefficients between these two scales becomes

$$\begin{pmatrix} C_1(\mu_1) \\ C_2(\mu_1) \\ \vdots \\ C_n(\mu_1) \end{pmatrix} = \hat{U}_c(\mu_1,\mu_2)\begin{pmatrix} C_1(\mu_2) \\ C_2(\mu_2) \\ \vdots \\ C_n(\mu_2) \end{pmatrix}. \tag{1.61}$$

The LLA scale evolution of the Wilson coefficients between two scales μ_1 and μ_2 has the form

$$\hat{U}_{c\mathrm{LLA}}(\mu_1,\mu_2) = \left[\frac{\alpha_s(\mu_1)}{\alpha_s(\mu_2)}\right]^{\frac{-(\hat{\gamma}^{(0)})^T}{2\beta_0}}, \tag{1.62}$$

where $\hat{\gamma}^{(0)}$ is the one-loop anomalous dimension matrix.

Bearing in mind that the next-to-leading logarithms are of $\mathcal{O}(\alpha_s)$, we are strongly motivated to go to the Next-to-Leading-Logarithm Approximation (NLLA). NLLA is also necessary to explore the scheme dependence, as the anomalous dimension starts to depend upon the choice of the scheme at this order. Going to NLLA requires the calculation of the two-loop QCD β function and the anomalous dimension for the operator in question. Results for these quantities in most interesting cases can be found in the literature. The general feature of the NLLA of the scale evolution of Wilson Coefficients between the scales μ_1 and μ_2 takes the form

$$\hat{U}_{\rm cNLLA}(\mu_1,\mu_2) = \left(1+\frac{\alpha_s(\mu_1)}{4\pi}\hat{J}\right)\hat{U}^{(0)}_{\rm cLLA}(\mu_1,\mu_2)\left(1-\frac{\alpha_s(\mu_2)}{4\pi}\hat{J}\right), \tag{1.63}$$

where the matrix $\hat{J}$ expresses the NLLA corrections to the scale evolution. Suppose the matrix $\hat{V}$ diagonalises $\left(\hat{\gamma}^{(0)}\right)^T$, and

$$\hat{\gamma}^{(0)}_D \equiv \hat{V}^{-1}\left(\hat{\gamma}^{(0)}\right)^T\hat{V}, \tag{1.64}$$

then we have

$$\hat{U}^{(0)}_{\rm cLLA}(\mu_1,\mu_2) = \hat{V}\left(\left[\frac{\alpha_s(\mu_1)}{\alpha_s(\mu_2)}\right]^{-\frac{\vec{\gamma}^{(0)}}{2\beta_0}}\right)\hat{V}^{-1}, \tag{1.65}$$

where $\vec{\gamma}^{(0)}$ is the vector whose elements are just the diagonal elements of the diagonalised matrix $\hat{\gamma}^{(0)}_D$. If we define a matrix

$$\hat{G} = \hat{V}^{-1}\left(\hat{\gamma}^{(1)}\right)^T\hat{V}, \tag{1.66}$$

where $\hat{\gamma}^{(1)}$ is the two-loop anomalous dimension matrix, then the matrix $\hat{J}$ is given by

$$\hat{J} = \hat{V}\hat{H}\hat{V}^{-1}. \tag{1.67}$$

The matrix $\hat{H}$ has the elements

$$H_{ij} = \delta_{ij}\gamma_i^{(0)}\frac{\beta_1}{\beta_0} - \frac{G_{ij}}{2\beta_0+\gamma_i^{(0)}-\gamma_j^{(0)}}, \tag{1.68}$$

where $\beta_1 = 102 - 38n_f/3$ is from the two-loop QCD β function.

Similarly, we can solve the RGEs

$$\frac{d\vec{\mathcal{O}}}{d\ln\mu} = -\hat{\gamma}\vec{\mathcal{O}}, \tag{1.69}$$

and obtain the scale-evolution function of the operators

$$\hat{U}(\mu_1,\mu_2) = T_g\exp\left[\int_{g(\mu_2)}^{g(\mu_1)} dg'\frac{-\hat{\gamma}(g')}{\beta(g')}\right]. \tag{1.70}$$

The scale evolution of the operators between μ_1 and μ_2 is

$$\begin{pmatrix}\mathcal{O}_1(\mu_1)\\ \mathcal{O}_2(\mu_1)\\ \vdots\\ \mathcal{O}_n(\mu_1)\end{pmatrix} = \hat{U}(\mu_1,\mu_2)\begin{pmatrix}\mathcal{O}_1(\mu_2)\\ \mathcal{O}_2(\mu_2)\\ \vdots\\ \mathcal{O}_n(\mu_2)\end{pmatrix}, \tag{1.71}$$

which has a Next-to-Leading-Logarithm approximation

$$\hat{U}_{\mathrm{NLLA}}(\mu_1, \mu_2) = \left(1 + \frac{\alpha_s(\mu_1)}{4\pi}\hat{J}\right) \hat{U}^{(0)}_{\mathrm{LLA}}(\mu_1, \mu_2) \left(1 - \frac{\alpha_s(\mu_2)}{4\pi}\hat{J}\right). \tag{1.72}$$

Here the notation is analogous to the one used between equation (1.62) and equation (1.68), with the replacement

$$\left(\hat{\gamma}^{(0)}\right)^T \longrightarrow -\hat{\gamma}^{(0)}, \tag{1.73}$$

$$\left(\hat{\gamma}^{(1)}\right)^T \longrightarrow -\hat{\gamma}^{(1)}. \tag{1.74}$$

Chapter 2

Theoretical Tools

We have arrived at the stage where we know the general strategy for exploring flavour physics. However, we have not talked about how to control the non-perturbative strong-interaction effects, which is the main theme of this work. This chapter is devoted to an introduction on how to perform the non-perturbative QCD calculation for weak matrix elements in the framework of Lattice QCD. Because of some theoretical and technical difficulties which will be explained in the first section of this chapter, we need Heavy Quark Effective Theory and Chiral Perturbation Theory which can guide us to extract physically meaningful results from Lattice QCD simulations.

2.1 Lattice QCD

Lattice QCD is the Euclidean version of QCD obtained by discretising space-time with a finite lattice spacing a. This imposes a cut-off of order $1/a$ in momentum space. Putting Lattice QCD in a finite space-time, the number of degrees of freedom becomes finite, one can then non-perturbatively perform numerical calculations in this framework. This makes the lattice regularisation different from other regularisations (*e.g.*, Dimensional Regularisation) and renormalisation schemes (*e.g.*, the $\overline{\mathrm{MS}}$ scheme) introduced via perturbation theory. These latter schemes are inherently perturbative, and therefore they are not suitable for dealing with non-perturbative strong-interaction effects. Lattice QCD offers a tool to calculate the non-perturbative strong-interaction effects from *first principles*, and quantify the resulting systematic errors. In this section, we give an introduction to Lattice QCD. We will discuss in detail two sources of systematic errors, discretisation and operator matching. Quenching errors will be mentioned. These three systematic errors are the most significant in current lattice calculations of weak matrix elements, as the finite-size effects have been studied by Lüscher [20] and can be shown to give a systematic error under a few percent on the largest currently available lattices.

2.1.1 Euclidean Formulation of a Field Theory

A Euclidean field theory is constructed from a Minkowski one with the substitution

$$x_0 = -ix_4^E, \tag{2.1}$$

and with the definition of the Euclidean gamma matrices

$$\begin{aligned}
\gamma_j^E &= i\gamma_j \quad (j = 1,2,3), && (2.2)\\
\gamma_4^E &= \gamma_0, && (2.3)\\
\gamma_5^E &= \gamma_5, && (2.4)
\end{aligned}$$

which satisfy

$$\begin{aligned}
\left\{\gamma_\mu^E, \gamma_\nu^E\right\} &= 2\delta_{\mu\nu}, && (2.5)\\
\gamma_5^E &= -\gamma_1^E\gamma_2^E\gamma_3^E\gamma_4^E. && (2.6)
\end{aligned}$$

An important requirement, the reflection positivity, must be satisfied such that the analytic continuation from Euclidean space back to Minkowski space can be performed. Consider the Euclidean field

$$\phi(x) = e^{Hx^4}\phi(\vec{x},0)e^{-Hx^4} \tag{2.7}$$

and the Euclidean time-reflection operators

$$\begin{aligned}
\theta(\vec{x}, x^4) &= (\vec{x}, -x^4), && (2.8)\\
\Theta\phi(x) &= \overline{\phi(\theta x)}, && (2.9)
\end{aligned}$$

where the bar indicates complex conjugation. For a function F of the Euclidean fields at positive times, *e.g.*, a Schwinger function, reflection positivity means

$$\langle (\Theta F)\, F \rangle \geq 0. \tag{2.10}$$

This condition can be shown to be equivalent to the positivity of inner products in Hilbert space and the spectrum condition in the Minkowski formulation. On the lattice, a small complication arises from the difference between the *site reflection* and the *link reflection*. Reference [21] gives a detailed discussion of the Euclidean formulation of field theory on the lattice.

The Euclidean path integral takes the form of a partition function,

$$Z = \int \mathcal{D}\Phi e^{-S[\Phi]} \quad (\Phi \text{ is a field}), \tag{2.11}$$

in statistical mechanics. One can therefore gain further understanding of the theory by using Monte Carlo methods in performing numerical calculations.

2.1.2 Discretising QCD

Putting Euclidean QCD on a finite lattice can be done by replacing integrals with finite sums and derivatives with finite differences. The lattice fields are only defined on the lattice points. In a more formal treatment, one states that the lattice fields result from integrating out the physics at distances shorter than the lattice spacing in the dynamical variables. On the lattice, periodic (or anti-periodic) boundary conditions are usually imposed, and momenta are restricted to the first *Brillouin zone*

$$\mathcal{B} = \left[\frac{-\pi}{a}, \frac{\pi}{a}\right]. \tag{2.12}$$

1. **Gauge Fields**
   Gauge fields are represented by the link fields $U_\mu(x)$ which are group elements of colour $SU(3)$ in the fundamental representation. They are parallel transporters

$$U_\mu(x) \equiv U(x, x+a\vec{\mu}) = \exp\left[-iagA_\mu(x)\right] = \mathbf{I} - ig\mathcal{P}\int_x^{x+a\vec{\mu}} A_\mu(x)dx^\mu, \tag{2.13}$$

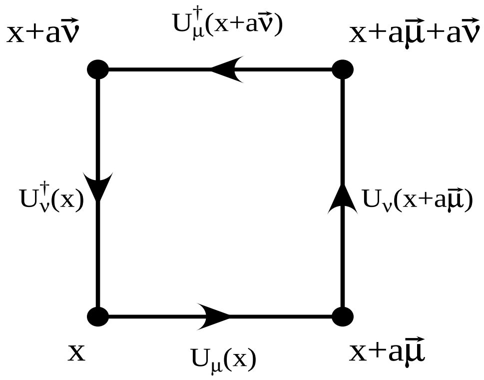

Figure 2.1: The plaquette in the $\mu\nu$ plane

where $A_\mu(x)$ are the gluonic fields, $\mathcal{P}$ means path-ordered. Under a local gauge transformation $\Lambda(x)$, the link fields transform as

$$U_\mu(x) \to \Lambda(x) U_\mu(x) \Lambda^{-1}(x + a\vec{\mu}). \tag{2.14}$$

The group integration is

$$\int \mathcal{D}U = \prod_{x,\mu} \int dU_\mu(x), \tag{2.15}$$

which is finite on a finite lattice and well-defined for any compact group if the measure satisfies

$$\int_G f(U)dU = \int_G f(VU)dU = \int_G f(UV)dU, \tag{2.16}$$

$$\int_G dU = 1, \tag{2.17}$$

where V is any element of the group G. Such a measure is called a Haar measure. The functional integral is also finite.

From equation (2.14), the gauge-invariant quantities in the pure Yang-Mills theory are closed loops formed by the link fields

$$U(x,x) = U(x,y_1)U(y_1,y_2)\ldots U(y_n,x), \tag{2.18}$$

amongst which the simplest is the plaquette $U^p_{\mu\nu}$ (figure 2.1)

$$U^p_{\mu\nu} = U_\mu(x)U_\nu(x+a\vec{\mu})U^\dagger_\mu(x+a\vec{\nu})U^\dagger_\nu(x), \tag{2.19}$$

with

$$U_\mu^\dagger(x) = U_{-\mu}(x + a\vec{\mu}). \tag{2.20}$$

The simplest pure gauge action for a $SU(N)$ gauge theory is the Wilson action [22]

$$S_{\mathrm{G}}^{\mathrm{W}} = \beta \sum_x \sum_{\mu<\nu} \left(1 - \frac{1}{N} \Re e \mathrm{Tr} U_{\mu\nu}^p(x)\right), \tag{2.21}$$

where $\beta = 2N/g^2(a)$. It can be shown that

$$S_{\mathrm{G}}^{\mathrm{W}} = S^{\mathrm{YM}} + \mathcal{O}(a^2). \tag{2.22}$$

2. **Fermion Fields**

Fermion fields on the lattice are anti-commuting spinors defined on the lattice sites. Under a local gauge transformation $\Lambda(x)$, they transform as

$$\psi(x) \;\rightarrow\; \Lambda(x)\psi(x), \tag{2.23}$$
$$\bar{\psi}(x) \;\rightarrow\; \bar{\psi}(x)\Lambda^{-1}(x). \tag{2.24}$$

Therefore the simplest way to obtain a gauge-invariant fermion action on the lattice is through the naive discretisation

$$\begin{aligned} S_{\mathrm{F}}^{\mathrm{N}} &= \sum_x \Big\{ \frac{1}{2} \sum_\mu \left[\bar{\psi}(x)\gamma_\mu U_\mu(x)\psi(x + a\vec{\mu}) - \bar{\psi}(x + a\vec{\mu}) U_\mu^\dagger(x)\gamma_\mu\psi(x)\right] \\ &+ m\bar{\psi}(x)\psi(x)\Big\}, \end{aligned} \tag{2.25}$$

where $m = am_{\mathrm{phys}}$ is a dimensionless mass parameter. This action suffers from the *fermion doubling problem* which arises because the Hermitian Dirac operator has only first derivatives, with an effective lattice spacing $2a$, and thus cannot distinguish the modes with momenta q and $\pi/a - q$.

Fermion doubling is related to the problem of discretising chiral fermions on the lattice via the Nielsen-Ninomiya no-go theorem [23, 24]. This states that if a lattice fermion action is

- ultra-local
- bilinear in fermion fields
- translationally invariant

- Hermitian

and has a continuous-like chiral symmetry ($m = 0$ in this case), then every left-handed fermion has a right-handed replica and every right-handed fermion has a left-handed replica. If one looks at the momentum-space Wilson-Dirac operator with $m = 0$, one finds this operator has two zeros in each dimension. It can be shown that these two zeros account for two propagating fermions with opposite chirality. This gives sixteen fermion species in a four-dimension space-time.

Wilson [25] proposed a way to avoid the doubling problem by adding an irrelevant operator to the naive fermion action

$$S^{\mathrm{W}} = \frac{r}{a}\sum_x \left[\bar{\psi}(x)\psi(x) - \frac{1}{2}\sum_\mu \left(\bar{\psi}(x+a\vec{\mu})U_\mu^\dagger(x)\psi(x) + \bar{\psi}(x)U\mu(x)\psi(x+a\vec{\mu})\right)\right], \tag{2.26}$$

where r is an arbitrary parameter which is usually set to unity. This term explicitly breaks chiral symmetry. The Wilson fermion action is usually written as

$$\begin{aligned} S_{\mathrm{F}}^{\mathrm{W}} &= \sum_x \Big\{\bar{\psi}(x)\psi(x) \qquad (2.27) \\ &+ \kappa\sum_\mu \bar{\psi}(x)\left[U\mu(x)(\gamma_\mu - r)\psi(x+a\vec{\mu}) - U_\mu^\dagger(x-a\vec{\mu})(\gamma_\mu + r)\psi(x-a\vec{\mu})\right]\Big\}, \end{aligned}$$

where

$$\kappa = \frac{1}{2m+8r} \tag{2.28}$$

is called the hopping parameter. In order to obtain the expression in equation (2.27), the fermion field has been rescaled by

$$\psi \longrightarrow \sqrt{2\kappa}\psi. \tag{2.29}$$

Here we stress some important features of the Wilson fermion action:

(a) It deviates from the continuum action by $\mathcal{O}(a)$, which means it approaches the continuum limit quite slowly. We will discuss the $\mathcal{O}(a)$ improvement of the Wilson fermion action later.

(b) Since chiral symmetry is explicitly broken by this action, there is nothing to prevent the quark mass from having an additive renormalisation, which raises a complication of finding the zero-quark-mass limit of the theory. Formulating this problem in terms of the hopping parameter, we define $\kappa_{\rm critical}$ ($\kappa_{\rm c}$) to be the point corresponding to the zero-quark-mass limit. At tree level, we have

$$\kappa_c = \frac{1}{8r}, \tag{2.30}$$

because of equation (2.28). However, this value changes significantly at one-loop, as the additive mass renormalisation constant receives a big correction at this order [26].

(c) It can be shown that, for the Wilson fermion action, chiral Ward identities are only satisfied with $\mathcal{O}(a)$ errors [27]. In the $\mathcal{O}(a)$ improved Wilson-type fermion actions, these errors can be reduced to $\mathcal{O}(\alpha_s^n a)$ or $\mathcal{O}(a^2)$. In the literature, one finds the terminology 'chiral limit of Wilson-type fermion actions'. Here we stress that this actually refers to the zero-quark-mass limit. There is no unambiguously-defined chiral limit in Wilson-type fermion actions at finite lattice spacing.

(d) There are other ways to avoid the fermion doubling problem and preserve chiral symmetry on the lattice, amongst which the most well-known ones are the staggered fermion action [28] and the domain-wall fermion action [29, 30]. The reason why we choose to use Wilson fermion action is simplicity and locality. The action and the operators are all local in Wilson's formalism[1].

(e) The Nielsen-Ninomiya theorem implies that one cannot discretise chiral fermions, hence cannot put the Standard Model directly on the lattice. This theorem can be proved by showing that the path-integral measure in Lattice QCD is invariant under the continuous-like chiral transformation, hence any lattice action which has a continuous-like chiral symmetry must be free of chiral anomaly, and this requires an opposite-chirality replica of each fermion field. There are new developments in this area [31, 32, 33], amongst which the most promising

[1]This is, however, not always true in the $\mathcal{O}(a)$-improved Wilson-type fermions.

actions are those which satisfy the Ginsparg-Wilson relation [34]. In these fermion actions, explicit chiral symmetry breaking is minimal, in the sense that its effects are localised at each lattice site, but sufficient to reproduce the chiral anomaly in the continuum limit. These actions are still far away from being used in practical calculations[2].

2.1.3 The Continuum Limit

The lattice regularises QCD with the cut-off a (lattice spacing). In order to simulate QCD in the continuum, we have to take the lattice spacing to zero. In the continuum limit ($a \to 0$), the correlation length

$$\xi = \frac{1}{m_{\mathrm{R}} a} \tag{2.31}$$

diverges, where m_{R} is the dimension-full renormalised mass. It can be shown that there is an ultra-violet fixed point $g(a) = 0$ along the line $m_{\mathrm{R}} a = 0$ in the parameter space $(g(a), m(a))$, while different values of the renormalised coupling constant g_{R} are allowed. Therefore, the continuum limit is formally reached as $\beta = 2N/g^2(a) \to \infty$.

2.1.4 Numerical Calculation in the Quenched Approximation

It is difficult to numerically simulate Grassmann variables directly. However, they can be integrated out analytically in Lattice QCD, provided the action is bilinear in the fermion fields. From

$$\int \prod_i d\bar{\psi}_i d\psi_i e^{-\bar{\psi}_j M_{jk} \psi_k} = \det M, \tag{2.32}$$

the vacuum expectation value of an operator $\mathcal{O}$ is

$$\langle \mathcal{O} \rangle = \frac{1}{Z} \int \mathcal{D}U \mathcal{O} \det M\,[U]\, e^{-S_{\mathrm{G}}[U]}. \tag{2.33}$$

[2]This is a rapidly developing field, therefore by the time this thesis is read, phenomenological calculations using these actions might already exist.

To perform the above functional integration, one can use a Monte Carlo simulation. The first step is to generate a set of gauge configurations

$$\{U_i\} \quad (i = 1, 2, \ldots, N_{\rm con}) \tag{2.34}$$

using a Markov process which samples the probability distribution

$$p(U)dU \sim \det M\,[U]\, e^{-S_{\rm G}[U]} dU. \tag{2.35}$$

Here $N_{\rm con}$ is the number of configurations. One then measures the operator $\mathcal{O}$ on these configurations to obtain a set of measurements $\{\mathcal{O}\,[U_i]\}$. In the limit of large $N_{\rm con}$, the average of these measurements is equal to the vacuum expectation value of the operator

$$\langle \mathcal{O} \rangle \sim \overline{\mathcal{O}} = \frac{1}{N_{\rm con}} \sum_{i=1}^{N_{\rm con}} \mathcal{O}\,[U_i]\,. \tag{2.36}$$

This means any Monte Carlo simulation contains a statistical error which decreases proportionally to $1/\sqrt{N_{\rm con}}$. Throughout this work, we estimate the statistical errors by using the bootstrap [35], a re-sampling technique.

The computation of the fermion matrix determinant in equation (2.33) is very expensive, and it has to be done in every update step in the Markov process. There are algorithms (*e.g.*, HMC [36]) which can generate the probability distribution in equation (2.35) in more efficient ways than the direct calculation of $\det M$. The common feature of these algorithms is that they all use auxiliary boson fields ϕ, ϕ^* and work in the configuration space (U, ϕ^*, ϕ). Because of the relation

$$\det M = \int \mathcal{D}\phi^* \mathcal{D}\phi \, \exp\left[- \int dx \phi^*(x) M^{-1} \phi(x) \right], \tag{2.37}$$

one can use a Markov process to sample the probability distribution

$$p\,(U, \phi^*, \phi)\, dU d\phi^* d\phi \sim \exp\left[S_{\rm G}\,[U] - \int dx \phi^*(x) M^{-1} \phi(x) \right] dU d\phi^* d\phi, \tag{2.38}$$

and this distribution will be effectively the same as the one in equation (2.35) when performing functional integral in the configuration space (U, ϕ^*, ϕ) using a Monte Carlo method. With this method, *one does not have to calculate the fermion matrix determinant directly.* However, when using these algorithms, one has to invert the fermion matrix, which is computationally expensive. Therefore most lattice calculations of weak matrix elements up to now have been performed in the *quenched approximation*, in which one sets $\det M$ to a constant. This approximation is equivalent to throwing away internal quark loops. It retains the two most important non-perturbative features of QCD, confinement and chiral symmetry breaking, although it does strongly distort physics in some cases. An example is that a resonance in quenched QCD is stable, as the internal quark loops are necessary to generate the width of the resonance. This is actually the reason why one can use the ρ-meson mass to set the lattice spacing in the quenched approximation, but not in dynamical-fermion calculation. Apart from these cases, many numerical results obtained by using this approximation agree quite well with experiments. This might be explained by the fact that lattice calculations give dimensionless results, therefore one has to rescale quantities by powers of lattice spacing, which is fixed using some physical quantity (*e.g.*, ρ-meson mass), to obtain results with correct dimensions. This rescaling procedure is equivalent to taking ratios between quantities, from which one expects cancellations of quenching errors.

Hadronic observables can be extracted from the mesonic or baryonic correlators which are constructed by the operators that carry the same quantum numbers as the process in question. They can be numerically calculated from proper manipulations of quark propagators $G_q(x, y)$ which are the inverse of the fermion matrix, obtained by solving

$$\sum_z \mathcal{M}(x, z) G_q(z, y) = \delta_{xy}. \tag{2.39}$$

This needs to be done on each gauge configuration U_i. It is important to use an efficient inversion algorithm here, since the fermion matrix $\mathcal{M}$ is large and highly non-local[3].

As a simple illustration, let's look at the mesonic two-point function

$$C(t; \vec{p}) = \sum_{\vec{x}} e^{-i\vec{p}\cdot\vec{x}} \langle A_4(\vec{x}, t) A_4^\dagger(0) \rangle, \tag{2.40}$$

where the Euclidean time $t > 0$ and A_4 is the fourth component of the Euclidean axial vector current $A_\mu = \bar{\psi}_1 \gamma_\mu \gamma_5 \psi_2$. After Wick contraction and the use of the

[3]This means the linear equations described by equation (2.39) are strongly coupled.

relation $G_q(x,0) = \gamma_5 G_q^\dagger(0,x)\gamma_5$, this correlator can be written as

$$C(t;\vec{p}) = \sum_{\vec{x}} e^{-i\vec{p}\cdot\vec{x}} \left\langle \mathrm{Tr}\left\{\gamma_4 G_2(0,x)\gamma_4 G_1^\dagger(0,x)\right\}\right\rangle . \tag{2.41}$$

By inserting a complete set of pseudo-scalar-meson energy eigenstates as intermediate states in equation (2.40) and using the translational invariance of the vacuum, the correlator is now

$$C(t;\vec{p}) = \sum_n \frac{|\langle 0|A_4(0)|n;\vec{p}\rangle|^2}{2E_n(\vec{p})} e^{-E_n(\vec{p})t}. \tag{2.42}$$

In the limit of large Euclidean time t, the ground state dominates, hence the above correlator (in the case $\vec{p}=0$) can be written as

$$C(t;0) \longrightarrow \frac{|\langle 0|A_4(0)|P\rangle|^2}{2M_P} e^{-M_P t}, \tag{2.43}$$

where $|P\rangle$ is the one-particle state and M_P is its mass. One can then take the correlator obtained from equation (2.41) and fit it with the function in equation (2.43) to extract $|\langle 0|A_4|P\rangle|$ and M_P.

The operators and the ground state in a hadronic correlator are not guaranteed to have a large enough overlap such that one can obtain a reasonable signal-to-noise ratio. This problem is more serious in heavy-quark systems. For instance, with a large meson mass, the correlator in equation (2.43) falls off exponentially very rapidly such that it might be 'buried' in the statistical noise before t is large enough to reach the ground-state-dominated region. Numerical techniques have been proposed to solve this problem by 'smearing' the operators, that is, by using operators with spatial extent instead of local ones [37]. In this work, we use fuzzed operators [38].

2.1.5 Discretisation Errors and $\mathcal{O}(a)$ Improvement

The Wilson fermion action has discretisation errors of $\mathcal{O}(a)$, while the gauge action has discretisation errors of $\mathcal{O}(a^2)$. This means, if one uses the Wilson fermion action,

1. simulation results have a strong dependence on the lattice spacing, therefore it is difficult to control the continuum extrapolation.

2. chiral Ward identities are violated at $\mathcal{O}(a)$ [27]. Therefore one expects to have large systematic errors when calculating quantities which are sensitive to chiral symmetry breaking, *e.g.*, the parameter B_K.

3. the error $\mathcal{O}(am_q)$, where m_q is the quark mass, is very large in the simulation of a heavy-quark system. This in turn makes the extrapolations in the heavy-quark masses unreliable. Note that one always wants $am_q < 1$ in the simulation so that the systematic errors $\mathcal{O}(a^n m_q^n)$ are under control.

Therefore $\mathcal{O}(a)$ improvement of the Wilson fermion action is strongly motivated.

Symanzik's programme [39, 40] provides a systematic way of understanding the improvement of lattice actions and operators. The most important idea of this programme is that in the vicinity of the continuum limit, with energy well below the cut-off $1/a$, Lattice QCD can be realised as a *local effective field theory* with the action

$$S_{\text{eff}} = S_0 + aS_1 + a^2 S_2 + \dots \tag{2.44}$$

where S_0 is just *the continuum QCD action.* Other terms are interpreted as (higher-dimensional) operator insertions *in the continuum theory* to define the effective theory. They are of the form

$$S_k = \int d^4x \mathcal{L}_k, \text{ with } k \geq 1, \tag{2.45}$$

where $\mathcal{L}_k$ are linear combinations of $k+4$ dimensional local composite operators. This realisation enables one to understand $\mathcal{O}(a)$ improvement in the framework of effective field theory [41, 42], with the continuum theory and the lattice theory identified as the 'full theory' and the 'local effective theory' respectively, *c.f.*, OPE and effective weak Hamiltonian discussed in Chapter 1. Similarly, in the local effective theory, any lattice operator can be represented by a local effective operator

$$\mathcal{O}_{\text{eff}} = \mathcal{O}_0 + a\mathcal{O}_1 + a^2\mathcal{O}_2 + \dots, \tag{2.46}$$

where $\mathcal{O}_0$ is the operator in the full theory. $\mathcal{O}_k$, with $k \geq 1$, are linear combinations of $(k + \dim[\mathcal{O}_0])$-dimensional operators. The coefficients in front of the operators, which appear in the linear combinations in forming $\mathcal{L}_k$ and $\mathcal{O}_k$, are not *a priori* known but might be calculated order by order in g.

When calculating the expectation value of $\mathcal{O}_{\text{eff}}$, there are two sources for $\mathcal{O}(a)$ operator insertions, $\mathcal{L}_1$ and $\mathcal{O}_1$. The idea of $\mathcal{O}(a)$ improvement is to add counter terms which cancel these operator insertions. For the QCD action, one can write down five dimension-five operators [40]. However, two of them amount to a renormalisation of the bare coupling constant and quark mass, and can therefore be dropped. When looking at on-shell quantities with external points well-separated, one can use classical equations of motion of the fields to eliminate two other operators. In the end, there is only one operator left, the Sheikholeslami-Wohlert term

$$c_{\text{SW}} \int d^4x \bar{\psi}(x) \frac{i}{4} \sigma_{\mu\nu} F^{\mu\nu}(x) \psi(x), \tag{2.47}$$

which was first obtained by Sheikholeslami and Wohlert [43]. A popular lattice representation of the Yang-Mills field tensor $F^{\mu\nu}(x)$ is the 'clover leaf', which is why this operator is sometimes called the 'clover term'. In Lattice QCD, the Sheikholeslami-Wohlert action (clover action) is formed by adding this clover term to the Wilson fermion action. To improve composite operators, one uses a similar procedure with symmetry constraints on the operators.

The coefficients in front of the counter term operators in this improvement programme can be calculated perturbatively to a certain order α_s^n by requiring that all $\mathcal{O}(a\alpha_s^m)$ $(m \leq n)$ discretisation errors are cancelled. They can also be non-perturbatively determined such that there is no $\mathcal{O}(a\alpha_s^m)$ $(\forall m)$ error left [40].

When using the clover action in a lattice calculation, interesting four-quark operators mix with operators of lower dimension or operators of the same dimension but different chirality. (We will come back to this issue in the next subsection). Taking into account operator mixing with higher-dimension operators is a very complicated task in this case. Fortunately, these four-quark operators are already tree-level improved if the tree-level clover action, in which $c_{\text{SW}} = 1$, is used. This is why tree-level improvement is frequently used in the calculation of these four-quark operators, although it only removes the $\mathcal{O}(a)$ error.

An important issue in $\mathcal{O}(a)$ improvement is the choice of renormalisation scheme. In order to solve the RGE in a simple way, one usually favours mass-independent schemes. However, $\mathcal{O}(a)$ improvement is not *a priori* compatible with a mass-independent scheme. That is, the perturbative expansions for the quark mass, gauge coupling and composite operators contain terms proportional to $am_q\alpha_s^n$, where m_q is the quark mass. One way to avoid this problem is to modify the bare quantities by

$$\tilde{g}_0^2 = (1 + b_g a m_q) g_0^2, \tag{2.48}$$

$$\tilde{m}_q = (1 + b_m a m_q) m_q, \tag{2.49}$$

$$\tilde{\mathcal{O}} = (1 + b_{\mathcal{O}} a m_q) \mathcal{O}. \tag{2.50}$$

b_g, b_m and $b_{\mathcal{O}}$ should be chosen so as to cancel the remaining cut-off effects properly. Again, they can be calculated perturbatively to a certain order α_s^n by requiring that all the remaining $\mathcal{O}(am_q\alpha_s^k)$ $(k \leq n)$ discretisation errors arising from choosing a mass-independent scheme are cancelled.

A similar way of understanding equation (2.50) is through the 'quark-field rotation' [44]. In this prescription, tree-level improvement requires a rotation of the quark field through

$$\psi \to \left(1 + \frac{1}{2} a m_q\right) \psi. \tag{2.51}$$

At tree level, the $\mathcal{O}(a)$ term which makes the Wilson fermion action different from the continuum fermion action can easily be eliminated by adding an operator to the Wilson fermion action. This operator contains next-to-nearest neighbour interactions, so does the resultant action. However, this next-to-nearest neighbour action can be made to contain only nearest neighbour terms by performing the transformation

$$\psi \to \left(1 + a\frac{r}{4} m\right) \left(1 - a\frac{r}{4} \not{D}\right) \psi, \tag{2.52}$$

$$\bar{\psi} \to \left(1 + a\frac{r}{4} m\right) \bar{\psi} \left(1 - a\frac{r}{4} \overleftarrow{\not{D}}\right). \tag{2.53}$$

The resultant action is the tree-level clover action. If we are looking at on-shell quantities with external points well separated, then the $\not{D}$ in equations (2.52) and (2.53) can be replaced by $-m$, using equations of motion. Hence they are equivalent to the transformation in equation (2.51) in this case.

To end this subsection, we address the point that it is difficult to control the discretisation errors of the form $a^n m_q^n$ in heavy-quark systems. A conventional method is to perform simulations in the charm-mass region then use Heavy Quark

Effective Theory to scale the matrix elements to the beauty-mass region. Based on an observation of the free-fermion propagator in Wilson fermion action, the authors of reference [45] propose to normalise the quark field by

$$\psi \to \sqrt{2\kappa}e^{am_1/2}\psi, \tag{2.54}$$

instead of using equation (2.51). Here m_1 is the pole mass of the quark, and is related to the bare quark mass m_0 in the Wilson fermion action by

$$am_1 = \ln(1 + am_0). \tag{2.55}$$

Evidence shows this normalisation (called the KLM normalisation) reduces discretisation errors in Lattice QCD calculation of heavy-quark systems.

2.1.6 Operator Matching

Let's recall the separation of short- and long-distance physics discussed in Chapter one. What Lattice QCD does is to provide a regularisation such that the operators, which contain long-distance QCD effects, can be calculated non-perturbatively. However, lattice operators are defined with a cut-off a, while the Wilson coefficients are usually perturbatively calculated in a continuum renormalisation scheme, *e.g.*, the NDR$-\overline{\mathrm{MS}}$ scheme. Therefore, the lattice operators have to be related to the operators in the same continuum scheme in which Wilson coefficients are calculated. Generically, one wants to establish the relation

$$\mathcal{O}_i^{\mathrm{cont}}(\mu) = Z_{ij}(\mu a, g)\mathcal{O}_j^{\mathrm{latt}}(a), \tag{2.56}$$

where μ is the renormalisation scale, and g is the strong coupling constant. i and j label the operator type, and mark the possibility of operator mixing. In addition to the operator mixing from colour exchange in perturbative QCD calculation, which happens in any regularisation, there might be extra operator mixing (with same or lower dimensional operators) on the lattice. In the following discussion, we focus on the Wilson-type fermions (including clover fermions) on the lattice.

All quark bilinears composed of quark fields at the same lattice site require renormalisation on the lattice with Wilson-type fermions, as none of them are symmetry currents. They can be multiplicatively renormalised [27, 46]. The vector and axial-vector currents do not depend on the renormalisation scale after being matched to the continuum scheme, in which they are symmetry currents.

Four-quark operators are more complicated, and they are all divergent. For simplicity, consider a four-fermion operator $\mathcal{O}$ which can be multiplicatively renormalised in a continuum scheme. The matching between the lattice and the continuum scheme is of the form

$$\mathcal{O}^{\rm cont} = Z\left(\mathcal{O}^{\rm latt} + Z_i'\mathcal{O}_i^{\rm latt}\right) + Z_i^{\rm low}\mathcal{O}_{i\rm low}^{\rm latt}, \tag{2.57}$$

where the 'diagonal operator' $\mathcal{O}^{\rm latt}$ has the same structure as $\mathcal{O}^{\rm cont}$, but is 'contaminated' by explicit chiral symmetry breaking so its matrix elements will not have the same chiral behaviour as the matrix elements of $\mathcal{O}^{\rm cont}$. The 'off-diagonal' operators in equation (2.57) fall into two categories:

1. $\mathcal{O}_{i\rm low}^{\rm latt}$ are lower dimensional operators which mix with $\mathcal{O}^{\rm latt}$ through some penguin contractions. The mixing with these operators is difficult to control, as the mixing coefficients $Z_i^{\rm low}$ asymptotically scale like the inverse powers of a; hence the renormalised operator $\mathcal{O}^{\rm cont}$ is obtained by subtracting a divergent quantity from $\mathcal{O}^{\rm latt}$, which is also divergent, when a approaches zero. In the weak-interaction processes examined in this work, there is no such operator mixing, so we will not discuss this any further.

2. $\mathcal{O}_i^{\rm latt}$ are of the same dimension as $\mathcal{O}^{\rm latt}$ but have different chirality. They mix with $\mathcal{O}^{\rm latt}$ as a consequence of explicit chiral symmetry breaking on the lattice. Hence this mixing is sometimes called 'chiral subtraction', as the coefficients Z_i' are tuned so that the matrix elements of $\mathcal{O}^{\rm latt} + Z_i'\mathcal{O}_i^{\rm latt}$ have more 'continuum-like' chiral behaviour.

There are non-perturbative methods to determine these renormalisation constants (matching coefficients) [47]. In this work, however, we only use renormalisation constants calculated from one-loop perturbation theory, as their non-perturbative determination for the action we use has not been done yet. This inevitably introduces systematic errors due to the truncation of perturbation series.

Perturbatively, up to one-loop level, the coefficients Z and Z'_i in equation (2.57) have the form

$$Z = 1 + \frac{\alpha_s}{4\pi}(\gamma^{(0)}\ln(\mu a) + d), \tag{2.58}$$

$$Z'_i = r^2 Z^*(r, g), \tag{2.59}$$

where $\gamma^{(0)}$ is the one-loop anomalous dimension and r is the same parameter in the Wilson fermion action (equation (2.26)). These coefficients have features which deserve some further discussion:

1. Schematically, $\mathcal{O}_i^{\rm latt}$ mix with $\mathcal{O}^{\rm latt}$ because a term in the quark propagator can violate chiral symmetry in loop diagrams. Therefore Z'_i are of $\mathcal{O}(\alpha_s)$.

2. From the universality of the one-loop anomalous dimension, $\mathcal{O}^{\rm cont}$ and $\mathcal{O}^{\rm latt}$ have the same anomalous dimension at one loop, which is $\gamma^{(0)}$ in equation (2.58). This means Z'_i do not depend upon $\ln(\mu a)$ at this order.

3. Obviously, Z'_i vanish in the limit $r = 0$, where chiral symmetry is restored.

4. The scheme-dependent term d [4] in the renormalisation constant Z might be cancelled by tuning the scale μ. However, in some cases, d is so large that to completely absorb it would result in a very big scale variation, which could make $\ln(\mu a)$ numerically large such that even higher-order logarithms, which we have not had a systematic way to deal with, contribute significantly. In practice, one performs one-loop operator matching at the matching scale $\mu \sim \mathcal{O}(1/a)$, such that $\ln(\mu a)$ in equation (2.58) is small.

5. An issue in performing operator matching using perturbation theory is the choice of expansion parameter. It turns out that the bare lattice coupling $\alpha_s^{\rm latt}$ gives poor convergence of the series. Lepage and Mackenzie [48] have shown that a renormalised coupling constant, at some optimal scale depending upon the operator in question, is a better choice. However, here we stress that *the systematic error arising from the truncation of the perturbation series has to be analysed no matter which coupling constant is used.*

[4]Note that this term is actually a next-leading logarithm.

2.1.7 Mean-Field (Tadpole) Improvement

An important origin of lattice artifacts is from the expansion of the link variable with respect to the strong coupling constant

$$U_\mu(x) = e^{iagA_\mu(x)} \to 1 + iagA_\mu(x). \tag{2.60}$$

The 'tadpole-diagram' contributions at higher orders in this expansion generate power divergences in $1/a$, which cancel the powers of a in the expansion. Lepage and Mackenzie [48] propose that a better expansion should be

$$U_\mu(x) \approx u_0 \left(1 + iagA_\mu(x)\right), \tag{2.61}$$

where u_0 is the mean value of U_μ and is meant to absorb most of the tadpole contributions. A gauge-invariant definition of u_0 is through the mean value of the plaquette variable

$$u_0 = \left\langle \frac{1}{3}\mathrm{Tr}U_p \right\rangle^{\frac{1}{4}}. \tag{2.62}$$

The central idea of the mean-field improvement prescription is to replace U_μ with U_μ/u_0 everywhere in the action and in operators when performing perturbative calculations. As can easily be seen from equation (2.21), with the Wilson gauge actions, this prescription is implemented through

$$g^2_{\mathrm{latt}} = \bar{g}^2 u_0^4, \tag{2.63}$$

and expanding in $\bar{g}$ instead of g. From equation (2.27), this prescription is implemented via

$$\kappa = \frac{\bar{\kappa}}{u_0}, \tag{2.64}$$

and using $\bar{\kappa}$, instead of κ, in the quark-field normalisation. For the clover action, one also has to replace c_{SW} by c_{SW}/u_0^3, which has to be done at the simulation time. This implemention also means that $\bar{g}$ should be a better expansion parameter than g_{latt} when performing lattice perturbation theory.

By using the mean-field improvement prescription, the large lattice artifacts from the contribution of tadpole diagrams can be reduced. Therefore, one expects the lattice theory should be more continuum-like. Evidence shows this is true. Some classical examples are:

1. The renormalisation constant (matching coefficient) for the lattice axial-vector current, Z_A, is closer to unity in this prescription.

2. In this prescription, the tree-level κ_c, which is $1/8u_0$ when $r = 1$, is closer to the non-perturbatively measured κ_c^{NP} (usually measured by PCAC relation).

In subsection 2.1.5, we have addressed the difficulty in going beyond tree-level $\mathcal{O}(a)$ improvement in the calculation of four-quark operator matrix elements. The mean-field improved clover action, in which $c_{\mathrm{SW}} = 1/u_0^3$, is a convenient way of achieving this goal, as it removes the tadpole contributions which are higher-order in α_s. However, here we stress that this prescription can *formally* control the discretisation error only at the same order as the tree-level clover action, *i.e.*, at $\mathcal{O}(a)$. Therefore, *formally* one does not have to take into account the operator mixing with higher-dimensional operators when using this prescription in lattice calculation.

2.2 Heavy Quark Symmetry

As mentioned in subsection 2.1.5, the $\mathcal{O}(a^n m_q^n)$ discretisation errors forbid direct application of Lattice QCD in the beauty-mass region, because a^{-1} is typically between two and three GeV in current lattice calculations. However, one can simulate heavy quark systems in the charm-mass region and scale the matrix elements to the beauty-mass region using Heavy-Quark-Effective-Theory inspired scaling relations.

Quarks in the Standard Model fall into two categories, heavy and light, according to the criterium that heavy quarks and light quarks have masses much larger and smaller than $\Lambda_{\mathrm{QCD}} \sim 200\mathrm{MeV}$ respectively. There are two features which might make the strong interactions involving heavy quarks simpler:

1. The heavy quark mass serves as a hard scale for performing an OPE.

2. The strong coupling at the heavy-quark-mass scale is small enough such that perturbation theory works for QCD.

As we shall see later in this section, these do help in simplifying strong-interaction effects in heavy-quark systems.

Consider a hadronic system containing a heavy quark and some light quarks. The typical momenta exchanged between the heavy and light quarks are of $\mathcal{O}(\Lambda_{\rm QCD})$. The Compton wavelength of the heavy quark, λ_Q, is much smaller than the hadronic size, $R_h \sim 1/\Lambda_{\rm QCD}$. Therefore, the soft gluons exchanged between the heavy and light quarks cannot resolve the quantum numbers of the heavy quark. This means the light degrees of freedom cannot 'feel' the flavour and the spin of the heavy quark in the limit $m_Q \to \infty$. m_Q is the heavy-quark mass. In this limit, there is a symmetry $SU(2N_f^Q)$, where N_f^Q is the number of heavy flavours. This Heavy Quark Symmetry has the properties:

1. It is not a symmetry of the QCD Lagrangian, but rather a symmetry of a low-energy effective theory of QCD which involves heavy quarks.
2. It does not tell us how to probe the light degrees of freedom in such a system, which is the difficult part. However, it does provide relations between the properties of heavy hadrons, like B and D mesons. These relations should be model-independent as they are derived from QCD in a well-defined kinematic limit.

The symmetry-breaking corrections to the Heavy Quark Symmetry can be systematically studied in the framework of Heavy Quark Effective Theory.

2.2.1 Heavy Quark Effective Theory

Using the techniques discussed in section 1.2, it is not difficult to obtain a low-energy effective theory describing strong interaction involving heavy quarks. The underlying idea is the same — integrating out the heavy degrees of freedom.

Consider a heavy-light meson. We want to build a low-energy effective theory to describe this system, in which the heavy quark is almost on-shell and acts as a static colour source in the meson rest frame since the momentum exchange of $\mathcal{O}(\Lambda_{\rm QCD})$ only changes the heavy-quark momentum by a negligible amount. According to this physical picture, we can write the heavy-quark momentum as

$$p_Q^\mu = m_Q v^\mu + k^\mu, \tag{2.65}$$

where v^μ is the *hadron* four-velocity and k^μ is the (off-shell) residual momentum. Since the meson is on-shell, we have $v^2 = 1$. In order to implement this physical picture, we can first factor out a phase $\exp(-im_Q v \cdot x)$ from the heavy-quark spinor Q

$$Q = \mathrm{e}^{-im_Q v\cdot x} Q_v, \tag{2.66}$$

such that the four-derivative acting upon Q_v in momentum space only produces the residual momentum k^μ. In constructing a low-energy effective theory which can describe this physical picture in the limit $m_Q \to \infty$, what we are integrating out is not the heavy quark. Rather, in the low-energy limit, we want to integrate out the heavy degrees of freedom such that pair creation cannot happen, as it takes $2m_Q$ to create a quark-antiquark pair. Consider the decomposition of Q_v

$$\begin{aligned} Q_v &= h_v + H_v, && (2.67)\\ h_v &= P_+ Q_v, && (2.68)\\ H_v &= P_- Q_v, && (2.69) \end{aligned}$$

where $P_\pm = (1 \pm \not{v})/2$ are projectors for positive and negative energy states. h_v is the big component of Q_v and annihilates a heavy quark with velocity v_μ, while H_v is the small component of Q_v and creates a heavy antiquark with the same velocity. If we express the heavy-quark sector of the QCD Lagrangian in terms of h_v and H_v, we find

$$\begin{aligned} \mathcal{L}^{(Q)}_{\rm QCD} &= \bar{h}_v i\,(v\cdot D)\,h_v - \bar{H}_v i\,(v\cdot D + 2m_Q)\,H_v, \\ &+ \bar{h}_v i\not{D}_\perp H_v + \bar{H}_v i\not{D}_\perp h_v, && (2.70) \end{aligned}$$

where $D_\perp^\mu = D^\mu - v^\mu\,(v\cdot D)$. We observe:

1. h_v is massless and H_v has a mass $2m_Q$.
2. the third and the fourth terms in the above expression account for the interaction between h_v and H_v, and are responsible for creating quark-antiquark pairs.

We lose the symmetry between particle and anti-particle in equation (2.70). However, this expression 'factors out' the phenomena (pair creation) we want to 'integrate out'. The fact that h_v is massless and H_v has a mass $2m_Q$ is just a shift of the zero energy.

So it is clear that we want to integrate out H_v to construct the effective theory, which is described by the Lagrangian

$$\mathcal{L}_{\mathrm{HQET}} = \bar{h}_v i\,(v \cdot D)\,h_v + \frac{1}{2m_Q}\bar{h}_v\,(i\not{D}_\perp)^2\,h_v + \frac{g}{4m_Q}\bar{h}_v \sigma_{\mu\nu} G^{\mu\nu} h_v + \mathcal{O}\left(\frac{1}{m_Q^2}\right), \quad (2.71)$$

where $gG^{\mu\nu} = -i\,[D_\mu, D_\nu]$. There are some interesting features of this effective theory

1. The leading term in $\mathcal{L}_{\mathrm{HQET}}$ does not depend upon the heavy-quark spin and mass, as it has an exact $SU(2N_f^Q)$ symmetry. The Heavy Quark Symmetry breaking effects are systematically dealt with in the $(1/m_Q)^n$ terms. The operator $\bar{h}_v \sigma_{\mu\nu} G^{\mu\nu} h_v$ is the colour magnetic term which then implements the dependence upon heavy-quark spin at $\mathcal{O}\,(1/m_Q)$.

2. As mentioned above, we lose quark-antiquark symmetry in the Heavy Quark Effective Theory. However, heavy antiquarks can be treated by the same procedure and included in the Lagrangian.

There are problems in choosing the expansion parameter in HQET, *i.e.*, the parameter m_Q has some ambiguities. These ambiguities can be shown not to affect physical results if other non-perturbative parameters in the theory are defined carefully [49, 50, 51, 52, 53]. However, in a lattice calculation, we can use the meson mass, which is well-defined in principle and is close to the heavy-quark mass, as the expansion parameter. This corresponds to a simple re-organisation of the expansion, and the procedure becomes free of these ambiguities.

2.2.2 The Scaling of Matrix Elements

We can use HQET to investigate the scaling property of matrix elements with respect to heavy-quark masses. The idea is, again, from the OPE introduced in section 1.2. We start by expressing the full heavy-quark spinor Q in terms of h_v. At tree level, we can use the classical QCD equation of motion for Q

$$(i\not{D} - m_Q)\, Q = 0. \tag{2.72}$$

Express this equation in terms of h_v and H_v, we find

$$H_v = \frac{1}{(iv \cdot D + 2m_Q - i\epsilon)} i\not{D}_\perp h_v, \tag{2.73}$$

which allows us to derive a $1/m_Q$ expansion for Q

$$Q = \mathrm{e}^{-im_Q v\cdot x} \left(1 + \frac{i\not{D}_\perp}{2m_Q} + \dots\right) h_v. \tag{2.74}$$

This expansion is used to construct the HQET operators at tree level. Note here 'tree level' is in the sense of hard-gluon exchanges. As an illustration, let's consider the axial-vector current $A_\mu = \bar{q}\gamma_\mu\gamma_5 Q$ composed of a light quark (q) and a heavy quark. In HQET, this current is represented as

$$\begin{aligned} A_\mu &= \mathrm{e}^{-im_Q v\cdot x} \bar{q}\gamma_\mu \left(1 + \frac{i\not{D}_\perp}{2m_Q} + \dots\right) h_v, \\ &\equiv \mathrm{e}^{-im_Q v\cdot x} A_\mu^{\mathrm{HQET}}. \end{aligned} \tag{2.75}$$

As for the external hadronic states, it is more convenient to use a mass-independent normalisation through the redefinition

$$|H(v)\rangle = \frac{1}{\sqrt{M_H}} |H(p)\rangle, \tag{2.76}$$

such that

$$\langle H(v')|H(v)\rangle = 2v^0 (2\pi)^3 \delta^3(\vec{p} - \vec{p}'). \tag{2.77}$$

We can then obtain the tree-level scaling properties for hadronic weak matrix elements. There are two sources of $1/m_Q$ corrections to matrix elements. One is from the corrections to the operators, as equation (2.75) shows. The other one is from the corrections in the HQET Lagrangian in equation (2.71), *i.e.*, corrections to the relation between heavy meson states in full QCD and those in HQET. For instance, at tree level,

$$\frac{\langle 0|A_0|P(\vec{p})\rangle}{\sqrt{M_P}} = \langle 0|A_0^{\mathrm{HQET}}|P(\vec{v})\rangle \sim a\left(1 + \frac{b}{M_P} + \frac{c}{M_P^2} + \dots\right), \tag{2.78}$$

where $|P\rangle$ is the pseudo-scalar-meson state and M_P is its mass. Here we use meson mass as the expansion parameter. From the above equation, we obtain the tree-level scaling law for the decay constant, f_P, of the pseudo-scalar meson

$$f_P\sqrt{M_P} \sim a\left(1 + \frac{b}{M_P} + \frac{c}{M_P^2} + \dots\right). \tag{2.79}$$

One can then perform the matching of QCD onto HQET using the idea introduced in section 1.2, which separates the short-distance and long-distance strong-interaction effects. Note that all quark bilinears require renormalisation in HQET, since the vector and axial-vector currents are not symmetry currents in this effective field theory. In this matching procedure, one takes into account the hard-qluon exchanges, and HQET operators also have logarithmic dependence upon heavy-quark masses beyond the tree level. Renormalisation Group techniques can be used to sum these logarithms when scaling the matrix elements between two heavy-quark masses.

2.3 Chiral Perturbation Theory

As mentioned in section 2.1, chiral symmetry is explicitly broken in Wilson-type fermions. This has the consequence

- There is an additive mass renormalisation.
- Lattice operators do not have the chiral behaviour of their continuum counterparts.

Chiral Perturbation Theory is heavily used in lattice calculations for the following reasons:

1. It offers a way to subtract the additive mass renormalisation (often represented by κ_c introduced in subsection 2.1.2) non-perturbatively.
2. In practice, it is very difficult to perform lattice simulations near the zero-quark-mass limit, as this requires a big lattice to accommodate the large

Compton wavelength of the very light particle, and the currently available fermion-matrix-inversion algorithms become inefficient when the light-quark mass is small. We therefore need ChPT to guide the extrapolation of matrix elements to the zero-quark-mass limit.

3. ChPT is a valid method to examine the chiral behaviour of matrix elements resulting from lattice calculations, and quantify systematic errors arising from the fact that lattice operators do not have the 'correct' chiral behaviour.

2.3.1 The Realisation of Chiral Symmetry in Strong Interactions

In the chiral limit, where u, d and s quarks are massless, the QCD Lagrangian has a global flavour symmetry $G = SU(3)_L \otimes SU(3)_R$ (We disregard the $U_A(1)$ anomaly for the time being, and baryon number $U_B(1)$ is not relevant in the present discussion). This means the Lagrangian is invariant under *independent* transformations of the left-handed and right-handed quarks (q_L and q_R) in flavour space

$$q_L \xrightarrow{G} g_L q_L, \tag{2.80}$$

$$q_R \xrightarrow{G} g_R q_R, \tag{2.81}$$

$$g_{L,R} \in SU(3)_{L,R}. \tag{2.82}$$

However, this chiral symmetry is not a symmetry of the light-hadron spectrum. Instead, what have been observed are:

1. there is no degenerate multiplets with opposite parity for hadrons in $SU(3)_V$ representations.

2. the octet of pseudo-scalar mesons is much lighter than all other hadronic states.

These strongly suggest that *the axial symmetry is spontaneously broken*, and the mesons in the pseudo-scalar octet are pseudo-scalar Goldstone bosons.

2.3.2 Constructing the Chiral Lagrangian

Chiral Perturbation Theory (ChPT) [54] is a low-energy effective field theory which describes the strong interaction between light hadrons with energy below the chiral-symmetry-breaking scale. It deals with hadrons, instead of quarks. Since we do not know how to directly (perturbatively) derive the hadronic interactions in this regime from QCD, due to confinement, we do not know how to match QCD onto ChPT. The techniques developed in section 1.2 do not apply in the chiral regime either, as there is no 'heavy scale' in this regime from which we can perform an OPE. These are the main reasons why strong interactions of light-quark systems are more difficult to understand than those of systems containing heavy quarks. However, we know the symmetry properties of the QCD Lagrangian in the chiral regime, and we know that any low-energy effective theory of QCD in this regime is constrained by these symmetry properties [41]. We can then parameterise the unknown QCD dynamics in a few parameters, which can be determined by comparison with experimental data, in the construction of ChPT.

Because of the mass gap between the pseudo-scalar octet and other hadrons, we can build a low-energy effective field theory containing only the pseudo-scalar Goldstone particles. This theory, as a valid effective theory of strong interactions in the chiral regime, should realise the chiral symmetry in the same way as described in the last subsection.

The dynamical variable is a unitary 3×3 field Σ. Under $SU(3)_L \otimes SU(3)_R$, it transforms as

$$\Sigma \rightarrow \Sigma' = L \Sigma R^\dagger, \tag{2.83}$$

where L (R) is an element of $SU(3_f)_{L(R)}$. The field Σ is written as

$$\Sigma = \exp\left[i \frac{\sqrt{2}}{f} \Phi \right], \tag{2.84}$$

where f is some constant which will be understood later, and Φ is constructed from the pseudo-scalar meson octet

$$\Phi = \frac{1}{\sqrt{2}}\phi_i T_i = \begin{pmatrix} \frac{1}{\sqrt{2}}\pi^0 + \frac{1}{\sqrt{6}}\eta & \pi^+ & K^+ \\ \pi^- & -\frac{1}{\sqrt{2}}\pi^0 + \frac{1}{\sqrt{6}}\eta & K^0 \\ K^- & \bar{K}^0 & -\frac{2}{\sqrt{6}}\eta \end{pmatrix}. \tag{2.85}$$

The effective Lagrangian $\mathcal{L}_{\text{eff}}$ is constructed from the dynamical variable Σ and is required to be invariant under the transformation in equation (2.84), and has a vacuum expectation value of the form

$$\langle\Sigma\rangle_{\text{VEV}} = \begin{pmatrix} 1 & 0 & 0 \\ 0 & 1 & 0 \\ 0 & 0 & 1 \end{pmatrix}, \tag{2.86}$$

which implements spontaneous chiral symmetry breaking. Since we are building up a low-energy effective theory, we expand $\mathcal{L}_{\text{eff}}$ in powers of four-momenta, *i.e.*, four-derivatives ∂^μ. Parity conservation requires an even number of derivatives in each term, so the lowest-order ($\mathcal{O}(p^2)$) non-trivial effective chiral Lagrangian is given by the term

$$\mathcal{L}_2 = \frac{f^2}{4}\text{Tr}\left(\partial_\mu\Sigma^\dagger\partial^\mu\Sigma\right). \tag{2.87}$$

However, as the low-energy effective theory of strong interaction, the chiral Lagrangian should explicitly break the chiral symmetry in the same way as the QCD Lagrangian does, *i.e.*, by any non-vanishing quark mass[5]. In this case, the lowest-order chiral Lagrangian is

$$\mathcal{L}_2 = \frac{f^2}{4}\text{Tr}\left(\partial_\mu\Sigma^\dagger\partial^\mu\Sigma\right) + v\,\text{Tr}\left(\mathcal{M}\Sigma + \Sigma^\dagger\mathcal{M}^\dagger\right), \tag{2.88}$$

where v is some unknown parameter, and $\mathcal{M}$ is the quark-mass matrix

$$\mathcal{M} = \begin{pmatrix} m_u & 0 & 0 \\ 0 & m_d & 0 \\ 0 & 0 & m_s \end{pmatrix}, \tag{2.89}$$

[5]A more complicated pattern of chiral symmetry breaking has been investigated by Knecht and Stern in [55]. This leads to a slightly different effective theory known as the Generalised Chiral Perturbation Theory.

This lowest-order chiral Lagrangian contains a lot of interesting information. By expanding Σ in powers of Φ, one obtains the relation between *quark masses* and *squared meson masses* [56]

$$M_{\pi^\pm}^2 = M_{\pi^0}^2 = \frac{4v}{f^2}(m_u + m_d), \tag{2.90}$$

$$M_\eta^2 = \frac{4v}{f^2}\left(\frac{m_u + m_d + 4m_s}{3}\right), \tag{2.91}$$

$$M_{K^\pm}^2 = \frac{4v}{f^2}(m_u + m_s), \tag{2.92}$$

$$M_{K^0}^2 = \frac{4v}{f^2}(m_d + m_s). \tag{2.93}$$

These relations tell us the term $v\mathrm{Tr}\left(\mathcal{M}\Sigma + \Sigma^\dagger\mathcal{M}^\dagger\right)$ is of $\mathcal{O}(p^2)$. The unknown parameters f and v can be identified as

$$f = f_\pi \approx 132\mathrm{MeV}, \tag{2.94}$$

$$-2v = \langle 0|\bar{u}u|0\rangle \text{ (chiral condensate)}, \tag{2.95}$$

in the lowest order.

One can perform loop calculations using the Lagrangian in equation (2.88) for interesting low-energy hadronic phenomenology. These loops from the $\mathcal{O}(p^2)$ chiral Lagrangian generate terms like $\frac{p^4 \ln(p^2/f^2)}{16\pi^2 f^4}$, which are called chiral logarithms and are of $\mathcal{O}(p^4)$. In addition, these loops also result in divergent terms which are of $\mathcal{O}(p^4)$. These divergences can be regularised by adding $\mathcal{O}(p^4)$ operators, whose coefficients can be determined by experiments, to the chiral Lagrangian[6]. There are ten such $\mathcal{O}(p^4)$ operators from the symmetry constraint. This is a general feature in the regularisation of ChPT, that higher-order couplings often depend upon the number of loops from the lower-order Lagrangian.

From the above discussion, we have seen two ingredients of the $\mathcal{O}(p^4)$ chiral Lagrangian

- One-loop graphs from the lowest-order Lagrangian.

[6] If a hard cut-off Λ is used to regularise the theory, there will be divergent terms proportional to Λ^4/f^4. However, these terms must vanish, since they imply the existence of a chirally invariant term constructed from Σ without derivatives and masses, in the chiral Lagrangian.

- The most general tree-level $\mathcal{O}(p^4)$ Lagrangian, $\mathcal{L}_4$, constrained by symmetry properties of the QCD Lagrangian.

We end this subsection by mentioning the third ingredient — the Wess-Zumino-Witten functional [57] which accounts for the chiral anomaly.

2.3.3 ChPT for Operators

The general strategy to deal with composite operators in ChPT consists of two steps [58]:

1. Construct the operator in each irreducible representation of $SU(3)_L \otimes SU(3)_R$ by a linear combination of all possible ChPT operators in that representation to a certain order in p. Again, the coefficients in this linear combination are not *a priori* known.

2. Up to the same order in p, express the operator in question by a linear combination of the irreducible operators constructed in the first step. This can be done using the standard trick of tensor decomposition.

We will leave the second step until we perform calculations for kaon mixing and decay in chapter 4

To classify a four-quark operator in a certain irreducible representation of $SU(3)_L \otimes SU(3)_R$, we label it by (a, b), where a is the $SU(3)_L$ and b is the $SU(3)_R$ irreducible representation for the operator. For instance, an operator labeled by (8,1) means it is '$SU(3)_L$ octet and $SU(3)_R$ singlet'. In ChPT, most interesting irreducible representations for four-quark operators have the generic forms

$$(8,1) \quad \rightarrow \quad \alpha \mathrm{Tr}\left(\lambda \partial^\mu \Sigma \partial_\mu \Sigma^\dagger\right) + \beta \mathrm{Tr}\left(\lambda \Sigma \mathcal{M} + \lambda \mathcal{M}^\dagger \Sigma^\dagger\right), \tag{2.96}$$

$$(27,1) \quad \rightarrow \quad \gamma T_{ij}^{kl} \left(\Sigma \partial^\mu \Sigma^\dagger\right)_{ik} \left(\Sigma \partial_\mu \Sigma^\dagger\right)_{jl}, \tag{2.97}$$

$$(8,8) \quad \rightarrow \quad \delta t_{ij}^{kl} \Sigma_{ik} \Sigma_{jl}^\dagger, \tag{2.98}$$

to the lowest order in which these operators scale non-trivially. α, β, γ and δ are unknown parameters to be determined by experimental data or lattice calculations. λ is the constant matrix which picks out the suitable octet components for the operator in question. T and t are tensors arising from tensor decomposition for the operators. Obviously, the values of their components depend upon the operators in question.

In lattice calculations for weak matrix elements in the chiral regime, relations such as those given in equations (2.96), (2.97) and (2.98) can guide the chiral extrapolation with respect to meson mass and recoil variable. For instance, when external mesonic states are on-shell and carry the same momentum, ChPT at $\mathcal{O}(p^2)$ predicts matrix elements for $(8,8)$ operators approach constants (equation (2.98)), while matrix elements for $(8,1)$ and $(27,1)$ operators approach zero in the chiral limit (equations (2.96) and (2.97)).

Chapter 3

B^0–$\bar{B}^0$ Mixing & Heavy-light Decay Constants

Being a FCNC process, B^0–$\bar{B}^0$ mixing system is a good testing ground for heavy-flavour physics and possible new physics beyond the Standard Model. In particular, the study of B^0–$\bar{B}^0$ oscillations allows a clean extraction of the magnitude of the poorly known CKM matrix element V_{td}. However, the accuracy of this determination is currently limited by the theoretical uncertainty in the calculation of the matrix element,

$$\begin{aligned}\mathcal{M}_{bd} &= \langle \bar{B}^0 | \mathcal{O}^{\Delta B=2}_{LL,d} | B^0 \rangle \\ &= \langle \bar{B}^0 | \bar{b}\gamma_\rho(1-\gamma_5)d\bar{b}\gamma^\rho(1-\gamma_5)d | B^0 \rangle \ . \end{aligned} \tag{3.1}$$

In this chapter, we review here the phenomenological analysis of this mixing process in detail, as many of the same ideas can be used in the kaon system, which will be discussed in the next chapter. We then present a high-statistics lattice calculation of matrix elements and ratios relevant for extracting $|V_{td}|$ from neutral B meson mixing. These include the matrix elements for B^0–$\bar{B}^0$ mixing and B^0_s–$\bar{B}^0_s$ mixing, the bag parameters associated with these matrix elements, the decay constants f_B and f_{B_s}, and the ratios amongst them.

There have been many lattice calculations of f_B and f_{B_s}. However, for the matrix elements of $B^0_{(s)}$–$\bar{B}^0_{(s)}$ mixing processes and their bag parameters, lattice calculations have only been done using propagating heavy quarks from the Wilson fermion action[1] [59, 60, 61, 62] or static heavy quarks [63, 64, 65]. As discussed in subsection 2.1.5, lattice calculations of these matrix elements and bag parameters using the Wilson fermion action have potentially large $\mathcal{O}(a^n m_q^n \alpha_s^k)$ systematic errors, as $B^0_{(s)}$–$\bar{B}^0_{(s)}$ mixing processes involve heavy quarks. Using static heavy quarks in lattice calculations avoids this problem, as the static theory[2] does not involve the mass of the heavy quark. However, lattice calculations for the matrix elements of four-quark operators using static heavy quarks contain big systematic errors arising from the operator matching between the lattice and the continuum scheme [66], as the one-loop corrections to the matching coefficients are large [67].

In this work, we use propagating heavy quarks from the mean-field improved clover action, which is the most-improved Wilson-type fermion action available in calculating matrix elements of four-quark operators so far (*c.f.*, the discussion in subsection 2.1.5). We perform lattice simulations at two small values of lattice spacing, corresponding to $\beta = 6.0$ and $\beta = 6.2$. Given the fact that discretisation errors play an important role in lattice calculations of heavy-quark systems, using the mean-field improved clover action is expected to significantly reduce the systematic errors. Combining this feature with the use of propagating heavy quarks, we can more reliably investigate the heavy-quark-mass scaling of $B^0_{(s)}$–$\bar{B}^0_{(s)}$ mixing matrix elements and their bag parameters. Decay constants for D_s and D mesons are also calculated in this work.

3.1 Phenomenology of B^0–$\bar{B}^0$ Mixing

In the Standard Model, neutral meson mixing can occur from the flavour mixing implemented via the CKM matrix. In this section, we first give a review of a purely phenomenological analysis of the B^0–$\bar{B}^0$ mixing process. We then show

[1]This is known as 'the conventional method' in the literature. In this method, lattice simulations are done at several heavy-quark masses. HQET is then used to scale the matrix elements to the physical B meson mass

[2]The static theory is the leading-order heavy quark effective theory in the mesonic rest frame.

how the Standard Model dynamics describes this process. After factorising out the matrix element which requires a non-perturbative calculation due to confinement of QCD, we discuss how to approximate this matrix element by vacuum saturation and how to parameterise it in terms of the bag parameter.

3.1.1 Phenomenological Description

In this subsection, we relate the strength of B^0–$\bar{B}^0$ oscillations to a quantity which can be measured in experiments. By looking at the time evolution, we can work out the mass eigenstates of this oscillation system, and the mass difference between these eigenstates. This mass difference is then experimentally measurable. In order to achieve this, we only have to resort to quantum mechanics.

The states $|B^0\rangle$ and $|\bar{B}^0\rangle$ are eigenstates of the strong interaction, but they are not eigenstates of the weak interaction, through which they can decay. Obviously, they are not CP eigenstates either. Here we choose the convention such that under the CP transformation

$$\mathrm{CP}|B^0\rangle = -|\bar{B}^0\rangle, \tag{3.2}$$

$$\mathrm{CP}|\bar{B}^0\rangle = -|B^0\rangle. \tag{3.3}$$

Under flavour mixing, the time evolution of the B^0–$\bar{B}^0$ system can be described by a 2×2 'effective Hamiltonian matrix' $\hat{H}$, which can be decomposed as

$$\hat{H} = \hat{M} - \frac{i}{2}\hat{\Gamma}, \tag{3.4}$$

where $\hat{M}$ and $\hat{\Gamma}$ are both Hermitian matrices with positive eigenvalues, so $\hat{M}$ accounts for the propagation part and $\hat{\Gamma}$ accounts for the decay part of the B^0–$\bar{B}^0$ oscillation system. If we write the B^0–$\bar{B}^0$ system as a two-component wave function

$$|\psi(t)\rangle = \begin{pmatrix} A(t) \\ B(t) \end{pmatrix} = A(t)|B^0\rangle + B(t)|\bar{B}^0\rangle, \tag{3.5}$$

then the time-evolution equation is

$$i\frac{d}{dt}|\psi(t)\rangle = \hat{H}|\psi(t)\rangle. \tag{3.6}$$

The diagonal elements of $\hat{H}$ should be equal, as required by CPT invariance of equation (3.6). Also, Hermiticity of $\hat{M}$ and $\hat{\Gamma}$ implies $M_{21} = M_{12}^*$ and $\Gamma_{21} = \Gamma_{12}^*$. Therefore, $\hat{H}$ has the general form

$$\hat{H} = \begin{pmatrix} h & p^2 \\ q^2 & h \end{pmatrix}, \tag{3.7}$$

where h, p^2 and q^2 are complex numbers. Note that the off-diagonal elements p^2 and q^2 serve as effective Hamiltonians for the transition from $\bar{B}^0$ to B^0 and the transition from B^0 to $\bar{B}^0$ respectively.

Diagonalising this matrix, we find that the eigenstates are

$$|B_{\mathrm{L,S}}\rangle = \frac{1}{\sqrt{|p|^2 + |q|^2}} \left[p|B^0\rangle \pm q|\bar{B}^0\rangle \right]. \tag{3.8}$$

From equation (3.2) and (3.3), $|B_{\mathrm{L,S}}\rangle$ will be CP eigenstates if $p = q$. This condition, together with Hermiticity of $\hat{M}$ and $\hat{\Gamma}$, implies that M_{12} and Γ_{12} are real if there is no CP violation through $B^0-\bar{B}^0$ oscillation. This means

$$\frac{1+\bar{\epsilon}}{1-\bar{\epsilon}} \equiv \frac{p}{q} = \sqrt{\frac{M_{12} - \frac{i}{2}\Gamma_{12}}{M_{12}^* - \frac{i}{2}\Gamma_{12}^*}} = 1, \tag{3.9}$$

which then tells us

$$\langle B^0|\mathcal{H}_{\mathrm{eff}}|\bar{B}^0\rangle \sim M_{12} - \frac{i}{2}\Gamma_{12} = M_{21} - \frac{i}{2}\Gamma_{21} \sim \langle \bar{B}^0|\mathcal{H}_{\mathrm{eff}}|B^0\rangle, \tag{3.10}$$

where $\mathcal{H}_{\mathrm{eff}}$ is a low-energy effective Hamiltonian for this process.

In the real world, however, it might be the case that $p \neq q$. Therefore M_{12} and Γ_{12} are not real, and CP violation can occur[3]. As we will see in the next subsection, the dominant Standard-Model contributions to $B^0-\bar{B}^0$ oscillations are the box diagrams involving top quarks in the loops. Therefore, one can show, by using perturbative calculations in scattering theory and complex analysis, that it is reasonable to assume

$$\frac{\mathrm{Im}M_{12}}{\mathrm{Re}M_{12}} \ll 1, \tag{3.11}$$

$$\frac{\mathrm{Im}\Gamma_{12}}{\mathrm{Re}\Gamma_{12}} \ll 1. \tag{3.12}$$

[3]Here we stress that neutral meson mixing does not necessarily mean that there will be CP violation, but it does provide interfering amplitudes that can cause CP violation.

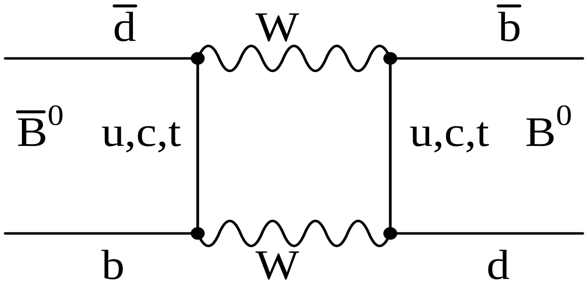

Figure 3.1: One of the Standard Model $\Delta B = 2$ box diagrams for B^0–$\bar{B}^0$ mixing.

The eigenvalues of $\hat{H}$ are non-degenerate, and their difference is

$$\begin{aligned} \Delta h &= (m_L - m_S) - \frac{i}{2}(\Gamma_L - \Gamma_S) \\ &= \Delta m - \frac{i}{2}\Delta\gamma \simeq 2\mathrm{Re}M_{12} - i\mathrm{Re}\Gamma_{12}, \end{aligned} \tag{3.13}$$

where we have used the assumption in equations (3.11) and (3.12). Δm and $\Delta\gamma$ can be experimentally measured from the time development of a neutral B meson state which is produced via a strong-interaction process, and therefore starts as either a pure B^0 or $\bar{B}^0$ at $t = 0$. On the other hand, they can be theoretically calculated because M_{12} and Γ_{12} account for the effective Hamiltonian $\mathcal{H}_{\mathrm{eff}}$ of B^0–$\bar{B}^0$ mixing

$$M_{B^0}\sqrt{(2\mathrm{Re}M_{12})^2 + (\mathrm{Re}\Gamma_{12})^2} = |\langle \bar{B}^0|\mathcal{H}_{\mathrm{eff}}|B^0\rangle|, \tag{3.14}$$

where M_{B^0} is the B^0 meson mass, and it appears due to the normalisation of pseudo-scalar meson states.

3.1.2 B^0–$\bar{B}^0$ Mixing via the $\Delta B = 2$ Box Diagram

In this subsection, we discuss $\mathcal{H}_{\mathrm{eff}}$, which appears in equation (3.14), in the absence of QCD. QCD effects will be discussed in the next two subsections.

In the framework of the Standard Model, the dominant short-distance electroweak contribution to the B^0–$\bar{B}^0$ mixing comes from the $\Delta B = 2$ box diagram shown in figure 3.1. Disregarding QCD effects, we can perform the OPE in the pure electroweak sector and write the effective Hamiltonian of this $\Delta B = 2$ process as (keeping the leading local operator)

$$\mathcal{H}_{\text{eff},d}^{\Delta B=2} = \frac{G_F^2}{16\pi^2} M_W^2 \sum_{i,j} (V_{ib}V_{id}^*)(V_{jb}V_{jd}^*) S_0\left(x_i, x_j\right) \mathcal{O}_{LL,d}^{\Delta B=2}, \tag{3.15}$$

where $x_i = m_i^2/M_W^2$ and $i = u, c, t$. The left-left four-quark operator is

$$\mathcal{O}_{LL,d}^{\Delta B=2} = \left[\bar{b}\gamma_\mu(1-\gamma_5)d\right]\left[\bar{b}\gamma^\mu(1-\gamma_5)d\right]. \tag{3.16}$$

$S_0(x_i, x_j)$ is the relevant Inami-Lim function [16] which can be written as

$$S_0(x_i, x_j) = \left(1 + \frac{1}{4}x_i x_j\right) A_0(x_i, x_j) - 2x_i x_j B_0(x_i, x_j), \tag{3.17}$$

where

$$A_0(x_i, x_j) = \frac{1}{(1-x_i)(1-x_j)} + \left[\frac{x_i^2 \ln x_i}{(x_i - x_j)(1-x_i)^2} + (i \leftrightarrow j)\right], \tag{3.18}$$

$$B_0(x_i, x_j) = \frac{1}{(1-x_i)(1-x_j)} + \left[\frac{x_i \ln x_i}{(x_i - x_j)(1-x_i)^2} + (i \leftrightarrow j)\right]. \tag{3.19}$$

The u-quark contribution in the loop can be eliminated using the unitarity of the CKM matrix and setting $x_u = 0$. Therefore, the $\Delta B = 2$ effective Hamiltonian can be written as

$$\mathcal{H}_{\text{eff},d}^{\Delta B=2} = \frac{G_F^2}{16\pi^2} M_W^2 \left[(V_{cb}V_{cd}^*)^2 F(x_c) + (V_{tb}V_{td}^*)^2 F(x_t) + 2(V_{cb}V_{cd}^*)(V_{tb}V_{td}^*) G(x_c, x_t)\right] \mathcal{O}_{LL,d}^{\Delta B=2} \tag{3.20}$$

where $F(x)$ and $G(x, y)$ are functions given in [16]. In the limit $x_c \ll 1$ and $x_t \gg 1$, they have the asymptotic behaviour

$$F(x_c) \sim x_c, \tag{3.21}$$

$$F(x_t) \sim x_t, \tag{3.22}$$

$$G(x_c, x_t) \sim \ln\frac{x_t}{x_c}. \tag{3.23}$$

Note that in equation (3.20), all the CKM factors are of $\mathcal{O}(\lambda^6)$. Therefore, the internal top quark dominates the loop in the $\Delta B = 2$ box diagram, because of the large m_t. The $\Delta B = 2$ effective Hamiltonian can then be written as

$$\mathcal{H}_{\text{eff},d}^{\Delta B=2} = \frac{G_F^2}{16\pi^2} M_W^2 (V_{tb}V_{td}^*)^2 S_0(x_t) \mathcal{O}_{LL,d}^{\Delta B=2}, \tag{3.24}$$

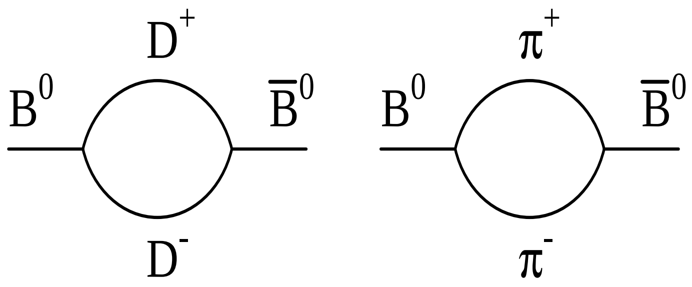

Figure 3.2: The long-distance electroweak contributions to the B^0–$\bar{B}^0$ mixing

to a very good approximation. $S_0(x_t)$ is just the abbreviation for $S_0(x_t, x_t)$, and is actually $F(x_t)$ in this case. This effective Hamiltonian is roughly proportional to m_t^2 because of the asymptotic behaviour of the Inami-Lim function $S_0(x_t)$ (equation (3.22)).

There are also long-distance electroweak contributions to B^0–$\bar{B}^0$ mixing in the framework of the Standard Model. Figure 3.2 shows the diagrams for these contributions. They involve only the charm or up quarks in the intermediate states, and are actually composed of two $\Delta B = 1$ decay process. Therefore,

1. the long-distance effects are suppressed by the factor $(M_B^2/m_t^2) \approx 4 \times 10^{-3}$ in comparison with short-distance effects[4], given the fact that the CKM factors in front of them are the same as the ones in the $\Delta B = 2$ box diagram.
2. the Γ_{12} contribution in equation (3.14) is suppressed, *i.e.*, $\mathrm{Re}\Gamma_{12} \ll 2\mathrm{Re}M_{12}$, as $\hat{\Gamma}$ is determined by the rate of the decay of the neutral mesons.

We then can conclude that the $\Delta B = 2$ box diagram with the top quark in the loop dominates the electroweak contribution to the B^0–$\bar{B}^0$ oscillation. The effective Hamiltonian, in the absence of QCD, is given by equation (3.24), and its matrix element can be related to the mass difference of the eigenstates of this oscillating system through equation (3.14)

$$\Delta m_d = 2M_{B^0}\,|M_{12}| = \left|\langle \bar{B}^0|\mathcal{H}^{\Delta B=2}_{\text{eff},d}|B^0\rangle\right|, \tag{3.25}$$

[4]The factor M_B^2 is from the phase space of B meson decays

where we have used the fact that $\mathrm{Im}M_{12} \ll \mathrm{Re}M_{12}$ and $\mathrm{Re}\Gamma_{12} \ll 2\mathrm{Re}M_{12}$. M_{B^0} is the mass of the B^0 meson, and the factor $2M_{B^0}$ arises from the normalisation of the neutral-meson state. We see $B^0-\bar{B}^0$ mixing has the property that it allows a clean extraction of $|V_{td}|$, as it is experimentally measurable and only involves the top-quark contribution in its theoretical evaluation[5]. The analyses of other neutral meson mixing processes are less clear and therefore do not allow clean extractions of CKM matrix elements. For instance:

1. $D^0-\bar{D}^0$ mixing is much less clean than $B^0-\bar{B}^0$ mixing. The short-distance $\Delta C = 2$ box diagram has d, s and b quarks in the loop. The b-quark contribution is suppressed by its CKM factor, and the GIM cancellation suppresses the d- and s-quark contributions. Worse is that the long-distance electroweak effect receives an $\mathcal{O}(10^2)$ enhancement from CKM factors, in comparison with the box diagram. Therefore, we cannot reliably predict the propagation part ($\mathrm{Re}M_{12}$) of this mixing process, as it is unclear how the long-distance effect contributes.

2. In $K^0-\bar{K}^0$ mixing, the c-quark contribution to the loop in the $\Delta S = 2$ box diagram is not suppressed. Instead, it is about sixteen times bigger than the t-quark contribution. This is because the c-quark CKM factor is of $\mathcal{O}(\lambda^2)$, while the t-quark CKM factor is of $\mathcal{O}(\lambda^{10})$. This mixing process also receives an important contribution from the long-distance effects, since the long-distance contributions involve pions as intermediate meson states such that the CKM factor is also $\mathcal{O}(\lambda^2)$, and the mass ratio (M_K^2/m_c^2) is not small and can be compensated by the large $\Delta I = 1/2$ enhancement of non-leptonic kaon decays.

3.1.3 Next-to-Leading-Logarithm Analysis of Short-Distance QCD Effect

Using the techniques introduced in section 1.2, we can examine the short-distance QCD effect in $\mathcal{H}_{\mathrm{eff},d}^{\Delta B=2}$. There is no operator mixing from gluon exchange in this

[5] $|V_{tb}|$ is well-constrained to be very close to unity.

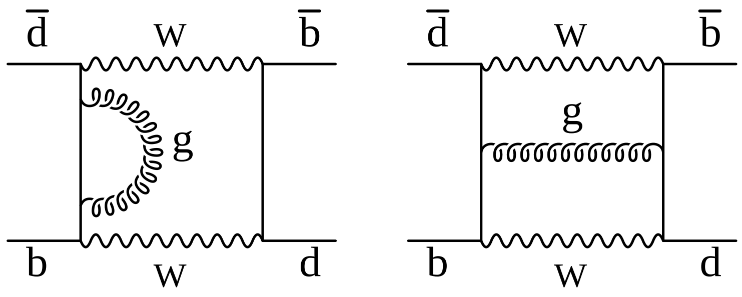

Figure 3.3: Some examples of two-loop diagrams which contribute to $B^0-\bar{B}^0$ mixing in the full Standard Model

process, as the Fierz transformed left-left operator reproduces itself. Taking into account the short-distance QCD effects, the effective Hamiltonian can be written as

$$\mathcal{H}_{\text{eff},d}^{\Delta B=2} = \frac{G_F^2}{16\pi^2} M_W^2 (V_{td} V_{tb}^*)^2 C^{\Delta B=2}(\mu) \mathcal{O}_{LL,d}^{\Delta B=2}(\mu). \tag{3.26}$$

Note that the four-quark operator is divergent and requires renormalisation. The dependence of the renormalisation scale μ in the operator $\mathcal{O}_{LL,d}^{\Delta B=2}(\mu)$ and the Wilson coefficient $C^{\Delta B=2}(\mu)$ should cancel each other, since the box diagram in the full Standard Model is finite and made up of symmetry currents. Solving the RGE, the Wilson coefficient $C^{\Delta B=2}(\mu)$ can be found to have the form

$$C^{\Delta B=2}(\mu) = U_c^{\Delta B=2}(\mu, M_W) C^{\Delta B=2}(M_W), \tag{3.27}$$

as in equation (1.47). The Next-to-Leading-Logarithm Approximation (NLLA) of this Wilson coefficient [68] is obtained from one-loop matching and two-loop running, in which the next-to-leading logarithms are summed and the $\mathcal{O}(\alpha_s)$ scheme ambiguity is removed. One-loop matching requires calculation of two-loop diagrams in the full Standard Model, as shown in figure 3.3. In LLA, matching is performed at tree-level and $C_{\text{LLA}}^{\Delta B=2}(M_W)$ only depends upon the Inami-Lim function $S_0(x_t)$. However, $C_{\text{NLLA}}^{\Delta B=2}(M_W)$ takes the form

$$C_{\text{NLLA}}^{\Delta B=2}(M_W) = S_0(x_t) + \frac{\alpha_s(M_W)}{4\pi} \left[S_1(x_t) + F(M_W, \mu_t) S_0(x_t) + B_t S_0(x_t) \right], \tag{3.28}$$

where μ_t is the renormalisation scale for the top-quark mass. $S_1(x_t)$ is function arising from the two-loop calculation in the full Standard Model. B_t and

$F(M_W, \mu_t)$ are of the form (in the NDR-$\overline{\rm MS}$ scheme)

$$F(M_W,\mu_t) = \gamma_m^{(0)} x_t \frac{\partial S_0(x_t)}{\partial x_t} \ln\frac{\mu_t^2}{M_W^2}, \tag{3.29}$$

$$B_t = 5\frac{N-1}{2N} + 3\frac{N^2-1}{2N}, \tag{3.30}$$

where N is the number of colours, $\gamma_m^{(0)}$ is the one-loop γ function for the running top-quark mass. Note that the μ_t dependences of $S_0(x_t)$, $S_1(x_t)$ and $F(M_W,\mu_t)$ in equation (3.28) should cancel amongst each other at $\mathcal{O}(\alpha_s)$. This μ_t dependence actually amounts to a 9% variation of the matrix element $\langle \bar{B}^0 | \mathcal{H}^{\Delta B=2}_{\text{eff},d} | B^0 \rangle$ in LLA, if μ_t is varied in the range $100\text{GeV} < \mu_t < 300\text{GeV}$. However, this ambiguity is reduced to 1% in NLLA [6]. The NLLA scale-evolution function for the Wilson coefficient (between M_W and $\mu \sim \mathcal{O}(1\text{GeV})$) takes the form (*c.f.*, equation (1.63))

$$U^{\Delta B=2}_{c\text{NLLA}}(\mu, M_W) = \left[1 + \frac{\alpha_s(\mu)}{4\pi} J_+\right] \left[\frac{\alpha_s(\mu)}{\alpha_s(M_W)}\right]^{-d_+} \left[1 - \frac{\alpha_s(M_W)}{4\pi} J_+\right], \tag{3.31}$$

where

$$J_+ = d_+ \frac{\beta_1}{\beta_0} - \frac{\gamma_+^{(1)}}{2\beta_0}, \tag{3.32}$$

$$d_+ = \frac{\gamma_+^{(0)}}{2\beta_0}. \tag{3.33}$$

$\beta_1 = 102 - 38n_f/3$, form the two-loop QCD β function. $\gamma_+^{(0)}$ and $\gamma_+^{(1)}$ are one- and two-loop anomalous dimensions of the operator $\mathcal{O}^{\Delta B=2}_{LL,d}$ in the NDR-$\overline{\rm MS}$ scheme, $\gamma_+^{(0)} = 4$ and $\gamma_+^{(1)} = -7 + 4n_f/9$. This evolution function sums up leading and next-to-leading logarithms and gives a 1% scale uncertainty when being used to run between $\mathcal{O}(M_W)$ and $\mathcal{O}(1\text{GeV})$. It is convenient to factor out the μ dependent part of $U^{\Delta B=2}_{c\text{NLLA}}(\mu, M_W)$ as

$$b^{\Delta B=2}_{\text{NLLA}}(\mu) = (\alpha_s(\mu))^{-d_+} \left[1 + \frac{\alpha_s(\mu)}{4\pi} J_+\right]. \tag{3.34}$$

The NLLA scale-evolution function for the $\Delta B = 2$ four-fermion operator (between two scales μ_1 and μ_2) has the form (*c.f.*, equation (1.72))

$$U^{\Delta B=2}_{\text{NLLA}}(\mu_1, \mu_2) = \left[1 - \frac{\alpha_s(\mu_1)}{4\pi} J_+\right] \left[\frac{\alpha_s(\mu_1)}{\alpha_s(\mu_2)}\right]^{d_+} \left[1 + \frac{\alpha_s(\mu_2)}{4\pi} J_+\right]. \tag{3.35}$$

3.1.4 Vacuum Saturation and the Bag Parameter

We have reviewed the phenomenology of B^0–$\bar{B}^0$ mixing, the construction of $\mathcal{H}_{\text{eff}}^{\Delta B=2}$ and the analysis of short-distance QCD effects in NLLA. However, the hadronic matrix element $\langle \bar{B}^0|\mathcal{O}_{LL,d}^{\Delta B=2}(\mu)|B^0\rangle$ requires a non-perturbative calculation due to confinement of QCD. Before presenting the lattice calculation of this matrix element, we introduce the vacuum-saturation (VS) approximation [69] which leads to parameterising non-perturbative four-quark matrix elements in terms of the Bag parameters (B parameters).

The idea of VS is to insert the lowest-lying state (the vacuum) in every possible way between the currents which compose the four-quark operator in question.

This approximation is certainly dubious. However, we will see why it is instructive to look at the vacuum-saturated matrix elements of four-quark operators.

We now proceed with the matrix element

$$\left\langle \bar{B}^0 \left|\mathcal{O}_{LL,d}^{\Delta B=2}(\mu)\right| B^0\right\rangle = \left\langle \bar{B}^0 \left|\left[\bar{b}\gamma_\mu(1-\gamma_5)d\right]\left[\bar{b}\gamma^\mu(1-\gamma_5)d\right]\right| B^0\right\rangle, \tag{3.36}$$

which has to be calculated non-perturbatively. We insert the vacuum state between the currents. There are four possible ways to perform the insertion, as there are four quark propagators and the external states are colour singlets. This is equivalent to stating that there are four possible Wick contractions. These four contractions are equal in pairs, which gives a symmetry factor 2. Therefore, the result of the VS approximation of the above matrix element is

$$\begin{aligned}\left\langle \bar{B}^0 \left|\mathcal{O}_{LL,d}^{\Delta B=2}(\mu)\right| B^0\right\rangle_{\text{VS}} = 2 \quad \Big\{ \quad & \left\langle \bar{B}^0 \left|\bar{b}_\alpha\gamma_\mu(1-\gamma_5)d_\alpha\right| 0\right\rangle \left\langle 0 \left|\bar{b}_\beta\gamma^\mu(1-\gamma_5)d_\beta\right| B^0\right\rangle \\ + \quad & \left\langle \bar{B}^0 \left|\bar{b}_\alpha\gamma_\mu(1-\gamma_5)d_\beta\right| 0\right\rangle \left\langle 0 \left|\bar{b}_\beta\gamma^\mu(1-\gamma_5)d_\alpha\right| B^0\right\rangle \Big\},\end{aligned} \tag{3.37}$$

where α and β are colour indices. From parity and Lorentz invariance, the vector current matrix element between vacuum and a B meson should be zero. Therefore, only the axial-vector current contributes to the right-hand side of equation (3.37). Its matrix elements between the vacuum and a B meson are

$$\left\langle 0 \left|\bar{b}_\alpha\gamma^\mu\gamma_5 d_\alpha\right| B^0(p)\right\rangle \quad = \quad -if_B p^\mu \exp(-ip\cdot x),$$

$$\left\langle 0 \left| \bar{b}_\alpha \gamma^\mu \gamma_5 d_\beta \right| B^0(p) \right\rangle = -i\frac{\delta_{\alpha\beta}}{3} f_B p^\mu \exp(-ip\cdot x), \tag{3.38}$$

where the second equation follows from the fact that the B meson is a colour singlet. p^μ is the four-momentum carried by the B meson and f_B is the B-meson decay constant. Therefore, the VS approximation gives the relation

$$\langle \bar{B}^0 | \mathcal{O}^{\Delta B=2}_{LL,d}(\mu) | B^0 \rangle_{\mathrm{VS}} = \frac{8}{3} f_B^2 M_B^2. \tag{3.39}$$

An immediate observation tells us the VS approximation cannot be right in this case. The matrix element $\langle \bar{B}^0 | \mathcal{O}^{\Delta B=2}_{LL,d}(\mu) | B^0 \rangle$ depends upon the renormalisation scale μ, while the vacuum saturated one does not. Hence we introduce the *Bag parameter* (B parameter). *The B parameter for a four-quark matrix element is defined to be the ratio between the matrix element itself and its vacuum-saturated counterpart.* In the case of $\mathcal{O}^{\Delta B=2}_{LL,d}$, the B parameter B_B is

$$B_B(\mu) = \frac{\langle \bar{B}^0 | \mathcal{O}^{\Delta B=2}_{LL,d}(\mu) | B^0 \rangle}{\langle \bar{B}^0 | \mathcal{O}^{\Delta B=2}_{LL,d}(\mu) | B^0 \rangle_{\mathrm{VS}}} = \frac{\langle \bar{B}^0 | \mathcal{O}^{\Delta B=2}_{LL,d}(\mu) | B^0 \rangle}{\frac{8}{3} f_B^2 M_B^2}. \tag{3.40}$$

B_B depends upon μ in the same way as $\mathcal{O}^{\Delta B=2}_{LL,d}$ does, so we can define the renormalisation-scale independent B parameter $\hat{B}_B$ by multiplying it by $b(\mu)$ introduced in equation (3.34)

$$\hat{B}_B = b^{\Delta B=2}(\mu) B_B(\mu). \tag{3.41}$$

3.2 Lattice Calculation

Our goal is to non-perturbatively calculate the matrix element

$$\mathcal{M}_{bd}(\mu) = \langle \bar{B}^0 | \mathcal{O}^{\Delta B=2}_{LL,d}(\mu) | B^0 \rangle, \tag{3.42}$$

using Lattice QCD to extract $|V_{td}|$ from B^0–$\bar{B}^0$ oscillations. However, this matrix element is of dimension four. Hence it has a strong dependence upon lattice spacing a, which is typically determined in quenched calculations at the level of 10%. Furthermore, there will be discretisation errors proportional to $\mathcal{O}(a^n m_q^n \alpha_s^k)$, where m_q is quark mass. Since m_q is quite large for a heavy quark, these systematic errors could be sizable. Therefore, $\mathcal{M}_{bd}$ is expected to be determined with rather large uncertainties. There are two remedies to these problems:

1. The experimental error on $|V_{ts}|$ is constrained to be within 10%. Therefore, we can calculate the flavour-$SU(3)$ breaking ratio

$$r_{sd} = \frac{\mathcal{M}_{bs}}{\mathcal{M}_{bd}}, \tag{3.43}$$

from which we can extract $|V_{ts}/V_{td}|$. It is reasonable to expect that many theoretical uncertainties in the calculations of $\mathcal{M}_{bs}$ and $\mathcal{M}_{bd}$ will cancel in this ratio. First, it is obvious that this dimensionless quantity has a milder dependence upon a than the matrix elements themselves. Secondly, if we use the *same heavy-quark masses* for $\mathcal{M}_{bs}$ and $\mathcal{M}_{bd}$ in the lattice calculation of r_{sd} then use HQET to extrapolate it to the beauty-mass regime, we expect significant cancellations of the discretisation errors in $\mathcal{M}_{bs}$ and $\mathcal{M}_{bd}$. Also, the renormalisation-scale dependence of $\mathcal{M}_{bs}$ and $\mathcal{M}_{bd}$ will cancel which means we can reduce systematic errors arising from

   - operator matching between the lattice and the continuum scheme.
   - running in the continuum scheme.

2. From the discussion in the last section, it is clear we can calculate the B parameter B_B and the decay constant f_B, then use them and the experimentally measured B^0 meson mass to obtain $\mathcal{M}_{bd}$. B_B is a dimensionless quantity formed by taking ratio between some closely related matrix elements ($\mathcal{M}_{bd}$ and $|\langle 0|A_\mu|B^0\rangle|^2$), so we expect that it will suffer less from the discretisation errors than the matrix element $\mathcal{M}_{bd}$. f_B is of dimension one, which is still expected to be better controlled than $\mathcal{M}_{bd}$.

In this work, we calculate r_{sd} directly from $\mathcal{M}_{bs}/\mathcal{M}_{bd}$ and indirectly by combining B_{B_s}/B_B and f_{B_s}/f_B. We also present results of the B parameters and decay constants. We estimate the statistical errors of these quantities using a bootstrap analysis [35]. One thousand bootstrap samples are created in the analysis.

Table 3.1: Simulation parameters

β	$c_{\rm SW} = 1/u_0^3$	lattice size	# of configs.
6.0	1.48	$16^3 \times 48$	498
6.2	1.44	$24^3 \times 48$	188

3.2.1 Simulation Details

Lattice simulations are performed in the quenched approximation at two β values using the mean-field (tadpole) improved Sheikholeslami-Wohlert (clover) action

$$S_{\rm SW}^{\rm TI} = S_{\rm W} - \frac{ig}{u_0^3}\frac{\kappa}{2}\sum_{x,\mu,\nu}\bar{q}(x)\sigma_{\mu\nu}P_{\mu\nu}q(x), \tag{3.44}$$

where $u_0 = \langle {\rm Tr} U_p/3\rangle^{1/4}$, $S_{\rm W}$ is the standard Wilson fermion action, $P_{\mu\nu}$ is the clover-leaf representation of the Yang-Mills field-strength tensor. The Wilson r parameter is set to unity in the simulation. Table 3.1 gives some simulation parameters. The quenched gauge configurations are generated using an over-relaxed [70, 71] Cabibbo-Marinari [72] algorithm. The quark propagators are generated using the algorithms described in reference [73].

We use three κ values for the light-quark masses, which then give six light-meson masses ranging from approximately 435 MeV to 815 MeV[6]. We use propagating heavy quarks in the charm-mass regime and use HQET to extrapolate matrix elements, B parameters, decay constants and flavour-$SU(3)$ breaking ratios to the beauty-mass regime. We have five κ values for heavy-quark masses at each β. However, only three of them are used in calculating four-fermion operator matrix elements and B parameters at $\beta = 6.2$. This is due to a shortage of disk space. The κ values are summarised in table 3.2.

Throughout this work, we only fuzz [38] the propagator of the heavier quark in a heavy-light and light-light meson. For a light-light meson composed of degenerate quarks, we fuzz one of the quarks. The other quark in the meson is always non-fuzzed (and non-smeared).

[6]As we will show later, the central values of the lattice spacing are $a^{-1} = 1.96$ GeV at $\beta = 6.0$ and $a^{-1} = 2.57$ GeV at $\beta = 6.2$.

Table 3.2: κ values used for quark masses. κ_l and κ_h are κ values for light- and heavy-quark masses. $aM_{\rm L}^{\rm PS}$ means the mass of the degenerate light-light pseudo-scalar meson formed by (κ_l, κ_l) in lattice unit. $aM_{\rm H}^{\rm PS}$ means the mass of the heavy-light pseudo-scalar meson formed by (κ_h, κ_{lh}) in lattice unit, where κ_{lh} is the κ value corresponding to the heaviest light-quark mass

β	κ_l	$aM_{\rm L}^{\rm PS}$	κ_h	$aM_{\rm H}^{\rm PS}$
6.0	0.13700	0.414	0.114	1.157
			0.118	1.053
	0.13810	0.293	0.122	0.943
			0.126	0.825
	0.13856	0.227	0.130	0.695
6.2	0.13640	0.304	0.120	0.877
			0.123	0.792
	0.13710	0.223	0.126	0.702
			0.129	0.604
	0.13745	0.171	0.132	0.496

In this work, we want to use the KLM normalisation[7] introduced in equation (2.54). Therefore, we have to multiply the lattice quark field q by $\sqrt{1+am_0}\sqrt{2\kappa_q}$,

$$q_{\rm KLM} = \sqrt{1+am_0}\sqrt{2\kappa_q}\,q = \sqrt{1+\frac{1}{2}\left(\frac{1}{2\kappa_q}-\frac{1}{2\kappa_c}\right)}\sqrt{2\kappa_q}\,q. \tag{3.45}$$

The critical hopping parameter κ_c in the above equation is determined non-perturbatively by a spectral calculation, which will be presented in subsection 3.4.1. Taking into account the mean-field improvement, we have to modify the κ values according to equation (2.64), so

$$q_{\rm KLM}^{\rm TI} = \sqrt{1+am_0^{\rm TI}}\sqrt{2\kappa_q u_0}\,q = \sqrt{1+\frac{1}{2u_0}\left(\frac{1}{\kappa_q}-\frac{1}{\kappa_c}\right)}\sqrt{2\kappa_q u_0}\,q. \tag{3.46}$$

where $m_0^{\rm TI}$ denotes the mean-field improved bare quark mass. u_0 is determined

[7]The KLM normalisation is based upon the observation of the tree-level fermion propagator in the Wilson fermion action. The clover term in equation (3.44) is of $\mathcal{O}(g)$, so the tree-level fermion propagator is the same as the one in the Wilson fermion action.

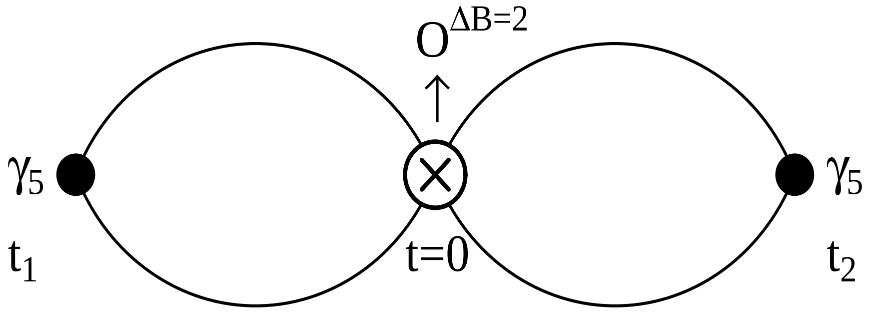

Figure 3.4: Three-point function for the B^0–$\bar{B}^0$ mixing.

non-perturbatively from the numerical calculation of $\langle \mathrm{Tr} U_p/3\rangle^{1/4}$ as obtained from the gauge configurations we have.

3.2.2 Correlation Functions

In order to extract the matrix elements $\mathcal{M}_{bd}$, $\mathcal{M}_{bs}$ and the B parameters B_B and B_{B_s}, we use the three-point correlation function

$$C^3(t_1,t_2) = \sum_{\vec{x},\vec{y}} \langle P_{\mathrm{F}}^{\dagger}(\vec{y},t_2)\mathcal{O}_{\mathrm{L}}^{\Delta B=2}(\vec{0},0)P_{\mathrm{F}}^{\dagger}(\vec{x},t_1)\rangle, \tag{3.47}$$

where $P_{\mathrm{F}}(\vec{x},t) = \bar{h}\gamma_5 l$ is the fuzzed operator such that $P_{\mathrm{F}}^{\dagger}(\vec{x},t)$ creates a pseudoscalar meson composed of the heavy antiquark h and the light quark l, at position $\vec{x}$ and (Euclidean) time t. $\mathcal{O}_{\mathrm{L}}^{\Delta B=2}(\vec{0},0)$[8] is a $\Delta B = 2$ operator at position $\vec{0}$ and time 0, the subscript L means that it is not smeared and not fuzzed. The summation over the spatial points $\vec{x}$ and $\vec{y}$ means this correlation function describes interactions of zero-spatial-momentum mesons. On the lattice, there is more than one $\Delta B = 2$ operator which can contribute to this mixing process because of explicit chiral symmetry breaking. We will discuss this issue in the next section. This correlation function can be written as a product of four quark propagators through Wick contraction, which is schematically depicted in figure 3.4.

[8] We perform the lattice simulation with heavy-quark masses around that of the charm, and light-quark masses around that of the strange. Mesons composed these quarks do not have counterparts in the real world. Therefore, strictly speaking, here we should call this operator $\mathcal{O}^{\Delta H=2}$. However, to avoid cumbersome notation, we still call it $\mathcal{O}^{\Delta B=2}$.

Here we want to discuss the time slices t_1 and t_2 in equation (3.47). The correlation function in this equation means there is a neutral meson at t_1 and its anti-particle is at t_2. We move these two time slices along the time direction and always keep the operator $\mathcal{O}_{\rm L}^{\Delta B=2}(\vec{0},0)$ at the space time point $(\vec{0},0)$. Suppose we have a lattice with T lattice points along the time direction. Periodic boundary condition means $t=0$ is equivalent to $t=T$. Therefore, we choose

$$\frac{T}{2} < \quad t_1 \quad < T, \tag{3.48}$$

$$0 < \quad t_2 \quad < \frac{T}{2}. \tag{3.49}$$

In order to extract the matrix element $\langle \bar{P}|\mathcal{O}_{\rm L}^{\Delta B=2}|P\rangle$ ($|P\rangle$ is the pseudo-scalar meson state) from this correlation function, we have to use the translational invariance of vacuum and insert two sets of Hamiltonian eigenstates. When t_2 and $T-t_1$ are both large enough, the correlation function is dominated by the ground-state contributions, and thus has the form

$$C^3(t_1,t_2) \sim \langle 0|P_{\rm F}^\dagger|\bar{P}\rangle\langle\bar{P}|\mathcal{O}_{\rm L}^{\Delta B=2}|P\rangle\langle P|P_{\rm F}^\dagger|0\rangle \exp\left[-aM_P(T-t_1+t_2)\right], \tag{3.50}$$

where aM_P is the mass of $|P\rangle$ in lattice units. $P_{\rm F}^\dagger$ is at the space-time point $(\vec{0},0)$. However, the asymptotic behaviour in equation (3.50) is contaminated by the 'backward contributions'

$$C_{b1}^3(t_1,t_2) \quad \sim \quad \langle 0|P_{\rm F}^\dagger|\bar{P}\rangle\langle\bar{P}|P_{\rm F}^\dagger|PP\rangle\langle PP|\mathcal{O}_{\rm L}^{\Delta B=2}|0\rangle \exp\left[-aM_P(t_2+t_1)\right], \tag{3.51}$$

$$C_{b2}^3(t_1,t_2) \quad \sim \quad \langle 0|\mathcal{O}_{\rm L}^{\Delta B=2}|\bar{P}\bar{P}\rangle\langle\bar{P}\bar{P}|P_{\rm F}^\dagger|P\rangle\langle P|P_{\rm F}^\dagger|0\rangle \exp\left[-aM_P(2T-t_2-t_1)\right]. \tag{3.52}$$

Assuming all the matrix elements appearing in equations (3.50), (3.51) and (3.52) have similar magnitudes, we can estimate the backward contamination at each time slice by looking at the ratio

$$\frac{C_{b1}^3(t_1,t_2)}{C^3(t_1,t_2)} \quad \sim \quad \exp\left[-aM_P(2t_1-T)\right], \tag{3.53}$$

$$\frac{C_{b2}^3(t_1,t_2)}{C^3(t_1,t_2)} \quad \sim \quad \exp\left[-aM_P(T-2t_2)\right]. \tag{3.54}$$

These equations tell us that we cannot take t_1 and t_2 too far away from the interaction point, *i.e.*, $t=0$ or $t=T$, otherwise the backward contributions

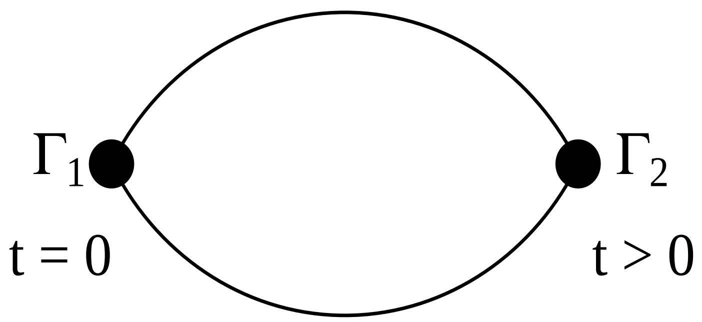

Figure 3.5: A correlator

become significant. As an example, let's look at the heavy-light pseudo-scalar meson with mass $aM_H^{PS} = 0.702$ in table 3.2. When $t_1 = 9$, the ratio in equation (3.54) is $C_{b2}^3/C^3 \sim 7\times 10^{-10}$. However, when $t_1 = 22$, this ratio becomes $C_{b2}^3/C^3 \sim 0.06$, which is a non-negligible contribution.

To get the $B^0 - \bar{B}^0$ -mixing matrix elements and B parameters, we have to take ratios between the above three-point function and two-point correlation functions (correlators). Generically, a zero-spatial-momentum correlator can be written as

$$C_{\Gamma_1\Gamma_2}(t) = \sum_{\vec{x}} \left\langle (\bar{q}_1(\vec{x},t)\Gamma_2 q_2(\vec{x},t))(\bar{q}_1(\vec{0},0)\Gamma_1 q_2(\vec{0},0))^\dagger \right\rangle \tag{3.55}$$

where $t > 0$. q_1 and q_2 are quark fields, and Γ_1 and Γ_2 are Dirac matrices. A correlator can be written as the product of two quark propagators, as depicted in figure 3.5. After inserting a complete set of Hamiltonian eigenstates between the quark bilinears, the asymptotic behaviour of a correlator at large t is found to be proportional to $\exp(-aMt)$, where aM is the meson mass in lattice unit. Again, it is contaminated by the backward contribution due to the periodic boundary condition. The ratio between the backward and forward contributions is of order $\exp\left[-aM(T-2t)\right]$ in this case.

To extract B parameters, B_P (P means pseudo-scalar), we need the ratio

$$\frac{C^3(t_1,t_2)}{\frac{-8}{3}C_{PA}^{FL}(t_1)C_{PA}^{FL}(t_2)}, \tag{3.56}$$

which reduces to

$$\frac{\langle \bar{P}|\mathcal{O}_{\mathrm{L}}^{\Delta B=2}|P\rangle}{\frac{8f_P^2M_P^2}{3Z_A}} = B_P^{\mathrm{latt}}, \tag{3.57}$$

in the limit where t_2 and $T-t_1$ are large enough to isolate the ground-state contribution. Here Z_A is the renormalisation constant (matching coefficient) which matches the lattice axial-vector current to its continuum counterpart. The superscript 'latt' in $B_P^{\rm latt}$ means it is the bare lattice result, which still has to be renormalised (matched to a continuum renormalisation scheme). We will discuss the issue of operator matching in the next section. Note that the KLM normalisation factors cancel between the three- and two-point correlation functions. f_P is the decay constant of the pseudo-scalar meson. $C_{PA}^{FL}(t)$ means a correlator formed by a local (non-smeared) operator $(\bar{h}\gamma_5\gamma_4 l)^\dagger$ at the origin and a fuzzed operator $\bar{h}\gamma_5 l$ at time t. In the above equation, we have used the periodic boundary condition and the property of the correlator C_{PA} under the time-reversal transformation

$$C_{PA}(t) = -C_{PA}(-t). \tag{3.58}$$

That is, we have

$$C_{PA}^{FL}(T-t_1) = -C_{PA}^{FL}(t_1-T) = -C_{PA}^{FL}(t_1). \tag{3.59}$$

An example of the plateau of the ratio in equation (3.56) is shown in figure 3.6(a).

To extract the matrix elements $\mathcal{M}_{bd}$ and $\mathcal{M}_{bs}$, we need the ratio

$$Z_{5\rm F}^2\,(2\kappa_h\kappa_l)\left(1+\frac{1}{2u_0}\left(\frac{1}{\kappa_h}-\frac{1}{\kappa_c}\right)\right)\left(1+\frac{1}{2u_0}\left(\frac{1}{\kappa_l}-\frac{1}{\kappa_c}\right)\right)\frac{C^3(t_1,t_2)}{C_{PP}^{FF}(t_1)C_{PP}^{FF}(t_2)} \to a^4\mathcal{M}_{hl}^{\rm latt} \tag{3.60}$$

where the KLM normalisation is made explicit. Lattice simulations only give dimensionless results, so we get the dimensionless matrix element $a^4\mathcal{M}_{hl}^{\rm latt}$. $C_{PP}^{FF}(t)$ means a correlator formed by a fuzzed operator $(\bar{h}\gamma_5 l)^\dagger$ at the origin and a fuzzed operator $\bar{h}\gamma_5 l$ at time t. The correlator C_{PP} is invariant under the time-reversal transformation, therefore

$$C_{PP}^{FF}(T-t_1) = C_{PP}^{FF}(t_1). \tag{3.61}$$

$Z_{5\rm F}$ is the matrix element $\langle 0|P_{\rm F}|P\rangle$, where $P_{\rm F}$ is the fuzzed operator $\bar{h}\gamma_5 l$ and $|P\rangle$ is the pseudo-scalar meson state. It can be determined by fitting the correlator $C_{PP}^{FF}(t)$ to

$$C_{PP}^{FF}(t) \to \frac{Z_{5\rm F}^2}{4a^2M_P^2}{\rm e}^{-aM_P\frac{T}{2}}\cosh\left[aM_P\left(\frac{T}{2}-t\right)\right]. \tag{3.62}$$

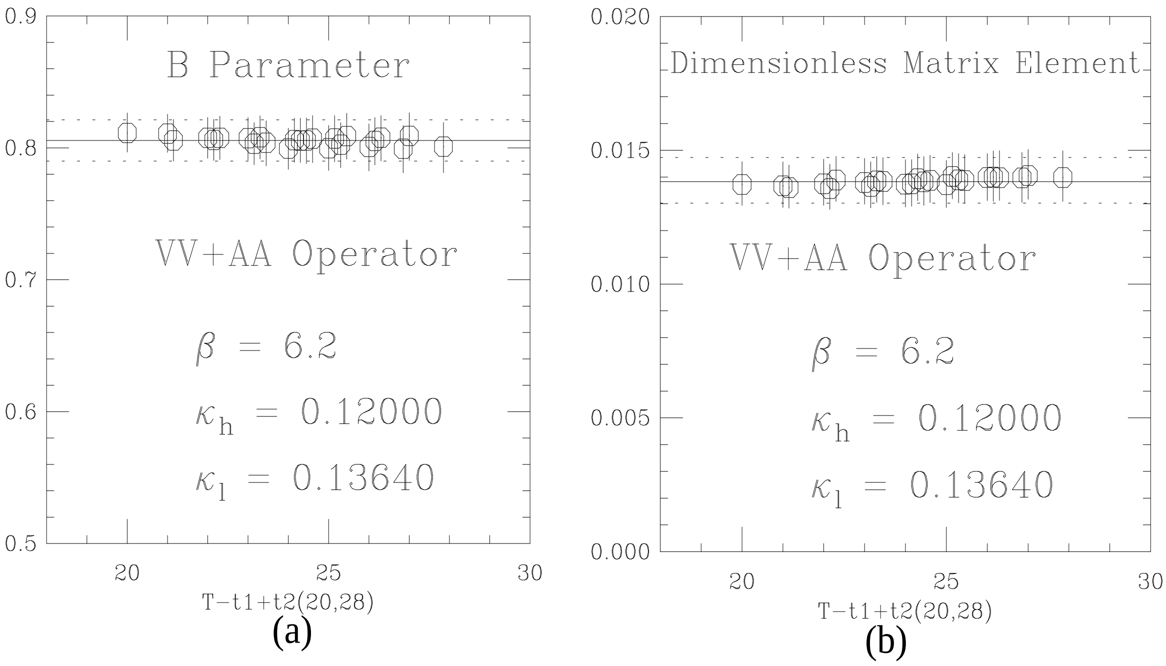

Figure 3.6: (a) A B-parameter plateau for a $\Delta B = 2$ lattice operator. The data points correspond to the ratio of equation (3.56) in the time-slice range $10 \le t_2 \le 14$ and $10 \le T - t_1 \le 14$. Points with the same $T - t_1 + t_2$ are shifted for clarity. The straight line is the fit to the ratio. (b) A plateau for the matrix element of the same $\Delta B = 2$ lattice operator. The data points correspond to the ratio of equation (3.60). Other details are the same as (a).

The cosh in the above equation comes from the backward contribution which has a time dependence $\exp(T-t)$. An example of the plateau of the ratio in equation (3.60) is shown in figure 3.6(b).

Since we have to perform a light-quark-mass extrapolation and heavy-quark-mass extrapolation to get the physical matrix elements, we have to determine certain spectral quantities. We will discuss this issue in detail in section 3.4. Here we just want to show that the pseudo-scalar-meson masses can be determined using the fit

$$C_{PP}^{FL}(t) \to \frac{Z_{5\mathrm{LF}}}{4a^2M_P^2}\mathrm{e}^{-aM_P\frac{T}{2}}\cosh\left[aM_P\left(\frac{T}{2}-t\right)\right], \tag{3.63}$$

where

$$Z_{5\mathrm{LF}} = Z_{5\mathrm{F}}Z_{5\mathrm{L}}, \tag{3.64}$$

$$Z_{5\mathrm{L}} = \langle 0|P_L|P\rangle, \tag{3.65}$$

P_L is the non-smeared operator $\bar{q}_1\gamma_5 q_2$. At this point, it is convenient to introduce the effective mass for a pseudo-scalar meson, which mimics the lattice meson mass aM_P

$$M_P^{\mathrm{eff}}(t) = -\ln\left[\frac{C_{PP}(t+1)+\sqrt{C_{PP}^2(t+1)-C_{PP}^2(\frac{T}{2})}}{C_{PP}(t)+\sqrt{C_{PP}^2(t)-C_{PP}^2(\frac{T}{2})}}\right]. \tag{3.66}$$

The effective mass plateau is a good tool to judge the onset of the large-time asymptotic behaviour of correlators. Figure 3.7(a) shows a plot of the effective mass plateau and the mass fit of equation (3.63) for a heavy-light meson in this work.

Similarly, vector-meson masses can be determined by looking at the large$-t$ asymptotic behaviour of the correlator

$$\begin{aligned} C_{VV}^{FL}(t) &= \sum_{i=1}^{3}\sum_{\vec{x}}\langle(\bar{q}_1(\vec{x},t)\gamma_i q_2(\vec{x},t))(\bar{q}_1(\vec{0},0)\gamma_i q_2(\vec{0},0))^\dagger\rangle \\ &\to \frac{\sum_{i=1}^{3}V_{LF}^i}{4a^2M_V^2}\mathrm{e}^{-aM_V\frac{T}{2}}\cosh\left[aM_V\left(\frac{T}{2}-t\right)\right], \end{aligned} \tag{3.67}$$

where aM_V is the vector-meson mass in lattice unit. V_{LF}^i are the vector-meson counterparts of the quantity in equation (3.64).

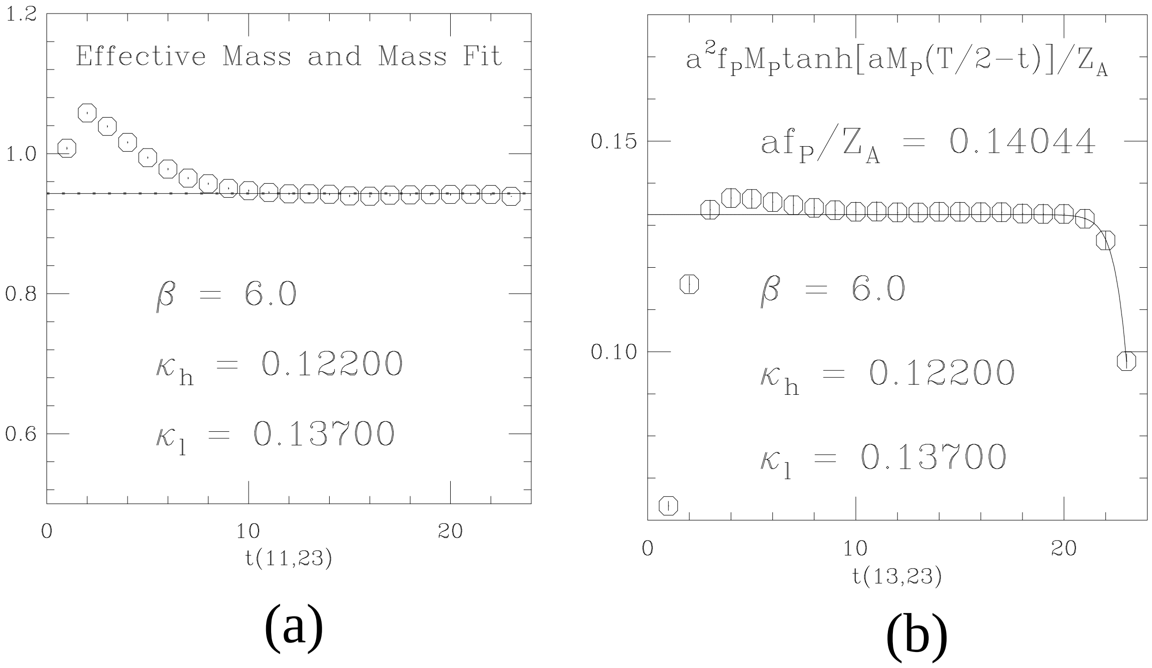

Figure 3.7: (a) A plot of effective mass and mass fit for a pseudo-scalar meson in the simulation. The data points are effective masses at each time slice obtained from equation (3.66), the straight line is the mass fit, *i.e.*, the parameter aM_P in equation (3.63). The fitting time-slice range is from 11 to 23. (b) A plot of the fit to equation (3.68). The data points are the left-hand side of the equation at each time slice. The curve is drawn according to the right-hand side of the equation with fitted $\frac{af_P}{Z_A}$. The fitting time-slice range is from 13 to 23.

To calculate the decay constants, we fit the following ratio (in the limit t is large enough)

$$Z_{5F}\,(2\sqrt{\kappa_1\kappa_2})\sqrt{1+\frac{1}{2u_0}\left(\frac{1}{\kappa_1}-\frac{1}{\kappa_c}\right)}\sqrt{1+\frac{1}{2u_0}\left(\frac{1}{\kappa_2}-\frac{1}{\kappa_c}\right)}\frac{C^{LF}_{AP}(t)}{C^{FF}_{PP}(t)}$$

$$\to\ \frac{af_P}{Z_A}(aM_P)\tanh\left[aM_P\left(\frac{T}{2}-t\right)\right], \qquad (3.68)$$

where Z_A is the renormalisation constant which relates the lattice axial-vector current to its continuum counterpart. Again, the KLM normalisation is taken into account. The tanh comes from the fact that C_{AP} and C_{PP} have different behaviours under time reversal. In the above fit, we plug in aM_P determined by equation (3.63). Figure 3.7(b) shows the result of such a fit.

3.3 Operator Matching

We have seen that we need the operators $\mathcal{O}^{\Delta B=2}_{LL,d(s)}$ and $\bar{q}_1\gamma_4\gamma_5 q_2$ to study $B^0_{(s)}$–$\bar{B}^0_{(s)}$ mixing and extract $|V_{td}|$. In a lattice calculation, we have to perform operator matching for these operators between the lattice regularisation and a continuum scheme. In this work, we match the four-fermion operators to the NDR-$\overline{\rm MS}$ scheme, since most Wilson coefficients are calculated in this scheme.

3.3.1 From Lattice to the Continuum Scheme

The matching between the lattice and the continuum scheme[9] is done using one-loop perturbation theory. Note that the clover term in equation (3.44) is of $\mathcal{O}(g)$. Therefore, the factor $1/u_0^3$ in the same equation does not generate any extra diagrams at the one-loop level, as the perturbative expression of u_0 at $\mathcal{O}(\alpha_s)$ is [48]

$$u_0=\left\langle\frac{1}{3}\mathrm{Tr}U_p\right\rangle^{\frac{1}{4}}=1+\frac{\alpha_s}{4\pi}X \quad (X=-\frac{4\pi^2}{3}). \qquad (3.69)$$

This tells us that we can use the renormalisation constants calculated using the

[9] Strictly speaking, there is no 'continuum scheme' for the axial-vector current since it does not require renormalisation in the continuum theory.

Table 3.3: Numerical values of relevant quantities for the matching of local quark bilinears between the lattice (tree-level clover action) and the continuum scheme [46] at $r = 1$. Δ_{Σ_1} is from the renormalisation of the fermion wave function, other quantities are from the matching of vertices. The local bilinears $\bar{q}_1 q_2$, $\bar{q}_1\gamma_5 q_2$ and $\bar{q}_1\sigma_{\mu\nu}q_2$ are matched to the NDR-$\overline{\mathrm{MS}}$ scheme.

Δ_I	Δ_{γ_5}	Δ_{γ_μ}	$\Delta_{\gamma_5\gamma_\mu}$	$\Delta_{\sigma_{\mu\nu}}$	Δ_{Σ_1}
-10.42	-13.50	-6.21	-4.67	-1.94	-9.11

tree-level clover action with appropriate modification to accommodate mean-field improvement.

Let's first consider the axial-vector current $\bar{q}_1\gamma_\mu\gamma_5 q_2$ in the absence of mean-field improvement. Using the KLM normalisation, the lattice current is

$$(\bar{q}_1\gamma_\mu\gamma_5 q_2)^{\mathrm{latt}}_{\mathrm{KLM}}(a) = \sqrt{1+am_1}\sqrt{1+am_2}\sqrt{2\kappa_1}\sqrt{2\kappa_2}\,(\bar{q}_1\gamma_\mu\gamma_5 q_2)^{\mathrm{latt}}(a), \qquad (3.70)$$

where am_1 and am_2 are bare quark masses. We want to perform the matching

$$(\bar{q}_1\gamma_\mu\gamma_5 q_2)^{\mathrm{cont}} = Z_A(\alpha_s; c_{\mathrm{SW}} = 1)\,(\bar{q}_1\gamma_\mu\gamma_5 q_2)^{\mathrm{latt}}_{\mathrm{KLM}}(a), \qquad (3.71)$$

where $Z_A(\alpha_s; c_{\mathrm{SW}} = 1)$ is the renormalisation constant calculated from the tree-level clover action. It does not contain scale-dependent logarithms because the axial-vector current is a symmetry current in the continuum and is finite. $Z_A(\alpha_s; c_{\mathrm{SW}} = 1)$ has the expression [46]

$$Z_A(\alpha_s; c_{\mathrm{SW}} = 1) = 1 + \frac{\alpha_s}{4\pi}\left[\frac{4}{3}\left(\Delta_{\gamma_\mu\gamma_5} + \Delta_{\Sigma_1}\right)\right], \qquad (3.72)$$

where $\Delta_{\gamma_\mu\gamma_5}$ is the contribution from the matching of the vertex, and Δ_{Σ_1} is from the wave-function renormalisation. Their values at $r = 1$ can be found in table 3.3.

Now we take into account mean-field improvement. According to equation (3.46), the current $(\bar{q}_1\gamma_\mu\gamma_5 q_2)^{\mathrm{latt}}_{\mathrm{KLM}}(a)$ in equation (3.70) should be modified by

$$(\bar{q}_1\gamma_\mu\gamma_5 q_2)^{\mathrm{latt}}_{\mathrm{TI-KLM}}(a) = \sqrt{1+am_1^{\mathrm{TI}}}\sqrt{1+am_2^{\mathrm{TI}}}\sqrt{2\kappa_1}\sqrt{2\kappa_2}\,u_0\,(\bar{q}_1\gamma_\mu\gamma_5 q_2)^{\mathrm{latt}}(a), \qquad (3.73)$$

where u_0 is non-perturbatively determined from the numerical calculation of $\langle \mathrm{Tr}U_p/3\rangle^{1/4}$ using a Monte Carlo method. The factor $\sqrt{2\kappa}$ arises from the fact that the quark fields are rescaled by this factor in Wilson-type fermion actions, so the replacement

$$\kappa \longrightarrow \kappa u_0 \tag{3.74}$$

is equivalent to using a different prescription to normalise the quark field. This then has an effect upon Δ_{Σ_1} in the renormalisation constant $Z_A(\alpha_s; c_{\mathrm{SW}} = 1)$. On the other hand, $\Delta_{\gamma_\mu\gamma_5}$ is not affected, since there is no extra vertex arising from mean-field improvement at this order. Therefore, implementing mean-field improvement results in the one-loop renormalisation constant

$$Z_A(\alpha_s; \mathrm{tad}) = \frac{Z_A(\alpha_s; c_{\mathrm{SW}} = 1)}{u_0} = 1 + \frac{\alpha_s}{4\pi}\left[\frac{4}{3}\left(\Delta_{\gamma_\mu\gamma_5} + \Delta_{\Sigma_1}\right) - X\right], \tag{3.75}$$

where we have used the one-loop expression of u_0 in equation (3.69). Note that $(\Delta_{\gamma_\mu\gamma_5} + \Delta_{\Sigma_1})$ is a negative number. The term $-X$ is a positive number. This means mean-field improvement is reducing the one-loop correction for Z_A. The matching between the lattice and the continuum is then

$$(\bar{q}_1\gamma_\mu\gamma_5 q_2)^{\mathrm{cont}} = Z_A(\alpha_s; \mathrm{tad})\,(\bar{q}_1\gamma_\mu\gamma_5 q_2)^{\mathrm{latt}}_{\mathrm{TI-KLM}}(a). \tag{3.76}$$

We now turn to the matching of the four-quark operator. In the continuum scheme, there is no operator mixing for $\mathcal{O}^{\Delta B=2}_{LL,d(s)}$ operators. However, chiral symmetry is explicitly broken in Wilson-type fermion actions, so there is nothing to prevent this operator from mixing with other parity-conserving operators of the same dimension but different chirality. The following five parity-conserving operators form a complete basis under renormalisation:

$$\begin{aligned}
\mathcal{O}_1 &= \gamma_\mu \times \gamma_\mu + \gamma_\mu\gamma_5 \times \gamma_\mu\gamma_5, \\
\mathcal{O}_2 &= \gamma_\mu \times \gamma_\mu - \gamma_\mu\gamma_5 \times \gamma_\mu\gamma_5, \\
\mathcal{O}_3 &= I \times I + \gamma_5 \times \gamma_5, \\
\mathcal{O}_4 &= I \times I - \gamma_5 \times \gamma_5, \\
\mathcal{O}_5 &= \sigma_{\mu\nu} \times \sigma_{\mu\nu},
\end{aligned} \tag{3.77}$$

where a sum over Lorentz indices is implicit. $\Gamma \times \Gamma$ stands for $(\bar{q}_1\Gamma q_2)(\bar{q}_3\Gamma q_4)$ (In this case, $q_3 = q_1$ and $q_4 = q_2$). $\mathcal{O}_1$ has the same structure as the operator we want to calculate, therefore, the one-loop matching we are performing can be written in the following generic form:

$$\mathcal{O}_{LL}^{\Delta B=2}(\mu) = \mathcal{O}_1^{\mathrm{NDR-\overline{MS}}}(\mu) = Z_1(\alpha_s, a\mu; c_{\mathrm{SW}})\left(\mathcal{O}_1^{\mathrm{latt}}(a) + \sum_{i=2}^{5} Z_i(\alpha_s; c_{\mathrm{SW}})\mathcal{O}_i^{\mathrm{latt}}(a)\right). \tag{3.78}$$

These renormalisation constants, Z_1 and Z_i, have the generic features discussed in subsection 2.1.6. For the case of tree-level clover action with KLM normalisation, the lattice operators $\mathcal{O}_j$ $(j = 1, \ldots, 5)$ have the form

$$\mathcal{O}_j^{\mathrm{tree-latt}}(a) = (1 + am_1)(1 + am_2)(2\kappa_1 2\kappa_2)\left[(\bar{q}_1\Gamma q_2)(\bar{q}_1\Gamma q_2)\right]^{\mathrm{latt}}(a). \tag{3.79}$$

The renormalisation constants Z_j $(j = 1, \ldots, 5)$ can be related to the renormalisation constants of the local quark bilinears, as all the one-loop vertex diagrams for four-fermion operators can be brought into forms which are constructed by local quark bilinears [74]. This is achieved using Fierz transformations and charge conjugation. It saves a lot of time in calculating renormalisation constants for four-fermion operators. However, this can only be done in the DRED-$\overline{\mathrm{MS}}$ scheme. Therefore, the matching between the lattice and the NDR-$\overline{\mathrm{MS}}$ scheme is composed of two steps: From lattice to DRED-$\overline{\mathrm{MS}}$ [75] and from DRED-$\overline{\mathrm{MS}}$ to NDR-$\overline{\mathrm{MS}}$ [76]. The second step is only relevant for Z_1 at this order, since other renormalisation constants are of $\mathcal{O}(\alpha_s)$.

Taking into account mean-field improvement will modify the lattice operators in equation (3.79)

$$\mathcal{O}^{\mathrm{TI-latt}} = \left(1 + am_1^{\mathrm{TI}}\right)\left(1 + am_2^{\mathrm{TI}}\right)(2\kappa_1 2\kappa_2)\, u_0^2 \left[(\bar{q}_1\Gamma q_2)(\bar{q}_1\Gamma q_2)\right]^{\mathrm{latt}}. \tag{3.80}$$

Using this prescription will modify the renormalisation constants through the modification of the quark-field renormalisation constant. However, only Z_1 needs to be modified at one-loop level, since other renormalisation constants are of $\mathcal{O}(\alpha_s)$. The one-loop $Z_1(\alpha_s, a\mu; \mathrm{tad})$ is related to its counterpart from the tree-level clover action through

$$Z_1(\alpha_s, a\mu; \mathrm{tad}) = \frac{Z_1(\alpha_s, a\mu; c_{\mathrm{SW}} = 1)}{u_0^2}, \tag{3.81}$$

where the perturbative expression of u_0 in equation (3.69) should be used.

The matching coefficients between the lattice and the NDR-$\overline{\rm MS}$ scheme in the mean-field improvement prescription are

$$
\begin{aligned}
Z_1(\alpha_s, a\mu; \mathrm{tad}) &= 1 + \frac{\alpha_s}{4\pi} \times \\
&\left\{ -4\ln(a\mu) + \frac{1}{3}\left[5\left(\Delta_{\gamma_\mu} + \Delta_{\gamma_\mu\gamma_5}\right) - (\Delta_I + \Delta_{\gamma_5}) + 8\Delta_{\Sigma_1}\right] - 2 - 2X \right\},
\end{aligned}
\tag{3.82}
$$

$$
Z_2(\alpha_s; \mathrm{tad}) = -\frac{11}{12}\frac{\alpha_s}{4\pi}\left[\Delta_I - \Delta_{\gamma_5}\right], \tag{3.83}
$$

$$
Z_3 = -\frac{4}{11}Z_2, \quad Z_4 = \frac{2}{11}Z_2, \quad Z_5 = -\frac{2}{11}Z_2, \tag{3.84}
$$

where we have used the quantities given in table 3.3. In equation (3.82), the factor (-4) in front of $\ln(a\mu)$ is just the one-loop anomalous dimension of $\mathcal{O}_1$, the term $(-2X)$ is from the perturbative expression of u_0^2 and the term (-2) is from the matching between DRED-$\overline{\rm MS}$ and NDR-$\overline{\rm MS}$ [76].

There is an ambiguity, which arises from the truncation of the perturbation series, when performing the operator matching in obtaining the B parameter in the NDR-$\overline{\rm MS}$ scheme. We use the ratio in equation (3.56) to fit the lattice bare B parameters, so the matching takes the form

$$
B^{\mathrm{NDR}-\overline{\mathrm{MS}}}(\mu) = \frac{Z_1(\alpha_s, a\mu; c_{\mathrm{SW}})}{Z_A^2(\alpha_s; c_{\mathrm{SW}})}\left(B_1^{\mathrm{latt}}(a) + \sum_{i=2}^{5} Z_i(\alpha_s; c_{\mathrm{SW}})B_i^{\mathrm{latt}}(a)\right). \tag{3.85}
$$

We can treat Z_A^2 as an overall factor, or combine its $\mathcal{O}(\alpha_s)$ correction with the one in Z_1. In this work, we always present the results of B parameters with Z_A^2 treated as an overall factor in the matching procedure. Actually, we observe that combining the one-loop correction of Z_A with the one in Z_1 makes an indistinguishable change to our results. This is because $Z_A(\alpha_s; \mathrm{tad})$ has a very small $\mathcal{O}(\alpha_s)$ correction.

Before the end of this subsection, we want to discuss the issue of choosing a coupling constant and a scale for the matching. As discussed in subsection 2.1.6, it is difficult to determine which coupling constant we should use and at which scale we should perform the matching, with only a one-loop calculation. According to the authors of reference [48], the coupling constant introduced in equation (2.63) is a good expansion parameter with the mean-field improvement

Table 3.4: Values of $\alpha_{\overline{\rm MS}}$ used in performing operator matching between the lattice and NDR-$\overline{\rm MS}$.

β	$\alpha_{\overline{\rm MS}}(1/a)$	$\alpha_{\overline{\rm MS}}(2/a)$	$\alpha_{\overline{\rm MS}}(\pi/a)$
6.0	0.192096	0.152163	0.134303
6.2	0.172993	0.140189	0.124985

prescription. However, we want to have a way of estimating the systematic errors arising from the truncation of the perturbative series. To this end, we use a $\overline{\rm MS}$ coupling constant, $\alpha_{\overline{\rm MS}}(\mu)$ (μ is the scale at which we perform the matching), and vary μ within the range $1/a \sim \pi/a$, which encompasses the range of typical ultra-violet scales on the lattice. We follow the procedure in reference [48] to determine $\alpha_{\overline{\rm MS}}(\mu)$:

First, we use the non-perturbatively determined u_0 and the relation

$$\ln(u_0) = \frac{\pi}{3}\alpha_V(3.41/a)(1 - 1.185\alpha_V), \tag{3.86}$$

and solve for $\alpha_V(3.41/a)$. α_V [77] is the coupling defined from the heavy-quark potential [78].

Second, we use the relation

$$\alpha_{\overline{\rm MS}}(3.41/a) = \alpha_V(\mathrm{e}^{5/6}3.41/a)\left(1 + \frac{2\alpha_V}{\pi}\right), \tag{3.87}$$

and solve for $\alpha_{\overline{\rm MS}}(3.41/a)$. Here we set $n_f = 0$ in β_0, since we are in the quenched approximation. The $\alpha_{\overline{\rm MS}}(\mu)$ at a different μ is then obtained from $\alpha_{\overline{\rm MS}}(3.41/a)$ using two-loop QCD $\beta-$function with $n_f = 0$. Varying q between $1/a$ and π/a causes a $\approx \pm 25\%$ variation in $\alpha_{\overline{\rm MS}}(\mu)$. This range covers the coupling constant obtained from equation (2.63). Table 3.4 lists the values of $\alpha_{\overline{\rm MS}}(\mu)$ we use in performing the operator matching between the lattice and the continuum scheme.

3.3.2 Running in the $\overline{\rm MS}$ Scheme

We have discussed the matching between the lattice and the NDR-$\overline{\rm MS}$ scheme at the scale $\mu \sim \mathcal{O}(1/a)$. In order to compare results at different μ and to compare our results with other calculations, we have to be able to run them to other scales (*e.g.*, 5 GeV) in the $\overline{\rm MS}$ scheme. In principle, we want to use the two-loop evolution function introduced in equation (3.35). However, there is an ambiguity in performing this running. Since we work in the quenched approximation, we do not know if we should take into account particle thresholds when using the two-loop $\overline{\rm MS}$ coupling constant. We choose to take into account the particle thresholds in this case, to be able to compare with what is commonly done. That means, we choose to perform matching using the following two steps:

1. Match from the lattice to NDR-$\overline{\rm MS}$ scheme at the scale μ with $n_f = 0$.

2. Run from μ to other scales in NDR-$\overline{\rm MS}$ scheme using two-loop evolution function introduced in equation (3.35) with particle thresholds taken into account.

μ serves as an intermediate scale between step one and step two. This procedure means we abandon the quenched approximation once we match the lattice to the NDR-$\overline{\rm MS}$ scheme. This is in contrast with the 'horizontal matching' used in reference [76], in which the running in the $\overline{\rm MS}$ scheme is done using $n_f = 0$. We stress here that both procedures are valid, and the difference will be quenching errors. However, these errors can only be truly quantified when data from dynamical-fermion simulations are available.

3.4 Analysis and Results

In the last two sections, we have seen how to use the lattice correlation functions to extract matrix elements of relevant lattice operators in the analysis of B^0–$\bar{B}^0$ mixing, and how to match these lattice operators to the operators in the NDR-$\overline{\rm MS}$ scheme. We then fit the plateaus for the following quantities:

1. The lattice bare pseudo-scalar decay constant af_P/Z_A (P means pseudo-scalar) for all light-light and heavy-light mesons we have. This is done using equation (3.68).

2. The lattice bare matrix elements $a^4\langle H^0|\mathcal{O}_H^{\mathrm{latt}-j}|\bar{H}^0\rangle = a^4\mathcal{M}_H^{\mathrm{latt}-j}$ ($j = 1,\ldots,5$), and B parameters, $B_H^{\mathrm{latt}-j}$, for all the basis operators in equation (3.77) (H^0 means a heavy-light pseudo-scalar meson) for all heavy-light mesons we have. This done using equations (3.60) and (3.56).

3. The matrix elements of the $\mathcal{O}_{LL}^{\Delta B=2}$ operators in the NDR-$\overline{\mathrm{MS}}$ scheme in lattice units, $a^4\langle H^0|\mathcal{O}_{LL}^{\Delta B=2}|\bar{H}^0\rangle = a^4\mathcal{M}_H$, and the B parameters, B_H of the same operators for all heavy-light mesons we have. This is done using the renormalisation constants in equations (3.82), (3.83) and (3.84) and the plateaus in equations (3.60) and (3.56).

We then obtain the NDR-$\overline{\mathrm{MS}}$ matrix elements and B parameters from two approaches

1. Fit the plateaus in equations (3.60) and (3.56) for each lattice operator in equation (3.77), then obtain NDR-$\overline{\mathrm{MS}}$ matrix elements and B parameters from these fits.

2. Form the 'NDR-$\overline{\mathrm{MS}}$ three-point correlation functions' by using NDR-$\overline{\mathrm{MS}}$ $\mathcal{O}_{LL}^{\Delta B=2}$ in equation (3.47) then fit according to equations (3.60) and (3.56)

We find, as expected, these two methods give nearly indistinguishable results, and we will present matrix elements and B parameters obtained from the second approach.

However, these matrix elements, B parameters and decay constants are calculated for heavy-quark masses around that of the charm, and light-quark masses around that of the strange. Therefore, we have to perform extrapolations/interpolations with respect to the quark masses to get results pertinent to $B_{(s)}$ and $D_{(s)}$ mesons. We start with a light-quark spectral calculation, which is necessary in order to determine the κ values corresponding to zero light-quark mass (κ_c) and strange-quark mass (κ_s). This spectral calculation is also necessary for determining the values of lattice spacing at each $\beta = 6/g_{\mathrm{bare}}^2$. We evaluate these spectral quantities for all the bootstrap samples that we use in fitting the matrix elements above, and use them in the bootstrap analysis for quark-mass extrapolations.

In fixing these light-hadron spectral quantities and performing light-quark-mass extrapolations for the matrix elements under investigation, we have to rely upon Chiral Perturbation Theory. In quenched approximation, the QCD Lagrangian has some extra ghost fields [79] which remove the internal quark loops. These ghost fields result in a larger chiral symmetry of the Lagrangian than the chiral symmetry of the unquenched QCD Lagrangian, as $U(1)_A$ anomaly is absent. In this case, the η' meson remains massless and should be treated as a pseudo-scalar Goldstone boson in the Quenched Chiral Perturbation Theory (QChPT) [80]. The η' field gives extra chiral logarithms when one performs one-loop calculations. These η' chiral logarithms diverge in the zero-quark-mass limit, hence are different from the chiral logarithms we have discussed in section 2.3. In principle, one should include these η' chiral logarithms when performing light-quark-mass extrapolations. Nevertheless, evidence suggests that they do not contribute significantly with the light-quark masses we work with [81]. Therefore, we will not include them in this work.

3.4.1 A Light-hadron Spectral Calculation

First of all, we have to find the limit of zero-quark mass for the theory (mean-field improved clover action), *i.e.*, κ_c. As has been discussed in the end of subsection 2.1.2, we need a non-perturbative method to determine κ_c, since one-loop perturbation theory gives a large correction to the additive mass renormalisation. We fix κ_c using the PCAC relation introduced in equation (2.90), *i.e.*, from the prediction of lowest order chiral perturbation theory. The pseudo-scalar-meson masses are determined using equation (3.63), while the bare quark masses are

$$am_q = \frac{1}{2}\left(\frac{1}{\kappa_q} - \frac{1}{\kappa_c}\right). \tag{3.88}$$

Therefore, for the pseudo-scalar meson composed of (κ_1, κ_2), we define

$$\frac{1}{\kappa_{\text{eff}}} = \frac{1}{2}\left(\frac{1}{\kappa_1} + \frac{1}{\kappa_2}\right), \tag{3.89}$$

and implement the PCAC relation through

$$a^2 M_P^2 \propto \frac{1}{\kappa_{\text{eff}}} - \frac{1}{\kappa_c}, \tag{3.90}$$

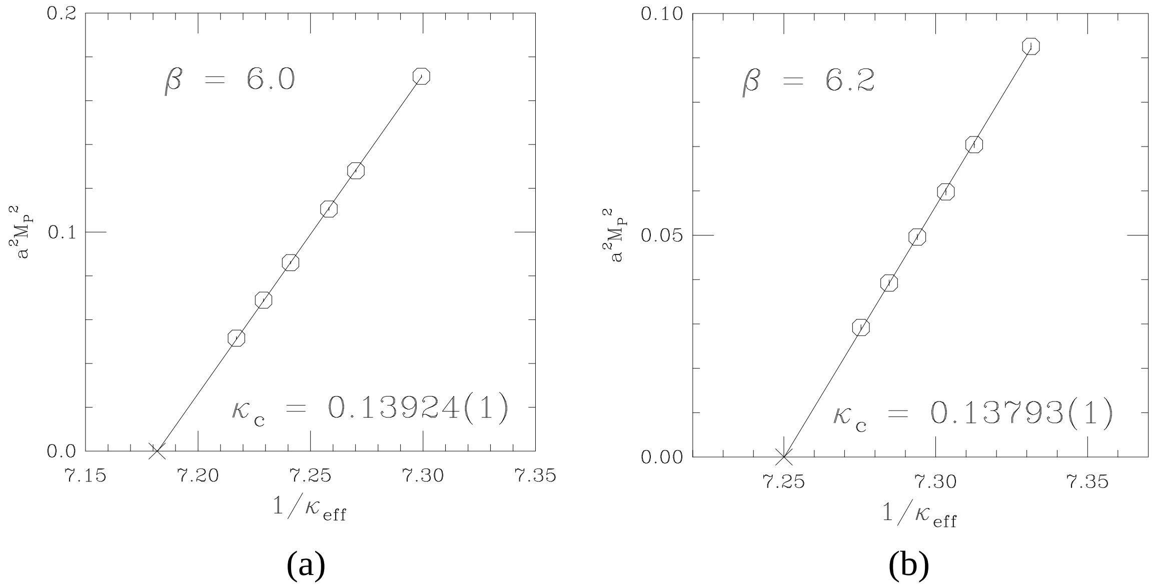

Figure 3.8: Implementation of equation (3.90) at (a) $\beta = 6.0$ and (b) $\beta = 6.2$ to determine κ_c

where aM_P is the pseudo-scalar-meson mass measured on the lattice. This relation then non-perturbatively fixes the value of the *bare quark mass* which corresponds to the *zero-quark-mass limit*[10]. Figure 3.8 shows the implementation of equation (3.90) at both β values we have.

The next task is to determine the $\rho-$meson mass in terms of lattice units. As discussed in subsection 2.1.4, the ρ mass can be used to set the lattice spacing in quenched approximation. We determine the lattice ρ mass using a linear relation between the vector-meson masses and the quark masses [82], which is implemented through

$$aM_V = A_V + B_V\left(\frac{1}{\kappa_{\rm eff}} - \frac{1}{\kappa_c}\right), \tag{3.91}$$

and extrapolating to $\kappa_{\rm eff} = \kappa_c$ [11]. Here aM_V is the vector-meson mass determined

[10]This is actually the *zero-pion-mass limit*.

[11]We can use a more complicated procedure to extrapolate aM_V to the κ value which corresponds to the physical pion mass, 135 MeV , instead of κ_c which corresponds to the zero-pion-mass limit. However, this will only give insignificant changes to the results of the matrix elements, B parameters and decay constants.

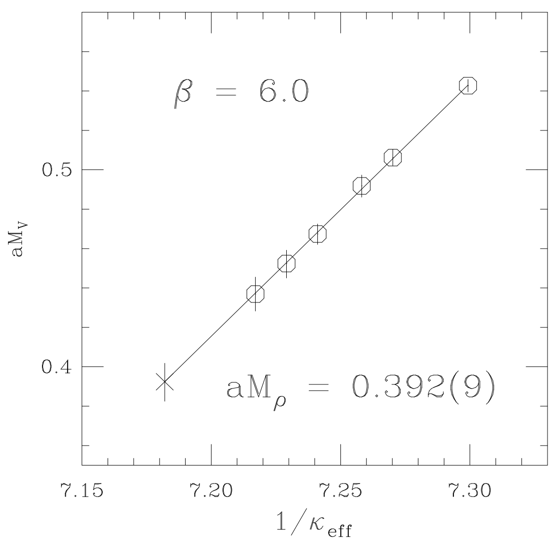

(a)

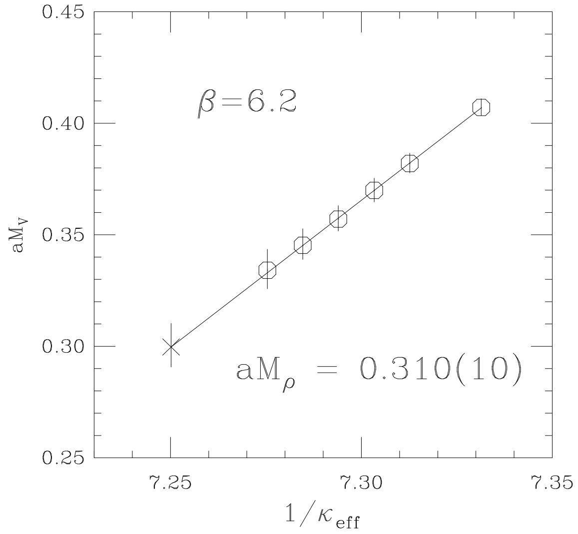

(b)

Figure 3.9: A linear fit of the vector-meson masses with respect to $1/\kappa_{\text{eff}}$ and extrapolate to $1/\kappa_c$ to determine to $\rho-$ meson mass in lattice unit (aM_ρ).

from equation (3.67), A_V and B_V are fitting parameters, with A_V identified as aM_ρ. Figure 3.9 shows the implementation of this equation and the determination of the ρ mass in lattice unit.

An issue in the above two extrapolations is the inclusion of higher-order terms of ChPT. A previous analysis of light-hadron spectrum using the same data set [81] shows that including these higher-order terms does not change κ_c and aM_ρ significantly. Therefore, we drop these terms in the fits as they increase the statistical errors.

Bearing in mind that we also want to investigate the $B_s^0-\bar{B}_s^0$ mixing, we need to fix the κ value (κ_s) which corresponds to the strange-quark mass. What we mean by 'strange-quark mass' is somewhat similar to the zero-quark-mass limit we have fixed using the PCAC relation, *i.e.*, we want to use a physical condition to fix κ_s. This time we use the kaon mass. The first step is to take the six light pseudo-scalar mesons we have, square their masses, then take one of the two κ values to κ_c for each meson and use PCAC to see how the squared meson mass changes. We then only have three independent light mesons left after this step.

Schematically, this can be seen as

$$a^2 M_P^2(\kappa_1,\kappa_2) \xrightarrow{\text{PCAC}} a^2 M_P^2(\kappa_c,\kappa_2), \tag{3.92}$$

where we have taken κ_1 to κ_c. Now we are ready to use the experimental kaon mass to fix κ_s. However, we have to determine the lattice spacing a, since we can only measure aM_P on the lattice. This can be effectively done by taking the ratio

$$\left(\frac{a^2 M_P^2(\kappa_c,\kappa_2)}{a^2 M_\rho^2}\right)^{\text{latt}} = \left(\frac{M_P^2(\kappa_c,\kappa_2)}{M_\rho^2}\right)^{\text{latt}}, \tag{3.93}$$

in which the lattice spacing cancels. We can then scale $\left(M_P^2(\kappa_c,\kappa_2)/M_\rho^2\right)^{\text{latt}}$ with respect to $1/\kappa_2$ according to PCAC, and interpolate to the point where

$$\left(\frac{M_P^2(\kappa_c,\bar{\kappa}_2)}{M_\rho^2}\right)^{\text{latt}} = \left(\frac{M_K^2}{M_\rho^2}\right)^{\text{exp}} = 0.413. \tag{3.94}$$

$\bar{\kappa}_2$ is then identified as κ_s.

Equation (3.93) is actually equivalent to setting the lattice spacing by taking the ratio

$$a^{-1} = \frac{M_\rho^{\text{exp}}}{(aM_\rho)^{\text{latt}}}. \tag{3.95}$$

In this work we set the lattice spacing using M_ρ and pion decay constant f_π. The latter is preferred in the calculation of pseudo-scalar-meson decay constants, as it removes the dependence of the mass-independent renormalisation constant (matching coefficient) Z_A in the calculation. In order to set the lattice spacing using f_π, we have to calculate af_π. Lattice simulations actually give the pseudo-scalar-meson decay constant (f_P) in the form af_P/Z_A, as can be seen in equation (3.68), which we call the bare lattice result for f_P. Inspired by Chiral Perturbation Theory, the bare lattice pion decay constant (af_π/Z_A) can be determined from the fit

$$\frac{af_P}{Z_A} = A_f + B_f\left(\frac{1}{\kappa_{\text{eff}}} - \frac{1}{\kappa_c}\right), \tag{3.96}$$

and extrapolation to $\kappa_{\text{eff}} = \kappa_c$[12]. A_f and B_f are fitting parameters, with A_f identified as af_P/Z_A. Figure 3.10 shows this extrapolation at both β values we have. af_π/Z_A can be used to set the lattice spacing through the relation

[12]As in footnote 11, we can extrapolate to the κ value which corresponds to $M_\pi = 135$ MeV, but this makes insignificant changes to the main results of this work.

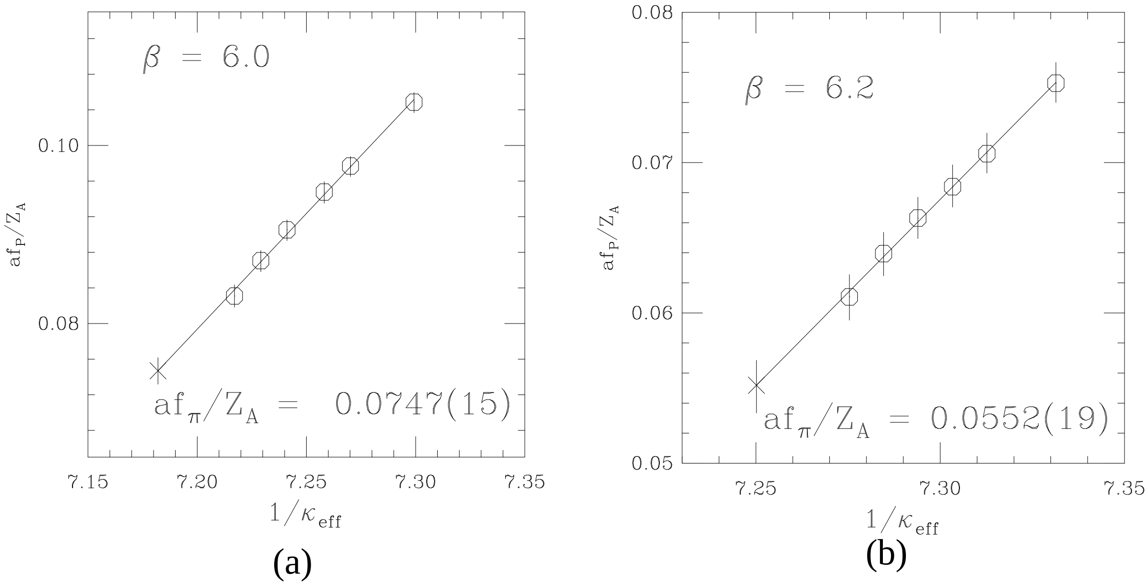

Figure 3.10: A linear fit of the pseudo-scalar-meson decay constant with respect to $1/\kappa_{\rm eff}$ and the extrapolation to $1/\kappa_c$ to determine f_π

$$a^{-1} = \left(\frac{f_\pi^{\rm exp}}{Z_A}\right)\left(\frac{af_\pi}{Z_A}\right)^{-1}. \tag{3.97}$$

Clearly, setting the lattice spacing using f_π has an ambiguity from the one-loop Z_A we use. In this work, we use $M_\rho^{\rm exp} = 769.9$ MeV and $f_\pi^{\rm exp} = 132$ MeV to set the lattice spacing. Table 3.5 lists the results of this light-hadron spectral calculation. Note that the values of lattice spacing set by M_ρ and f_π are compatible with each other.

Table 3.5: Results of the spectral quantities which we will use in performing chiral extrapolations. Errors bars quoted here are statistical. In setting the lattice spacing by f_π, we use Z_A with $\alpha_{\overline{\rm MS}}(1/a)$.

β	κ_c	κ_s	$a^{-1}(M_\rho)$ (GeV)	$a^{-1}(f_\pi)$ (GeV)
6.0	0.13924(1)	0.13757(8)	1.96(5)	1.92(4)
6.2	0.13793(1)	0.13670(9)	2.57(8)	2.58(9)

3.4.2 Light-quark-mass Extrapolations/Interpolations

After fixing κ_c and κ_s, we can perform light-quark-mass extrapolations/interpolations for $B^0-\bar{B}^0$ -mixing matrix elements, B parameters (B_H), af_H/Z_A and heavy-light-meson masses produced by fitting the ratios in equations (3.60), (3.56), (3.68) and (3.63). For clarity, we explicitly write the dependence upon κ values of these quantities, *i.e*,

$$\begin{aligned}
\text{NDR-}\overline{\text{MS}}\text{ Matrix Element in Lattice Unit} &= a^4\mathcal{M}_H(\kappa_h,\kappa_l),\\
\text{NDR-}\overline{\text{MS}}\text{ B Parameter} &= B_H(\kappa_h,\kappa_l),\\
\text{Bare Lattice Heavy-light Decay Constant} &= \frac{af_H(\kappa_h,\kappa_l)}{Z_A},\\
\text{Mass of Heavy-light Pseudo-scalar Meson Normalised by } M_\rho &= \frac{M_H(\kappa_h,\kappa_l)}{M_\rho}.
\end{aligned}$$

For each $R_H(\kappa_h,\kappa_l)$, where R can be $\mathcal{M}$, B, af/Z_A or M/M_ρ, we want to perform a light-quark-mass extrapolation to obtain $R_{Hd}(\kappa_h) \equiv R_H(\kappa_h,\kappa_c)$, and a light-quark-mass interpolation to obtain $R_{Hs}(\kappa_h) \equiv R_H(\kappa_h,\kappa_s)$. We have to perform light-quark-mass extrapolations/interpolations for the mass of the heavy-light pseudo-scalar meson because we want to use it as the expansion parameter in the heavy-quark-mass extrapolations. We also perform the light-quark-mass extrapolations/interpolations for the matrix elements and B parameters of $\mathcal{O}_1^{\mathrm{TI-latt}}$, as it has the left-left structure. We find it exhibits the same behaviour as the NDR-$\overline{\text{MS}}$ left-left operator. This is expected, as the renormalisation constants Z_i ($i = 2,\ldots,5$) are much smaller than Z_1. As mentioned before, we drop the η' chiral logarithms when investigating chiral behaviours of quantities of interest. With three light-quark masses, we can only investigate the linear dependence of these quantities with respect to light-quark masses. It turns out that the linear fits work quite well with the data we have. Examples of these extrapolations/interpolations are shown in figures 3.11, 3.12, 3.13 and 3.14. $R_H(\kappa_h,\kappa_l)$ in these examples are with the heaviest κ_h in this work. R_H with other κ_h are observed to behave similarly to the ones shown in the plots in light-quark-mass interpolations/extrapolations. From these plots, we can see the lines in the plots

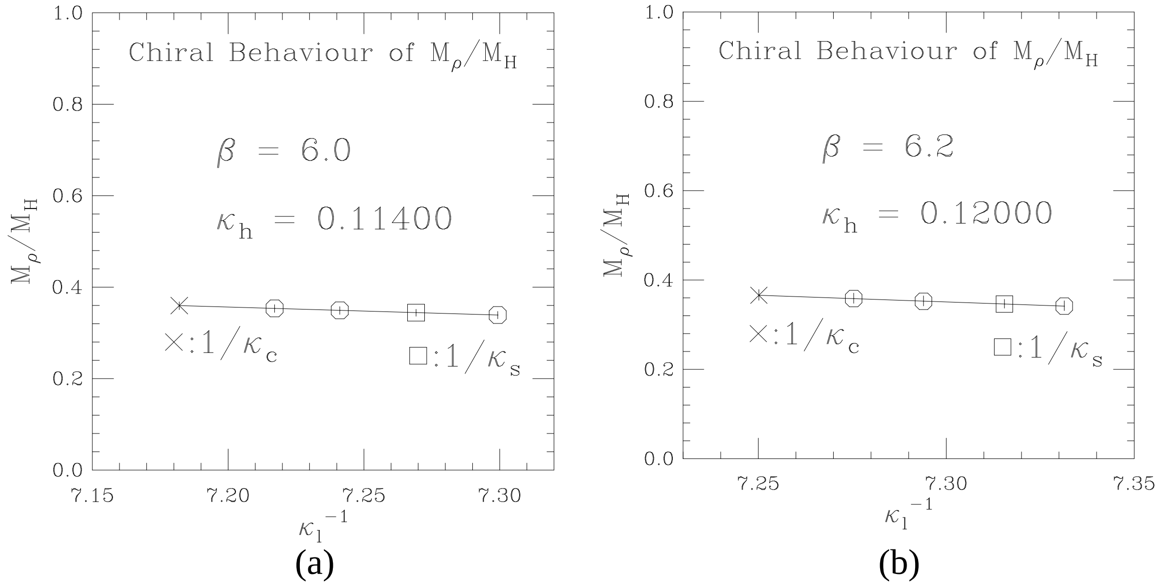

Figure 3.11: Light-quark-mass extrapolations of the inverse masses of the heavy-light mesons normalised by M_ρ with the heaviest κ_h at (a) $\beta = 6.0$ and (b) $\beta = 6.2$.

of B parameters are very flat, while the lines in the plots of $a^4\mathcal{M}_H$ are quite steep. This seems to suggest:

1. The flavour-$SU(3)$ breaking effect in B parameters should be small. The flavour-$SU(3)$ breaking in $\mathcal{M}_H$ comes mainly from f_H.

2. Numerically, it is more difficult to control the behaviour of $\mathcal{M}_H$ with respect to the light-quark mass, as any uncertainty in the determination of κ_c and κ_s will give a larger systematic error in the determination of $\mathcal{M}_{Hd}$ and $\mathcal{M}_{Hs}$, and one may also expect the need for a non-linear term in these extrapolations.

We can also see that the lines in figure 3.11 are very flat, which means M_ρ/M_{Hs} and M_ρ/M_{Hd} are quite close to each other in these plots. Actually,

$$\frac{M_{Hs} - M_{Hd}}{M_{Hd}} \sim 5\%, \tag{3.98}$$

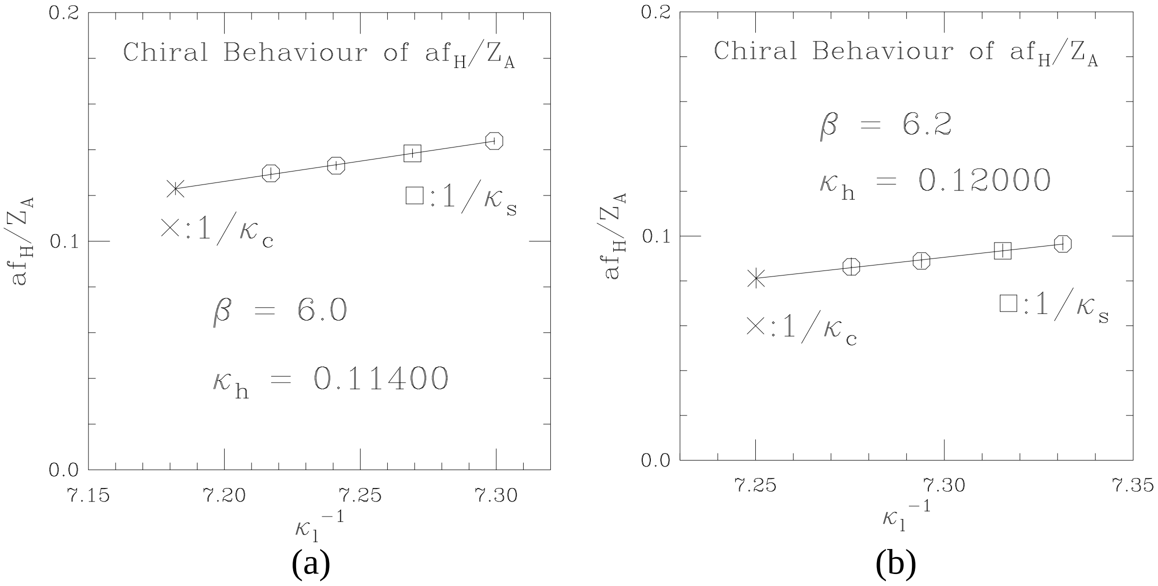

Figure 3.12: Light-quark-mass interpolation/extrapolations of af_H/Z_A with the heaviest κ_h at (a) $\beta = 6.0$ and (b) $\beta = 6.2$.

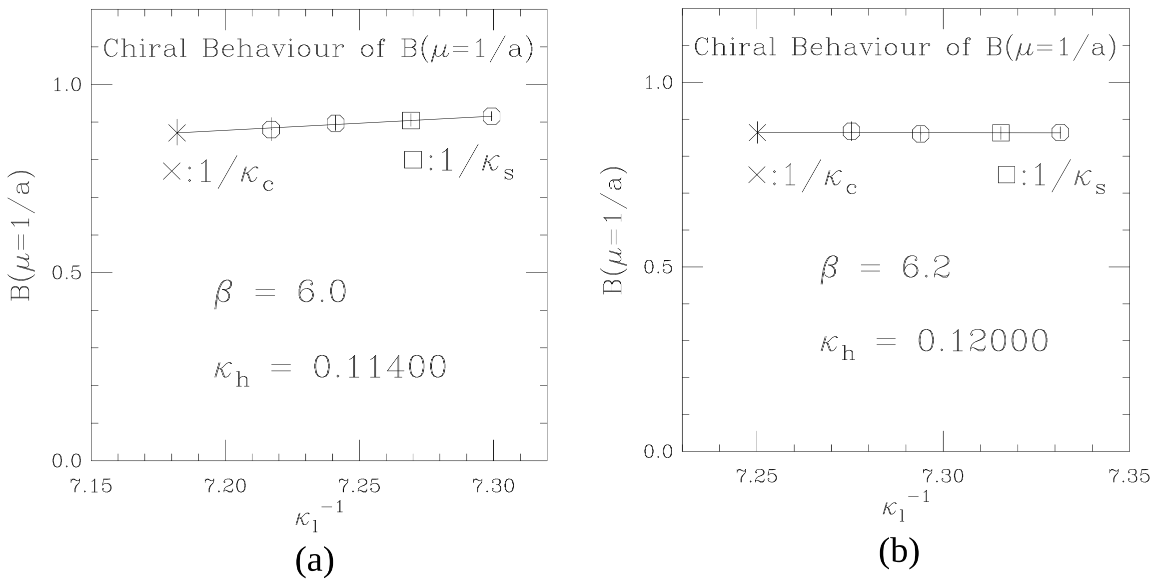

Figure 3.13: Light-quark-mass interpolation/extrapolations of NDR-$\overline{\rm MS}$ B_H matched at $\mu = 1/a$ with the heaviest κ_h at (a) $\beta = 6.0$ and (b) $\beta = 6.2$.

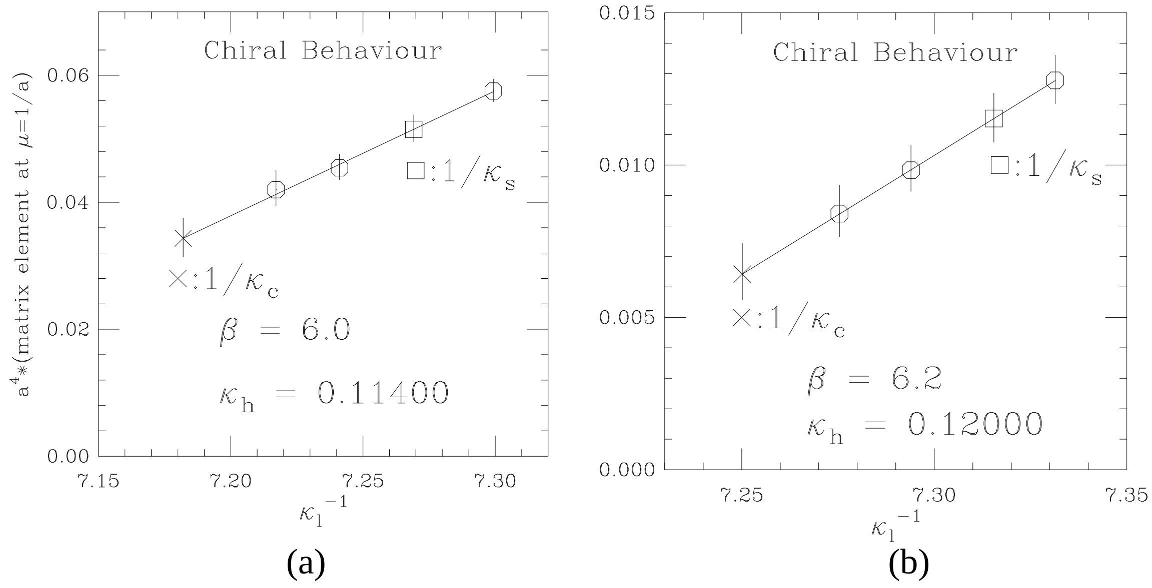

Figure 3.14: Light-quark-mass interpolation/extrapolations of NDR-$\overline{\text{MS}}$ $a^4\mathcal{M}_H$ matched at $\mu = 1/a$ with the heaviest κ_h at (a) $\beta = 6.0$ and (b) $\beta = 6.2$.

in both plots in figure 3.11. Again, this is trivially expected, since the mass of a heavy-light meson is dominated by the heavy-quark mass. With the lightest heavy quark in the simulation, we find

$$\frac{M_{Hs} - M_{Hd}}{M_{Hd}} \sim 10\%. \tag{3.99}$$

Therefore, we form the flavour-$SU(3)$ breaking ratios $S_H = R_{Hs}/R_{Hd}$, where R could be f, B or $\mathcal{M}$, and perform heavy-quark-mass extrapolations of S_H using the heavy-light-meson mass as expansion parameter.

3.4.3 Heavy-Quark Scaling

Now we are ready to investigate the heavy-quark-mass scaling properties of R_{Hd}, R_{Hs} and flavour-$SU(3)$ breaking ratios S_H defined in the last subsection. According to subsection 2.2.2, if we define

$$\Phi_f(M_H) \quad = \quad \frac{af_H}{Z_A}\sqrt{\frac{M_H}{M_\rho}}\left[\frac{\alpha_s(M_H)}{\alpha_s(M_B)}\right]^{\frac{2}{\beta_0}}, \tag{3.100}$$

$$\Phi_{\Delta F=2}(M_H) = a^4\mathcal{M}_H\left(\frac{M_\rho}{M_H}\right)\left[\frac{\alpha_s(M_H)}{\alpha_s(M_B)}\right]^{\frac{4}{\beta_0}}, \tag{3.101}$$

where F means the quantum number representing the heavy flavour, then for $X(M_H)$=$\Phi_f(M_H)$,$\Phi_{\Delta F=2}(M_H)$, $B_H(M_H)$ and S_H, HQET predicts

$$X(M_H) = A_X\left\{1+B_X\left(\frac{M_\rho}{M_H}\right)+C_X\left(\frac{M_\rho}{M_H}\right)^2+...\right\}, \tag{3.102}$$

in the LLA. The factors in the square brackets in equations (3.100) and (3.101) are from the re-summation of the leading logarithms. A_X, B_X and C_X are non-perturbative inputs in HQET, and can be fitted using lattice calculations.

Some important points in performing these extrapolations with respect to heavy-quark masses are:

1. In equation (3.102), $X(M_H)$ is what the lattice calculation produces *from QCD*. We are just using HQET to guide the extrapolation/interpolation of $X(M_H)$ in terms of heavy-quark mass. The HQET anomalous dimensions of the operators of interest are not big (4 for the four-fermion operator and 2 for the axial-vector current), and we are scaling $X(M_H)$ within the range of a few GeV. Therefore, the LLA approximation should work well enough.

2. $\beta_0 = 11$ in the above equations, because we work in the quenched approximation.

3. In the above equations, we always normalise the heavy-light-meson mass by M_ρ, *i.e.*, we set the lattice spacing by M_ρ for spectral quantities. We also set the lattice spacing using M_ρ for $\mathcal{M}_H$. However, we use f_π to set the lattice spacing for decay constants. Since these two scales are nearly identical, they make no difference on the main results in this work.

4. We use equations (3.100), (3.101) and (3.102) to perform extrapolations/interpolations to the physical meson masses [83]

$$M_B = 5.28 \text{ GeV},$$

$$
\begin{aligned}
M_{B_s} &= 5.37 \text{ GeV}, \\
M_D &= 1.86 \text{ GeV}, \\
M_{D_s} &= 1.97 \text{ GeV}.
\end{aligned}
$$

5. Using the heavy-light-meson mass as the expansion parameter avoids the renormalon ambiguity in the heavy-quark mass. However, in all of our heavy-quark-mass extrapolations, the choice of the expansion parameter is still arbitrary up to $\mathcal{O}(\Lambda_{\mathrm{QCD}}/m_Q)$ corrections (m_Q is the heavy-quark mass). For quantities which depend only on a single pseudo-scalar meson, we use the mass of the corresponding meson. For $SU(3)$ ratios, we use M_{Hd} but have checked that using M_{Hs} gives entirely compatible results.

Examples of heavy-quark-scaling behaviours of R_{Hd}, R_{Hs} and S_H are shown in figures 3.15, 3.16,..., 3.20. These figures have the features:

1. For decay constants and B parameters and their flavour-$SU(3)$ breaking ratios, we do see heavy-quark scaling. Figures 3.17 and 3.18 even suggest that the $1/m_Q^2$ corrections are small in B parameters.

2. In figure 3.19, we see the extrapolations of $\mathcal{M}_{Hs}$ and $\mathcal{M}_{Hd}$ to M_B are very large, as the HQET corrections are observed to be significant for these matrix elements. Therefore, it is more difficult to control the heavy-quark-scaling behaviours of $\mathcal{M}_{Hs}$ and $\mathcal{M}_{Hd}$.

3. In figure 3.20(a), we observe that the contribution from the quadratic term M_ρ^2/M_{Hd}^2 in the heavy-quark-mass extrapolation of the $SU(3)$ breaking ratio $\mathcal{M}_{Hs}/\mathcal{M}_{Hd}$ is larger than that from the linear term M_ρ/M_{Hd}. A plausible explanation is the large heavy-quark-mass dependence in the matrix elements $\mathcal{M}_{Hs}$ and $\mathcal{M}_{Hd}$ (*e.g.*, figure 3.19). Suppose we have the relations of heavy-quark-mass scaling for the matrix elements $\mathcal{M}_{Hs}$ and $\mathcal{M}_{Hd}$

$$
\Phi_{\Delta F_s=2} = A_X^s \left\{ 1 + B_X^s \left(\frac{M_\rho}{M_{Hs}}\right) + C_X^s \left(\frac{M_\rho}{M_{Hs}}\right)^2 + \ldots \right\}, \quad (3.103)
$$

$$
\Phi_{\Delta F_d=2} = A_X^d \left\{ 1 + B_X^d \left(\frac{M_\rho}{M_{Hd}}\right) + C_X^d \left(\frac{M_\rho}{M_{Hd}}\right)^2 + \ldots \right\}, \quad (3.104)
$$

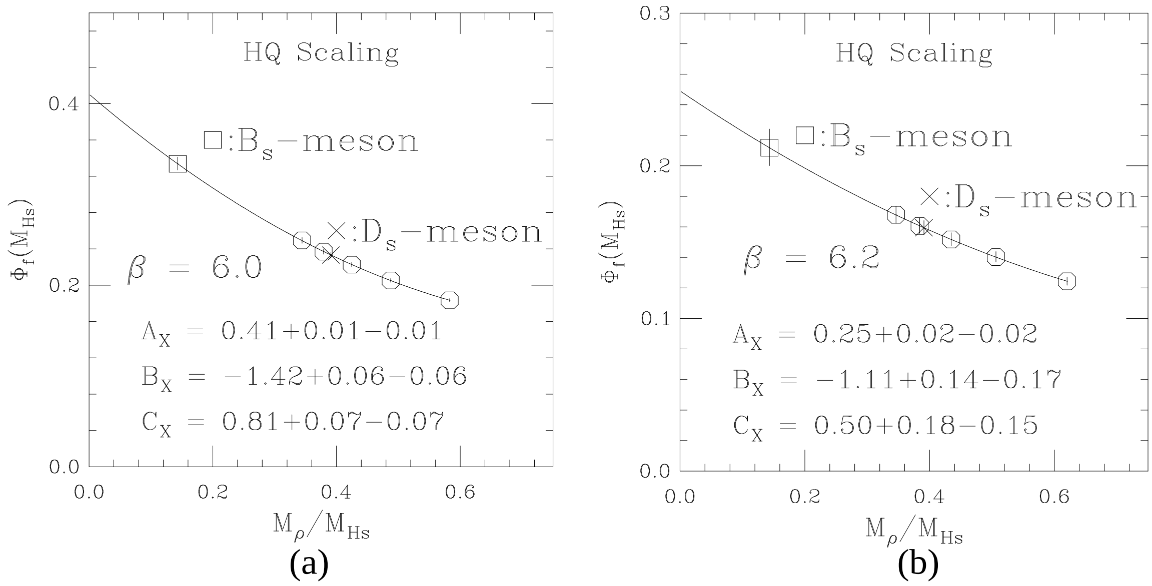

Figure 3.15: Scaling of $\Phi_f(M_{Hs})$ with respect to M_ρ/M_{Hs} at (a) $\beta = 6.0$ and (b) $\beta = 6.2$. Octagon Symbols indicate data points. The heaviest meson mass in each plot is about 2.1 GeV. Fitting parameters defined in equation (3.102) are shown in the plots. Here we see a quite significant quadratic-term contribution in the Heavy-Quark-Effective-Theory expansion.

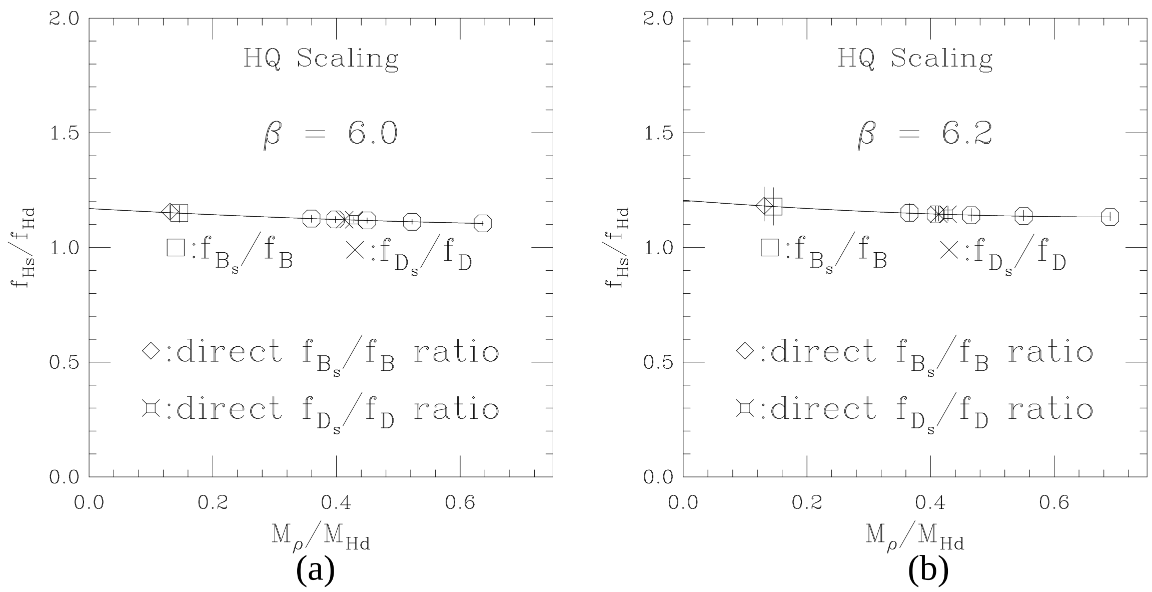

Figure 3.16: Scaling of the $SU(3)$ breaking ratio f_{Hs}/f_{Hd} with respect to M_ρ/M_{Hd} at (a) $\beta = 6.0$ and (b) $\beta = 6.2$. The fitted flavour-$SU(3)$ breaking ratios at B- and D-meson masses are consistent with the ratio taken between the extrapolated f_{B_s} and f_B, and the ratio between the interpolated f_{D_s} and f_D. The fitting parameters B_X and C_X are consistent with zero in both plots.

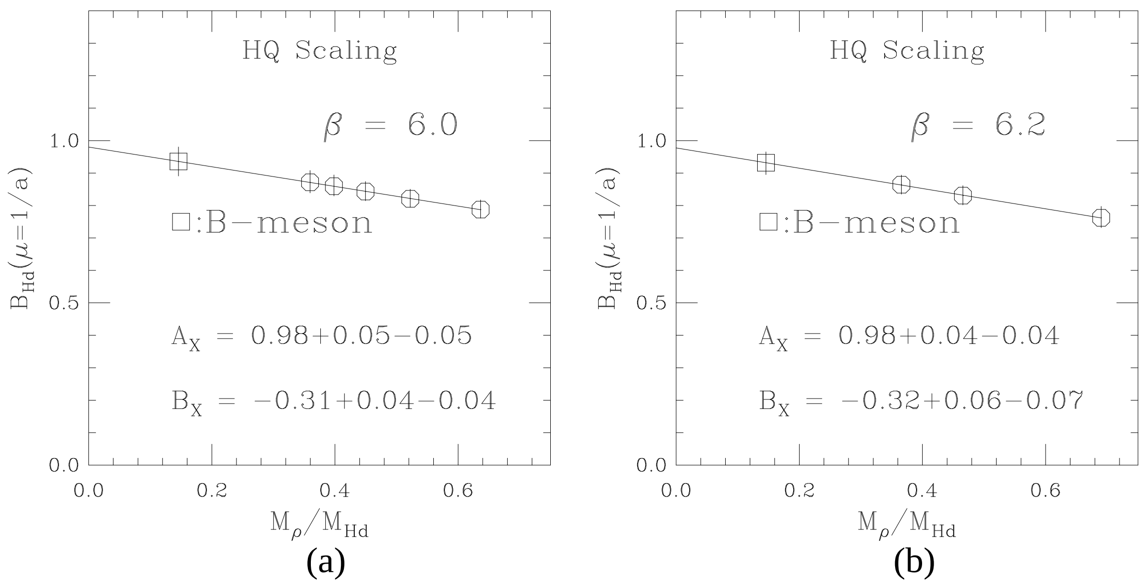

Figure 3.17: Scaling of B_{Hd} with respect to M_ρ/M_{Hd} at (a) $\beta = 6.0$ and (b) $\beta = 6.2$. We only show the linear extrapolations of B parameters with respect to M_ρ/M_{Hd}. As we have five heavy κ values at $\beta = 6.0$, we can investigate the contribution from the quadratic term M_ρ^2/M_{Hd}^2 in this heavy-quark-mass extrapolation. However, adding this quadratic term does not change A_X and B_X in (a), and the resulting C_X, which has a central value -1.76×10^{-5}, is consistent with zero. This suggests that the contribution from M_ρ^2/M_{Hd}^2 is very small in the heavy-quark-mass extrapolations for B parameters in our calculations. Therefore, the linear extrapolation in (b) should be reliable.

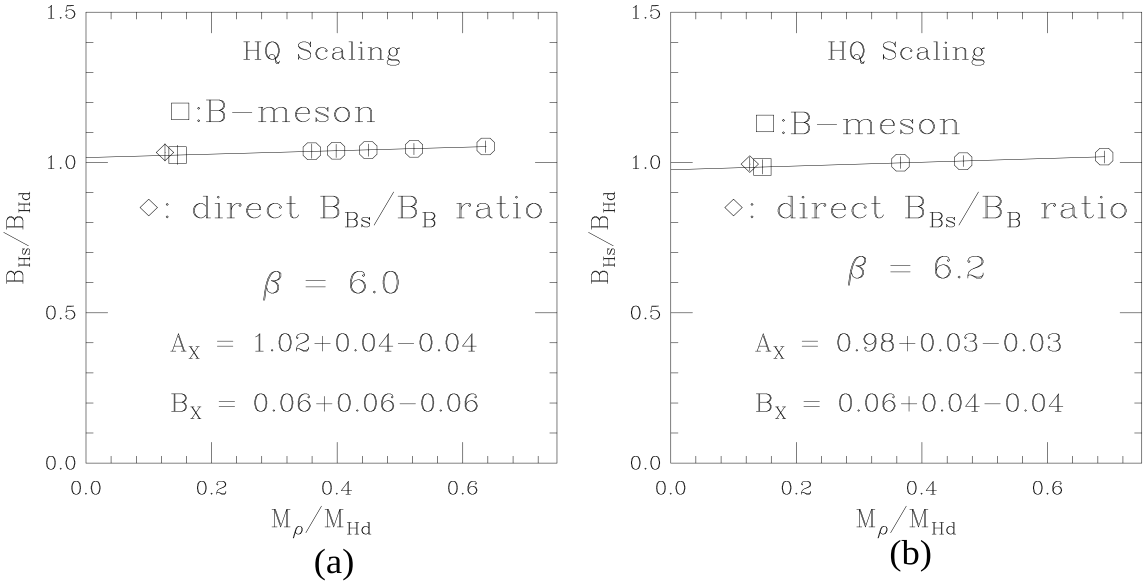

Figure 3.18: Scaling of B_{Hs}/B_{Hd} with respect to M_ρ/M_{Hd} at (a) $\beta = 6.0$ and (b) $\beta = 6.2$. The fitted flavour-$SU(3)$ breaking ratio at B-meson mass is consistent with the ratio taken between the extrapolated B_{B_s} and B_B. We only show the linear extrapolations of B_{Hs}/B_{Hd} with respect to M_ρ/M_{Hd}. As we have five heavy κ values at $\beta = 6.0$, we can investigate the contribution from the quadratic term M_ρ^2/M_{Hd}^2 in this heavy-quark-mass extrapolation. However, adding this quadratic term does not change A_X and B_X in (a), and the resulting C_X, which has a central value 2.14×10^{-5}, is consistent with zero.

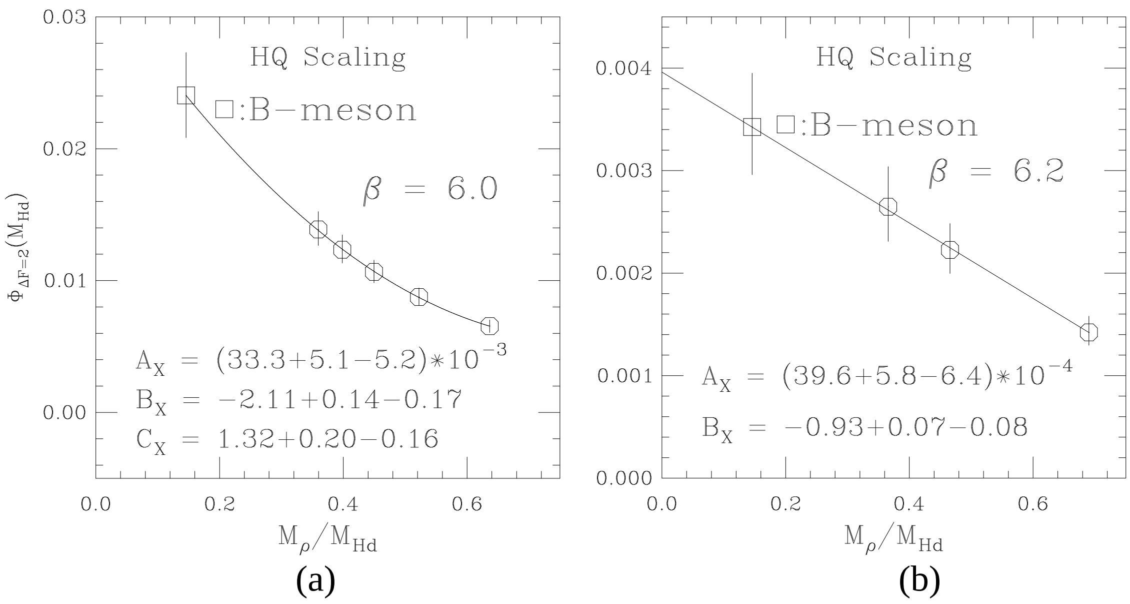

Figure 3.19: Scaling of $\Phi_{\Delta F=2}(M_{Hd})$ with respect to M_ρ/M_{Hd} at (a) $\beta = 6.0$ and (b) $\beta = 6.2$. The plot in (a) is a quadratic fit. It shows a large M_ρ/M_{Hd} dependence and a large M_ρ^2/M_{Hd}^2 dependence. B_X and C_X have opposite signs in this fit. The plot in (b) shows a smaller M_ρ/M_{Hd} dependence than the one in (a). However, from what is observed in (a), the extrapolation in (b) might not be a reliable one. This is because the M_ρ^2/M_{Hd}^2 dependence, which we are not able to investigate using three heavy-quark masses at $\beta = 6.2$, might be absorbed into the parameter B_X in this case.

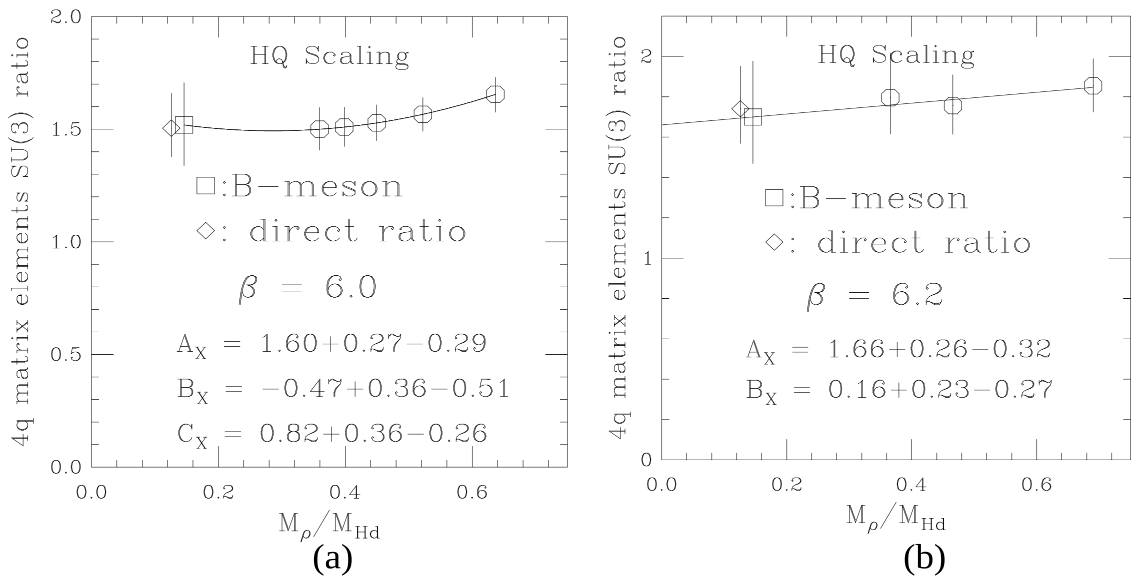

Figure 3.20: Scaling of $\mathcal{M}_{Hs}/\mathcal{M}_{Hd}$ with respect to M_ρ/M_{Hd} at (a) $\beta = 6.0$ and (b) $\beta = 6.2$. The fitted flavour-$SU(3)$ breaking ratio at B-meson mass is consistent with the ratio taken between the extrapolated $\mathcal{M}_{bs}$ and $\mathcal{M}_{bd}$. The plot in (a) is a quadratic fit. In this plot, we observe that the contribution from the quadratic term M_ρ^2/M_{Hd}^2 is larger than that from the linear term M_ρ/M_{Hd}. This might be explained by the large B_X observed in figure 3.19(a), see the text for details.

according to equations (3.101) and (3.102), where the meanings of the subscripts (superscripts) d and s are clear. The logarithmic dependences in $\Phi_{\Delta F_s=2}$ and $\Phi_{\Delta F_d=2}$ should be very similar. Assuming $B_X^d \sim B_X^s$, we expect that the $SU(3)$ breaking ratio $\mathcal{M}_{Hs}/\mathcal{M}_{Hd}$ has a small dependence upon the linear term M_ρ/M_{Hd} in its heavy-quark-mass extrapolation. However, a large B_X^d can result in a large M_ρ^2/M_{Hd}^2 dependence of this ratio, although it is reasonable to expect $C_X^s \sim C_X^d$.

These features show that heavy-quark-mass extrapolations are better controlled in the calculations of decay constants and B parameters than in the calculations of the mixing matrix elements. This point, together with what we have discussed in the last subsection, suggests that r_{sd} might be more reliably determined from the calculations of f_{B_s}/f_B and B_{B_s}/B_B, rather than from a direct calculation of $\mathcal{M}_{bs}$ and $\mathcal{M}_{bd}$.

3.4.4 Results and Systematic Errors

In this subsection, we present the results of heavy-light decay constants, B_{B_s}, B_B, their flavour-$SU(3)$ breaking ratios and r_{sd}. We do not present $\mathcal{M}_{bs}$ and $\mathcal{M}_{bd}$ because they contain large systematic errors, as we have discusses in the last two subsections. We also discuss the analysis of systematic errors. The systematic errors due to perturbative matching are estimated by using μ (the scale in $\alpha_{\overline{\rm MS}}(\mu)$ and the matching scale for four-fermion operators) at three different values, $1/a$, $2/a$ and π/a.

We first present the results of pseudo-scalar-meson decay constants and their flavour-$SU(3)$ breaking ratios at both β values (lattice spacing). They are summarised in table 3.6.

The results of decay constants presented in table 3.6 are from the method in which we set the lattice spacing using f_π. Hence they are free of the systematic errors due to perturbative matching. Here we mention that f_π varies for about 3% within the range of the strong coupling we use in Z_A. Therefore, if we set the lattice spacing by M_ρ, we will have a 3% systematic error due to the perturbative

Table 3.6: Results of decay constants and their flavour-$SU(3)$ breaking ratios. The error bars quoted here are only statistical.

β	f_{D_s} (MeV)	f_D (MeV)	f_{B_s} (MeV)	f_B (MeV)	f_{D_s}/f_D	f_{B_s}/f_B
6.0	239(6)	213(6)	221(7)	191(10)	1.12(1)	1.15(4)
6.2	221(9)	193(10)	190(12)	161(16)	1.15(4)	1.18(8)

matching, although the values of lattice spacing set by f_π (with $\alpha_{\overline{\mathrm{MS}}}(1/a)$ in Z_A) and M_ρ are very close to each other.

In table 3.6, we observe a quite large discrepancy between decay constants at the two different values of lattice spacing. The difference is about 2σ for f_D and f_B, and about 3σ for f_{D_s} and f_{B_s}. This strongly suggests that discretisation is the main source of systematic errors in lattice calculations of decay constants. In order to quantify these discretisation errors, we are undertaking analyses of heavy-light pseudo-scalar-meson decay constants

1. using the improved axial-vector current [40]

$$A_\mu^{\mathrm{I}} = A_\mu + c_A a \partial_\mu P, \tag{3.105}$$

   where P is the pseudo-scalar density. $a\partial_\mu P$ is a higher dimensional operator which serves as the counter term to remove the $\mathcal{O}(a)$ discretisation errors (recall the discussion in subsection 2.1.5). For tree-level improvement, $c_A = 0$. Formally, we do not have to take this operator mixing into account in the mean-field improvement prescription, as discussed in subsection 2.1.7. However, using this improved axial-vector current with the one-loop value for c_A [84], we can try to explore the $\mathcal{O}(am_q\alpha^s)$ discretisation errors (m_q is the quark mass) in the axial-vector current.

2. using different quark-field normalisations. From the discussion in subsection 2.1.5 and equation (2.50), we can see that using the one-loop value for b_A [84] in equation (2.50) can remove the $\mathcal{O}(am_q\alpha^s)$ errors arising from choosing a mass-independent renormalisation scheme.

These analyses will be finished in the near future, and hopefully will help us to quantify the discretisation errors in heavy-light decay constants. We temporarily quote the $\beta = 6.2$ results of decay constants and their $SU(3)$ ratios as our best estimates of these quantities (the discretisation errors in the $SU(3)$ ratios seem to be very small):

$$\begin{aligned} f_{D_s} &= 221(9)\ \text{MeV}, \\ f_D &= 193(10)\ \text{MeV}, \\ f_{B_s} &= 190(12)\ \text{MeV}, \\ f_B &= 161(16)\ \text{MeV}, \\ \frac{f_{D_s}}{f_D} &= 1.15(4), \\ \frac{f_{B_s}}{f_B} &= 1.18(8), \end{aligned}$$

where the errors are statistical.

Results of the B parameters and their flavour-$SU(3)$ breaking ratios at both β values are summarised in table 3.7. We present our results of B parameters renormalised at 5GeV in NDR-$\overline{\text{MS}}$ scheme. Here we actually use the two-step procedure introduced in subsection 3.3.2. The strong coupling used in the two-loop running in the NDR-$\overline{\text{MS}}$ scheme is run down from Z^0-boson mass M_Z using $\alpha_s(M_Z) = 0.118$ and two-loop QCD β function.

From the method we use to estimate the systematic errors due to perturbative matching, these errors are small for B parameters. Varying q amongst $1/a$, $2/a$ and π/a causes a less than 3% change in B parameters. The discretisation errors seem to be small too, as the values of B_{B_s} and B_B are quite stable with respect to the change of the lattice spacing. However, with only two values of the lattice spacing, it is difficult to draw strong conclusions. A plausible way of estimating the discretisation errors might be comparing our extrapolated static B parameters

Table 3.7: Results of B parameters in NDR-$\overline{\rm MS}$ scheme and their flavour-$SU(3)$ breaking ratios. The error bars quoted here are only statistical. $B_{B_s}^{\rm ext-sta}$ and $B_B^{\rm ext-sta}$ are the 'extrapolated-static' results, *i.e.*, results extrapolated to the limit $M_{B_{(s)}} \to \infty$.

β	B_{B_s}(5GeV)	B_B(5GeV)	B_{B_s}/B_B	$B_{B_s}^{\rm ext-sta}$(5GeV)	$B_B^{\rm ext-sta}$(5GeV)
6.0	0.86(2)	0.83(4)	1.03(3)	0.94(2)	0.93(5)
6.2	0.85(2)	0.85(3)	0.99(3)	0.90(2)	0.93(4)

with a calculation done using tadpole-improved-clover light quarks and static heavy quarks, although this static calculation might have systematic errors from other sources, which have to be analysed carefully. We have not found results of this kind in the literature. This calculation will be performed by the UKQCD Collaboration in the near future. However, given the evidence presented above, it is reasonable to give B_{B_s}, B_B and their $SU(3)$ breaking ratio using our results at $\beta = 6.2$

$$B_{B_s}(5\mathrm{GeV}) = 0.85(2),$$

$$B_B(5\mathrm{GeV}) = 0.85(3),$$

$$\frac{B_{B_s}}{B_B} = 0.99(3),$$

where the errors are only statistical.

Finally, we present our results of r_{sd} in table 3.8. Two approaches are used to calculate this $SU(3)$ breaking ratio:

1. The direct calculation from taking the ratio between the directly calculated $\mathcal{M}_{bs}$ and $\mathcal{M}_{bd}$. (*Direct method*)
2. The indirect calculation from combining the $SU(3)$ breaking ratios of $f_{B_{(s)}}$ and $B_{B_{(s)}}$. (*Indirect method*)

Table 3.8: Results of r_{sd} from direct and indirect calculations at both β values we have.

β	$\mathcal{M}_{bs}/\mathcal{M}_{bd}$	$\left(\frac{M_{B_s}f_{B_s}}{M_B f_B}\right)^2 \frac{B_{B_s}}{B_B}$
6.0	1.52(19)	1.38(7)
6.2	1.70(28)	1.37(13)

At both β values, the direct calculation of r_{sd} is compatible with the indirect calculation within error bars. However, the direct calculations have much bigger statistical errors, and might have larger systematic errors due to the uncertainties in quark-mass extrapolations, as we have discussed in the last two subsections. Therefore, we quote the indirect calculation at $\beta = 6.2$ with only statistical error as our best estimate of r_{sd}

$$r_{sd} = 1.37(13), \tag{3.106}$$

with a word of caution that we still need to improve the statistics in calculating this ratio by the direct method.

3.4.5 Comparison with Other Calculations

We now compare our results of B_{B_s}, B_B and r_{sd} with other lattice calculations. An extensive comparison of our results of decay constants and other calculations can be found in [85]. Here we just stress that our results for decay constants at $\beta = 6.2$ are well compatible with the two recent world averages in references [66] and [85]. As mentioned in the beginning of this chapter, lattice calculations of matrix elements of $B^0_{(s)}-\bar{B}^0_{(s)}$ mixing processes and their B parameters using static heavy quarks contain large systematic errors arising from the operator matching between the lattice and the continuum scheme. Therefore, here we only compare with the calculations using propagating heavy quarks.

In table 3.9, we can see that our results of B_{B_s} and B_B are consistent with other calculations using propagating heavy quarks from Wilson-type fermion actions. Here we add a word of caution that BBS and JLQCD perform lattice

Table 3.9: Comparison of our result of B_B and B_{B_s} with other calculations using propagating heavy quarks from Wilson-type fermion actions. $m_b = 5$ GeV. JLQCD presented calculations at $\beta = 6.1$ and $\beta = 6.3$, here we only quote their results at $\beta = 6.3$. The results from BBS are already extrapolated to the continuum limit.

Authors	c_{SW}	$B_B(m_b)$	$B_{B_s}(m_b)$
This Work	$1/u_0^3$	0.85(3)	0.85(2)
BBS[62]	0	0.96(12)	0.96(12)
JLQCD[61]	0	0.840(60)	0.878(32)
ELC[60]	0	0.84(5)	
BDHS[59]	0	0.95(14)	

simulations using heavy-quark masses in the beauty-mass regime, where $am_q > 1$ (m_q is the quark mass). These authors use meson kinetic masses, defined in [86] and [87], in investigating heavy-quark-mass scaling properties of matrix elements of four-fermion operators and their B parameters.

Table 3.10 shows that our results of r_{sd} are also consistent with other calculations using propagating Wilson-type fermion actions, although the results in this table all contain large errors. Here we choose to present our result at $\beta = 6.0$ when comparing r_{sd} calculated from direct method. This is because the heavy-quark-mass extrapolations at $\beta = 6.0$ are more reliable than those at $\beta = 6.2$ in calculating $\mathcal{M}_{bs}$ and $\mathcal{M}_{bd}$ (*c.f.*, figure 3.19). ELC presented $f_{B_s}^2 B_{B_s}/f_B^2 B_B = 1.19(10)$ in their paper [60], we then take this number and the $B_{(s)}-$meson masses from [83] to obtain the r_{sd} quoted here.

Table 3.10: Comparison of our result of r_{sd} with other calculations using propagating heavy quarks from the Wilson fermion action. Results from BBS are already extrapolated to the continuum limit.

Authors	direct	indirect
This Work	1.52(19)	1.37(13)
BBS[62]	$1.76(10)^{+57}_{-42}$	$1.42(5)^{+28}_{-15}$
ELC[60]		1.23(10)

Chapter 4

Kaon Mixing and Decays

FCNC processes in kaon systems have been crucial in the development of the Standard Model. For instance, in 1974, the charm-quark mass was estimated through low-energy phenomenology of kaon mixing [69] before the experimental discovery of the charm quark. However, a clean analysis of these FCNC processes is very difficult because of the long-distance effects enhanced by the $\Delta I = 1/2$ rule. In this chapter, we will not present any analysis of the $\Delta I = 1/2$ rule, as a precise lattice calculation of this phenomenon is still hard to achieve [88] due to the mixing with lower-dimension operators. The lattice calculations we present in this chapter include:

1. the short-distance electroweak contribution to K^0–$\bar{K}^0$ mixing, which helps to constrain the unitarity triangle in figure 1.1, and is a plausible description of indirect CP violation in $K_L \to \pi\pi$ [89].

2. B parameters of four-fermion-operator matrix elements of the purely $\Delta I = 3/2$ electromagnetic-penguin contributions in $K \to \pi\pi$ decays. These EM penguin contributions are potentially important for describing direct CP violation in kaon systems in the framework of the Standard Model.

We start with a brief review of the phenomenology of the processes examined in this chapter. We then present high-statistics lattice calculations of the B_K, $B_7^{3/2}$ and $B_8^{3/2}$ parameters. B_K is the B parameter of the matrix element of the $\Delta S = 2$ four-fermion operator, which appears in the analysis of the short-distance electroweak contribution to the $K^0 - \bar{K}^0$ mixing process. B_K is also a very interesting quantity to look at from the point of view of lattice field theory, as it is very sensitive to chiral symmetry breaking, and Wilson-type fermion actions break chiral symmetry explicitly. $B_7^{3/2}$ and $B_8^{3/2}$ are the B parameters relevant for purely $\Delta I = 3/2$ EM penguin contributions in non-leptonic kaon decays.

4.1 Phenomenology

In this section, we start with a phenomenological description of kaon CP violation. We then outline the anatomy of ϵ'/ϵ in the framework of the Standard Model.

4.1.1 CP Violation in Kaon Systems: the Story of ϵ'/ϵ

In this subsection, we review the phenomenology of direct and indirect kaon CP violations. Indirect CP violation is induced by the mixing of a neutral kaon and its anti-particle. Before discussing this $K^0 - \bar{K}^0$ mixing, we stress that all the results in the purely phenomenological analysis of $B^0 - \bar{B}^0$ mixing in subsection 3.1.1 apply to neutral kaon mixing, with B meson states replaced by kaon states. However, as we shall see in the next subsection, the Standard Model dynamics involved in $K^0 - \bar{K}^0$ mixing are very different from the ones in $B^0 - \bar{B}^0$ mixing.

Kaons can decay into pions non-leptonically. Let's consider $K \to \pi\pi$ decays. π^0 is a CP eigenstate, while π^+ and π^- are CP-conjugate with each other. We choose the phase convention such that

$$\mathrm{CP}|\pi^0\rangle = -|\pi^0\rangle, \tag{4.1}$$

$$\mathrm{CP}|\pi^+\rangle = -|\pi^-\rangle, \tag{4.2}$$

$$\mathrm{CP}|\pi^-\rangle = -|\pi^+\rangle. \tag{4.3}$$

The two final-state pions must be in a S-wave ($l = 0$) state, therefore all the two-pion final states are CP even

$$\mathrm{CP}|\pi\pi\rangle = |\pi\pi\rangle \tag{4.4}$$

Also, it is obvious that a three-pion final state is CP-odd. Therefore, in a CP-conserving world, the weak-interaction eigenstates, K_L and K_S, would be CP eigenstates (*c.f.* equation (3.8)) and only have the modes of non-leptonic decay into pions

$$K_{\mathrm{L}} \longrightarrow \pi\pi\pi, \tag{4.5}$$

$$K_{\mathrm{S}} \longrightarrow \pi\pi. \tag{4.6}$$

However, from the discussion in subsection 3.1.1, $K^0-\bar{K}^0$ oscillations might cause CP violation. This is called indirect CP violation, as it happens through the mixture of CP eigenstates in physical kaons. Define the states

$$|K^0_\pm\rangle = \frac{1}{\sqrt{2}}\left[|K^0\rangle \mp |\bar{K}^0\rangle\right], \tag{4.7}$$

which are CP eigenstates

$$\mathrm{CP}|K^0_\pm\rangle = \pm|K^0_\pm\rangle, \tag{4.8}$$

we can parameterise $|K_{\mathrm{L,S}}\rangle$ as

$$|K_{\mathrm{L,S}}\rangle = \frac{1}{\sqrt{1+|\bar{\epsilon}|^2}}\left[|K^0_\mp\rangle + \bar{\epsilon}|K^0_\pm\rangle\right], \tag{4.9}$$

where $\bar{\epsilon}$ is introduced via the kaon analogue of equation (3.9).

There is also possibility of direct CP violation, which occurs because of CP-violating terms in the effective Hamiltonian describing non-leptonic kaon decays. $|K^0_-\rangle$ might decay into a two-pion state, which is CP-even. In order to discuss the phenomenology of the search of both direct- and indirect-CP-violation signals in the decay

$$K_L \longrightarrow \pi\pi, \tag{4.10}$$

we have to look closely at the generic features of $K \to \pi\pi$ decays.

Since the two-pion state is a S-wave state, Bose-Einstein symmetry implies that it has a total isospin 0 or 2. Kaons have isospin 1/2, so each $K \to \pi\pi$ decay has a $\Delta I = 1/2$ part and a $\Delta I = 3/2$ part. The matrix elements of these processes can be parameterised as

$$\langle\pi\pi(I=0)|\mathcal{H}_{\mathrm{eff}}|K^0\rangle = A_0 \mathrm{e}^{i\delta_0}, \tag{4.11}$$

$$\langle\pi\pi(I=2)|\mathcal{H}_{\mathrm{eff}}|K^0\rangle = A_2 \mathrm{e}^{i\delta_2}, \tag{4.12}$$

where $\mathcal{H}_{\text{eff}}$ is the effective Hamiltonian for $K \to \pi\pi$ decays. It is not difficult to write down the same decay-process matrix elements for $\bar{K}^0$ in terms of A_0 and A_2. δ_0 and δ_2 are phase shifts due to $I = 0$ and $I = 2$ final-state pion interactions. Since they arise from strong interactions, they are called strong phases. From the unitarity of the S matrix and CPT invariance, one can show that A_0 and A_2 are real numbers if there is no direct CP violation (as CP invariance implies time-reversal invariance). However, in the presence of direct CP violation (which is implemented via the complex phase η in the CKM matrix in the framework of the Standard Model), A_0 and A_2 could be complex, so there are also weak phases ξ_0 and ξ_2 in this situation,

$$A_0 = |A_0|\mathrm{e}^{i\xi_0}, \tag{4.13}$$

$$A_2 = |A_2|\mathrm{e}^{i\xi_2}. \tag{4.14}$$

Now we look at the matrix elements of neutral kaons decaying into two-pion final states. First, we have the decompositions of neutral two-pion states:

$$\langle\pi^+\pi^-| \;=\; \sqrt{\frac{2}{3}}\langle\pi^+\pi^-(I=0)| + \sqrt{\frac{1}{3}}\langle\pi^+\pi^-(I=2)| \tag{4.15}$$

$$\langle\pi^0\pi^0| \;=\; \sqrt{\frac{2}{3}}\langle\pi^0\pi^0(I=2)| - \sqrt{\frac{1}{3}}\langle\pi^0\pi^0(I=0)|. \tag{4.16}$$

From these decompositions, we can write down the $K^0 \to \pi\pi$ decay amplitudes as

$$A_{K^0\to\pi^+\pi^-} \;=\; |A_0|\mathrm{e}^{i\xi_0}\mathrm{e}^{i\delta_0} + \frac{|A_2|}{\sqrt{2}}\mathrm{e}^{i\xi_2}\mathrm{e}^{i\delta_2} \tag{4.17}$$

$$A_{K^0\to\pi^0\pi^0} \;=\; |A_0|\mathrm{e}^{i\xi_0}\mathrm{e}^{i\delta_0} - \sqrt{2}|A_2|\mathrm{e}^{i\xi_2}\mathrm{e}^{i\delta_2}. \tag{4.18}$$

$\bar{K}^0 \to \pi\pi$ decay amplitudes can also be written down in a similar fashion.

At this stage, we already have all the necessary information in order to parameterise the indirect and direct CP violations in $K_L \to \pi\pi$ decays. The parameter $\bar{\epsilon}$ in equation (4.9) parameterises the indirect CP violation. However, it is phase-dependent. An alternative is to use the parameter ϵ defined as

$$\epsilon = \bar{\epsilon} + i\xi_0. \tag{4.19}$$

As we shall see, this parameter is phase-independent. Using equations (4.9), (4.17) and (4.18), a straightforward calculation leads to the following measures of CP violation:

$$\frac{\langle\pi^+\pi^-|\mathcal{H}_{\rm eff}|K_L\rangle}{\langle\pi^+\pi^-|\mathcal{H}_{\rm eff}|K_S\rangle} \equiv \eta_{+-} \equiv \epsilon + \epsilon', \tag{4.20}$$

$$\frac{\langle\pi^0\pi^0|\mathcal{H}_{\rm eff}|K_L\rangle}{\langle\pi^0\pi^0|\mathcal{H}_{\rm eff}|K_S\rangle} \equiv \eta_{00} \equiv \epsilon - 2\epsilon', \tag{4.21}$$

where the parameter

$$\epsilon' = \frac{i{\rm e}^{i(\delta_2-\delta_0)}}{\sqrt{2}}\left|\frac{A_2}{A_0}\right|(\xi_2-\xi_0) \tag{4.22}$$

characterises direct CP violation through its dependence upon $(\xi_2 - \xi_0)$.

In K^0–$\bar{K}^0$ mixing, $\Delta m/\Delta\gamma$ (*c.f.*, equation (3.13)) is experimentally measured as 0.478 ± 0.003. Approximating this value by $1/2$ and using the fact that both direct and indirect CP violations are small effects, we can write

$$\epsilon \simeq \frac{{\rm e}^{i\frac{\pi}{4}}}{\sqrt{2}}\left(\frac{{\rm Im}M_{12}}{2{\rm Re}M_{12}} + \frac{{\rm Im}A_0}{2{\rm Re}A_0}\right), \tag{4.23}$$

$$\epsilon' \simeq \frac{iw{\rm e}^{i(\delta_2-\delta_0)}}{\sqrt{2}}\left(\frac{{\rm Im}A_2}{2{\rm Re}A_2} - \frac{{\rm Im}A_0}{2{\rm Re}A_0}\right), \tag{4.24}$$

where $w \equiv {\rm Re}A_2/{\rm Re}A_0 \simeq 1/22$ ($\Delta I = 1/2$ rule). From the above two equations, we observe some important characters of ϵ and ϵ' parameters:

1. ϵ is sensitive to the (indirect) CP violation in the mass matrix $\hat{M}$. ϵ' comes from the contributions of purely $\Delta S = 1$ decays.

2. ϵ and ϵ' are independent of phase convention. A phase shift λ in K^0,

$$|K^0\rangle \longrightarrow {\rm e}^{i\lambda}|K^0\rangle, \tag{4.25}$$

$$|\bar{K}^0\rangle \longrightarrow {\rm e}^{-i\lambda}|\bar{K}^0\rangle, \tag{4.26}$$

   will have the effect

$$\frac{{\rm Im}A_I}{{\rm Re}A_I} \longrightarrow \frac{{\rm Im}A_I}{{\rm Re}A_I} + \lambda, \tag{4.27}$$

$$\frac{{\rm Im}M_{12}}{{\rm Re}M_{12}} \longrightarrow \frac{{\rm Im}M_{12}}{{\rm Re}M_{12}} - 2\lambda, \tag{4.28}$$

   which leaves ϵ and ϵ' unchanged.

3. Any theoretical calculation of ϵ' cannot avoid facing the the difficulty of resolving the $\Delta I = 1/2$ rule, because of the term $(\mathrm{Im}A_0/2\mathrm{Re}A_0)$ in equation (4.24)[1]. In the literature, one can see a widely used convention, in which $\mathrm{Im}A_0$ is set to zero. However, this is not convenient for the Standard Model prediction of direct CP violation, as here the A_0 amplitude does have a CP violating phase, implemented by the complex phase in the CKM matrix.

Indirect CP violation has been well confirmed by experiments [89]. However, searching for direct CP violation is still one of the most challenging task in testing the CP-violation scenario of the Standard Model. ϵ' and ϵ can be experimentally studied through the measurements of the decay amplitudes relevant to the matrix elements in equations (4.20) and (4.21). However, the current experimental situation on ϵ' is still unclear. While the result of the NA31 collaboration at CERN indicates direct CP violation [90], the result of E731 at Fermilab indicates that ϵ'/ϵ is consistent with zero [91]. The values of ϵ'/ϵ given by these two experimental groups are:

$$\left|\frac{\epsilon'}{\epsilon}\right| = \begin{cases} (23 \pm 7) \times 10^{-4} & [\mathrm{NA31}]\,. \\ (7.4 \pm 5.9) \times 10^{-4} & [\mathrm{E731}]\,. \end{cases} \tag{4.29}$$

A non-zero ϵ'/ϵ indicates that there is a complex phase in the CKM matrix, and therefore rules out the superweak models in which all the CKM matrix elements are assumed to be real. The experiments undertaken by the NA48 collaboration at CERN and the KTEV collaboration at Fermilab will hopefully constrain the experimental prediction of ϵ'/ϵ to a precision level with errors smaller than 10^{-4}.

4.1.2 Effective Hamiltonians

In the last subsection, we have reviewed the phenomenology of ϵ'/ϵ. In this subsection, we will discuss the Standard Model dynamics involved violations in the kaon sector.

[1] In equation (4.23), this term is assumed to be much smaller than $(\mathrm{Im}M_{12}/2\mathrm{Re}M_{12})$, as evidence shows direct CP violation is much smaller than indirect CP violation.

We start with the parameter ϵ. In equation (4.23), the important contribution is from ($\mathrm{Im}M_{12}/2\mathrm{Re}M_{12}$), as the direct CP violation is very small. Therefore, we have to examine what the Standard Model dynamics predicts for the mixing mass matrix $\hat{M}$. In analogy to equation (3.13), we have the relation

$$\Delta M_K \equiv \Delta m \simeq 2\mathrm{Re}M_{12}, \tag{4.30}$$

using the fact that CP violation is a small effect. ΔM_K can be measured by the time evolution of a neutral kaon state which is produced via a strong-interaction process, and hence starts as either a pure K^0 or $\bar{K}^0$. It has been very precisely measured to be

$$\Delta M_K = (3.522 \pm 0.016) \times 10^{-12}\ \mathrm{MeV}. \tag{4.31}$$

Therefore, we want to estimate $\mathrm{Im}M_{12}$. In the Standard Model, the leading short-distance electroweak contribution is from the $\Delta S = 2$ box diagrams, such as the one shown in figure 4.1. As already discussed in subsection 3.1.2, the c-quark contribution is an order of magnitude bigger than the t-quark contribution in the loop in the $\Delta S = 2$ box diagram. Also, CKM factor for the long-distance contributions via two $\Delta S = 1$ processes are of the same order as the c-quark contribution in the box diagrams. Therefore, these contributions should be suppressed by a factor $\simeq M_K^2/m_c^2 \simeq 1/10$ [2]with respect to the short-distance contribution. However, the $\Delta I = 1/2$ rule might modify this factor to be $(20M_K/m_c)^2 \simeq 40$. This makes it very difficult to be precise about the mass matrix $\hat{M}$, since there is still no reliable theoretical calculation of the $\Delta I = 1/2$ rule. In this work, we will only focus upon the short-distance electroweak contribution of K^0–$\bar{K}^0$ mixing, which results in the relation

$$2M_{K^0}\,(\mathrm{Im}M_{12})^{\mathrm{short-dist}} = \mathrm{Im}\langle\bar{K}^0|\mathcal{H}_{\mathrm{eff}}^{\Delta S=2}|K^0\rangle, \tag{4.32}$$

where M_{K^0} is the kaon mass. The factor $2M_{K^0}$ is from the normalisation of the kaon states. $\mathcal{H}_{\mathrm{eff}}^{\Delta S=2}$ is the effective Hamiltonian resulting from the $\Delta S = 2$ box diagram contributions. Using the same procedure as the one we used to obtain equation (3.20), this effective Hamiltonian can be written as (in the absence of QCD)

$$\mathcal{H}_{\mathrm{eff}}^{\Delta S=2} = \frac{G_F^2}{16\pi^2} M_W^2 \left[\lambda_c^2 F(x_c) + \lambda_t^2 F(x_t) + 2\lambda_c\lambda_t G(x_c, x_t)\right] \mathcal{O}_{LL}^{\Delta S=2}, \tag{4.33}$$

[2]The factor M_K^2 is from the phase space of kaon decays.

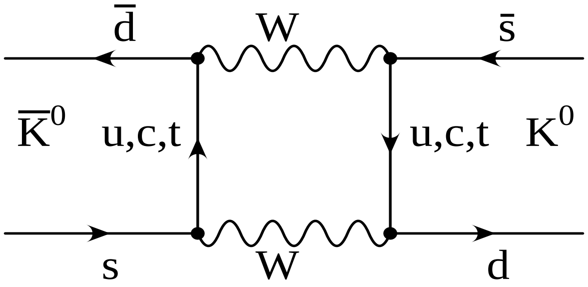

Figure 4.1: One of the Standard Model $\Delta S = 2$ box diagrams of $K^0{-}\bar{K}^0$ mixing

where $\lambda_c = V_{cs}V^*_{cd}$ and $\lambda_t = V_{ts}V^*_{td}$. The four-fermion operator $\mathcal{O}^{\Delta S=2}_{LL}$ is the left-left operator $[\bar{s}\gamma_\mu(1-\gamma_5)d\bar{s}\gamma^\mu(1-\gamma_5)d]$. The NLLA of the short-distance QCD effects in this effective Hamiltonian should have similar features as the one in $\mathcal{H}^{\Delta B=2}_{\text{eff}}$ in subsection 3.1.3, *i.e.*, the $\mathcal{O}(\alpha_s)$ scheme ambiguity and μ_t ambiguity should be removed. However, analysing the short-distance QCD effects in the $K^0{-}\bar{K}^0$ mixing process is more involved than the same analysis in the $B^0{-}\bar{B}^0$ mixing system, because of two reasons:

1. There are more terms in equation (4.33), which have to be evolved.
2. After performing an OPE at the scale of $\mathcal{O}(M_W)$, the c-quark is still a dynamical degree of freedom. Since the t-quark dominates the loop in the $\Delta B = 2$ box diagram, one does not have to take the c-quark into account. However, in the $K^0{-}\bar{K}^0$ mixing system, the c-quark contribution is significant in the loop in the $\Delta S = 2$ box diagram. Therefore, one has to deal with bilocal structures such as the one shown in figure 4.2, when evolving between the scales M_W and m_c.

NLLA calculations of the short-distance QCD effects in this $\Delta S = 2$ effective Hamiltonian can be found in references [68, 92, 93]. The resulting Hamiltonian is written as

$$\mathcal{H}^{\Delta S=2}_{\text{eff}} = \frac{G_F^2}{16\pi^2}M_W^2\left[\lambda_c^2\eta_1 S(x_c) + \lambda_t^2\eta_2 S(x_t) + 2\lambda_c\eta_3\lambda_t S(x_c,x_t)\right] b^{\Delta S=2}_{\text{NLLA}}(\mu)\mathcal{O}^{\Delta S=2}_{LL}(\mu), \tag{4.34}$$

where the Wilson coefficient has been split into two parts, the one in the square bracket only depends upon matching condition, while $b^{\Delta S=2}_{\text{NLLA}}(\mu)$ only accounts for

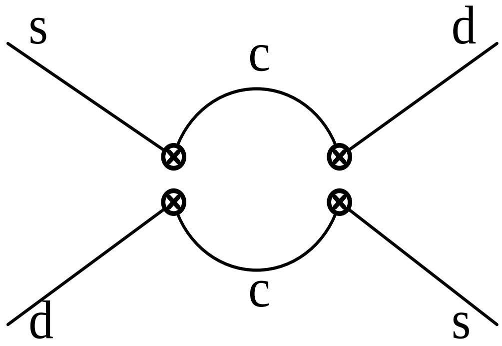

Figure 4.2: One of the bilocal structures obtained after performing OPE above the charm threshold for the $\Delta S = 2$ box diagrams.

the scale evolution and is independent of the matching condition. This $b^{\Delta S=2}_{\rm NLLA}(\mu)$ is actually identical to $b^{\Delta B=2}_{\rm NLLA}(\mu)$ introduced in equation (3.34), as the scale evolution is purely due to QCD effects, which are independent of the flavour content of the four-fermion operators to the leading order in the OPE. $S(x_i, x_j)$ is the relevant Inami-Lim function. η_1, η_2 and η_3 are from short-distance QCD effects. They do not depend upon the renormalisation scale μ, but they depend upon how the matching is done (*i.e.*, above or below the charm threshold).

Now we turn to the Standard Model dynamics which contribute to ϵ'. This time we need the $\Delta S = 1$ effective Hamiltonian, $\mathcal{H}^{\Delta S=1}_{\rm eff}$ (*c.f.*, equation (4.24)). The analysis of this Hamiltonian is a very complicated task, as there are ten operators which mix under renormalisation. Good reviews of this $\mathcal{H}^{\Delta S=1}_{\rm eff}$ and related subject can be found in references [94] and [95]. Here we will only give a very brief outline of the construction of this Hamiltonian, with stress upon the components we are calculating in this work, *i.e.*, the $\Delta I = 3/2$ part of electromagnetic penguin contributions. In constructing $\mathcal{H}^{\Delta S=1}_{\rm eff}$, we take into account the QED effects.

In the absence of QCD and QED, *i.e.*, $\alpha_s = \alpha_{\rm em} = 0$, there is only one $\Delta S = 1$ operator after integrating out the heavy W boson. It arises from the diagram in figure 1.5(a). This operator is traditionally called Q_2

$$Q_2 = (\bar{s}_\alpha u_\alpha)_{V-A} \, (\bar{u}_\beta d_\beta)_{V-A} \,, \tag{4.35}$$

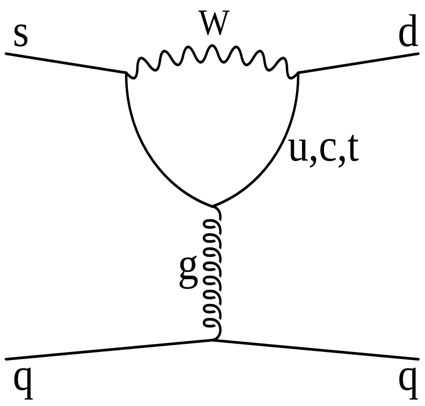

Figure 4.3: A QCD penguin diagram.

where α and β are colour indices, $(V \pm A)$ stand for the structure $\gamma_\mu(1 \pm \gamma_5)$. Taking QCD into account will introduce five more operators under renormalisation. Amongst these five operators, there is an operator Q_1 which is just the colour-mixed partner of Q_2,

$$Q_1 = (\bar{s}_\alpha u_\beta)_{V-A} (\bar{u}_\beta d_\alpha)_{V-A} = (\bar{s}_\alpha d_\alpha)_{V-A} (\bar{u}_\beta u_\beta)_{V-A} , \tag{4.36}$$

where we have used a Fierz transformation in the second step. The other four operators (Q_3, Q_4, Q_5 and Q_6) are called QCD penguins, as they come from penguin diagrams with a gluon propagator involved, figure 4.3

$$\begin{aligned}
Q_3 &= (\bar{s}_\alpha d_\alpha)_{V-A} \sum_{q=u,d,s} (\bar{q}_\beta q_\beta)_{V-A} , & (4.37)\\
Q_4 &= (\bar{s}_\alpha d_\beta)_{V-A} \sum_{q=u,d,s} (\bar{q}_\beta q_\alpha)_{V-A} , & (4.38)\\
Q_5 &= (\bar{s}_\alpha d_\alpha)_{V-A} \sum_{q=u,d,s} (\bar{q}_\beta q_\beta)_{V+A} , & (4.39)\\
Q_6 &= (\bar{s}_\alpha d_\beta)_{V-A} \sum_{q=u,d,s} (\bar{q}_\beta q_\alpha)_{V+A} . & (4.40)
\end{aligned}$$

It is instructive to look briefly at the kind of transition processes between K and $\pi\pi$ these operators can generate. First, we can see that Q_1 and Q_2 are singlet under $SU(3)_R$, as they both have purely left-left structure. In order to investigate the transformation properties of Q_1 and Q_2 under $SU(3)_L$, we look at the two operators

$$Q_1' = Q_1 - Q_2 = [(\bar{s}d)_L(\bar{u}u)_L - (\bar{s}u)_L(\bar{u}d)_L] , \tag{4.41}$$

$$Q_2' = Q_1 + Q_2 = [(\bar{s}d)_L(\bar{u}u)_L + (\bar{s}u)_L(\bar{u}d)_L]\,, \tag{4.42}$$

where spinors in the same parenthesis carry the same colour index, and we have written $V-A$ as 'left' (and we will write $V+A$ as 'right'). We can write Q_1' and Q_2' as the form

$$T^{ik}_{jl}\bar{q}^L_i q^L_j \bar{q}^L_k q^L_l, \tag{4.43}$$

where i, j, k, l are $SU(3)$ indices, with the convention

$$u \longrightarrow 1, \tag{4.44}$$

$$d \longrightarrow 2, \tag{4.45}$$

$$s \longrightarrow 3. \tag{4.46}$$

Then we see that for Q_1',

$$T^{31}_{21} = T^{13}_{12} = \frac{1}{2}, \;\; T^{31}_{12} = T^{13}_{21} = -\frac{1}{2}, \;\; \text{all other } T^{ik}_{jl} = 0. \tag{4.47}$$

Therefore, T is antisymmetric in the upper and lower indices, which means the four-quark operator Q_1' is antisymmetric under the exchange of two antiquarks and the exchange of two quarks. Bearing this in mind and using the tensor-algebra relations

$$(3 \times 3)_{\text{antisymm}} = \bar{3}, \tag{4.48}$$

$$(\bar{3} \times \bar{3})_{\text{antisymm}} = 3, \tag{4.49}$$

we can see that Q_1' can be represented as $3 \times \bar{3} = 8 + 1$ under the $SU(3)_L$ transformation. Since this operator describes the quark-level $s_L \to d_L$ transition, it cannot be flavour singlet. Therefore, we conclude that Q_1' is in the (8,1) representation under $SU(3)_L \times SU(3)_R$. We can apply this argument to Q_2'. In this case,

$$T^{31}_{21} = T^{13}_{12} = T^{31}_{12} = T^{13}_{21} = \frac{1}{2}, \;\; \text{all other } T^{ik}_{jl} = 0. \tag{4.50}$$

That is, T is symmetric in the upper and lower indices. This means we have to use the relations

$$(3 \times 3)_{\text{symm}} = 6, \tag{4.51}$$

$$(\bar{3} \times \bar{3})_{\text{symm}} = \bar{6}, \tag{4.52}$$

and Q_2' can be represented as $6 \times \bar{6} = 27 + 8 + 1$. However, this operator cannot be in the 27 representation since it is not traceless[3], and it cannot be in the singlet representation since it is not flavour singlet. We conclude that Q_2' is also in the (8,1) representation under $SU(3)_L \times SU(3)_R$. This can also be justified by the fact that Q_2' is related to Q_1' via gluon exchange, so they should be in the same irreducible representation under flavour $SU(3)_L \times SU(3)_R$. Therefore, Q_1 and Q_2 are both in (8,1) representation, as they are just linear combinations of Q_1' and Q_2'.

Using an argument which is very similar to the above one, we can show that Q_3 and Q_4 are also in the (8,1) representation under $SU(3)_L \times SU(3)_R$. As for Q_5 and Q_6, we can write them in the form

$$Q_{5,6} = (\bar{s}d)_L(\bar{u}u + \bar{d}d + \bar{s}s)_R \quad \text{(colour unmixed, mixed)}. \tag{4.53}$$

The $(\bar{s}d)_L$ is in the octet representation under $SU(3)_L$, and $(\bar{u}u + \bar{d}d + \bar{s}s)_R$ is singlet under $SU(3)_R$. That means $Q_{5,6}$ are both in the (8,1) representation under $SU(3)_L \times SU(3)_R$.

Therefore, the above six operators are all in the (8,1) representation. Q_1 and Q_2 can generate both $\Delta I = 1/2$ and $\Delta I = 3/2$ transitions. On the other hand, Q_3, Q_4, Q_5 and Q_6 only generate $\Delta I = 1/2$ transitions and only contribute to $(\mathrm{Im}A_0/2\mathrm{Re}A_0)$ in the estimate of ϵ' in equation (4.24). This is from the fact that these four operators involve a $s \to d$ transition, and the quark-qluon vertex must be flavour-singlet. It can be argued [96, 97] that the $(V-A)\times(V+A)$ chiral structure of Q_6 enhances its matrix elements by an order of magnitude[4]. Hence most analyses of $(\mathrm{Im}A_0/2\mathrm{Re}A_0)$ only include this operator. Calculating matrix elements of Q_6 is a very difficult task due to mixing with lower dimensional operators on the lattice, and is beyond the scope of this work.

In addition to the above six operators, there are also four electroweak-penguin (figure 4.4) operators

---

[3]From the tensor method for classifying irreducible representations of Lie groups, the highest-dimension irreducible representation must be traceless.

[4]Of course, matrix elements of Q_5 receive the same enhancement as well. However, the colour-mixed $(V-A)\times(V+A)$ structure has a larger overlap with pseudo-scalar-meson states than its colour-unmixed counterpart. We will discuss this point in subsection 4.2.2.

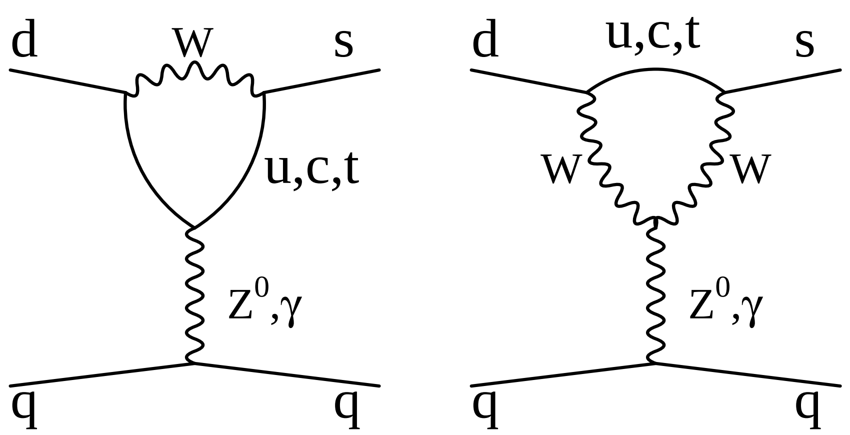

Figure 4.4: Electroweak penguin diagrams.

$$
\begin{aligned}
Q_7 &= \frac{3}{2}(\bar{s}_\alpha d_\alpha)_{V-A} \sum_{q=u,d,s} e_q\,(\bar{q}_\beta q_\beta)_{V+A}\,, &(4.54)\\
Q_8 &= \frac{3}{2}(\bar{s}_\alpha d_\beta)_{V-A} \sum_{q=u,d,s} e_q\,(\bar{q}_\beta q_\alpha)_{V+A}\,, &(4.55)\\
Q_9 &= \frac{3}{2}(\bar{s}_\alpha d_\alpha)_{V-A} \sum_{q=u,d,s} e_q\,(\bar{q}_\beta q_\beta)_{V-A}\,, &(4.56)\\
Q_{10} &= \frac{3}{2}(\bar{s}_\alpha d_\beta)_{V-A} \sum_{q=u,d,s} e_q\,(\bar{q}_\beta q_\alpha)_{V-A}\,, &(4.57)
\end{aligned}
$$

where e_q is the electric charge carried by the quark. We now look at the structures of these operators. For $Q_{7,8}$, we can write them in the form

$$Q_{7,8} = e(\bar{s}d)_L\left(\bar{u}u - \frac{1}{2}\bar{d}d - \frac{1}{2}\bar{s}s\right)_R \quad \text{(colour unmixed, mixed)}, \tag{4.58}$$

where e is the electron charge. The $(\bar{s}d)_L$ structure is clearly in the octet representation under $SU(3)_L$. The right-handed component $[\bar{u}u - (1/2)\bar{d}d - (1/2)\bar{s}s]_R$ is the traceless part in the $SU(3)$ algebraic relation $\bar{3}\times 3 = 8+1$, hence it is also in the octet representation. Therefore, Q_7 and Q_8 are in (8,8) under $SU(3)_L \times SU(3)_R$. They can contribute to both $\Delta I = 1/2$ and $\Delta I = 3/2$ transitions between K and $\pi\pi$. This can be seen from the fact that $(\bar{s}d)_L$ carries $\Delta I = 1/2$, and the right-handed part can be decomposed into a linear combination of $\Delta I = 0$ and $\Delta I = 1$ transitions according to

$$\left(\bar{u}u - \frac{1}{2}\bar{d}d - \frac{1}{2}\bar{s}s\right)_R = \frac{3}{4}\left(\bar{u}u - \bar{d}d\right)_R + \frac{1}{4}\left(\bar{u}u + \bar{d}d - 2\bar{s}s\right)_R. \tag{4.59}$$

Q_9 and Q_{10} can be shown to be in (27,1) representation under $SU(3)_L \times SU(3)_R$, and can also generate both $\Delta I = 1/2$ and $\Delta I = 3/2$ transitions.

From this observation, it has been argued [98] that the $\Delta I = 3/2$ parts of the EM penguin operators Q_7 and Q_8 contribute significantly to ϵ', although they are suppressed by a factor of $\alpha_{\rm em}/\alpha_s$ in comparison with the QCD-penguin operators. This argument is based upon two reasons

1. Q_7 and Q_8 transform as (8,8), while $Q_1, \ldots, Q_6$ transform as (8,1). From the predictions of Chiral Perturbation Theory, equations (2.96) and (2.98), we can see that $Q_1, \ldots, Q_6$ vanish in the chiral limit, while $Q_{7,8}$ contributions scale like constants[5].

2. The imaginary part of the matrix elements of purely $\Delta I = 3/2$ EM-penguin operators contribute to the phase of A_2. Since $\mathrm{Re}A_2$ is a small number in comparison with $\mathrm{Re}A_0$ ($\Delta I = 1/2$ rule), these operators might give significant contributions to ϵ' via the enhancement of $(\mathrm{Im}A_2/\mathrm{Re}A_2)$ in equation (4.24).

From the above discussion, we are strongly motivated to investigate the matrix elements of the $\Delta I = 3/2$ parts of Q_7 and Q_8. We will call them $\mathcal{O}_7^{3/2}$ and $\mathcal{O}_8^{3/2}$ throughout this work,

$$\mathcal{O}_7^{3/2} = \left(\bar{s}_\alpha \gamma_\mu^{\rm L} d_\alpha\right) \left[\bar{u}_\beta \gamma_{\rm R}^\mu u_\beta - \bar{d}_\beta \gamma_{\rm R}^\mu d_\beta\right] + \left(\bar{s}_\alpha \gamma_\mu^{\rm L} u_\alpha\right) \left(\bar{u}_\beta \gamma_{\rm R}^\mu d_\beta\right), \quad (4.60)$$

$$\mathcal{O}_8^{3/2} = \left(\bar{s}_\alpha \gamma_\mu^{\rm L} d_\beta\right) \left[\bar{u}_\beta \gamma_{\rm R}^\mu u_\alpha - \bar{d}_\beta \gamma_{\rm R}^\mu d_\alpha\right] + \left(\bar{s}_\alpha \gamma_\mu^{\rm L} u_\beta\right) \left(\bar{u}_\beta \gamma_{\rm R}^\mu d_\alpha\right), \quad (4.61)$$

where $\gamma_\mu^{\rm R} = \gamma_\mu(1+\gamma_5)$ and $\gamma_\mu^{\rm L} = \gamma_\mu(1-\gamma_5)$.

RG analysis of the scale evolution of $\mathcal{H}_{\rm eff}^{\Delta S=1}$ in NLLA [95, 99, 100] is much more involved than the one for $\mathcal{H}_{\rm eff}^{\Delta S=2}$. In addition to the fact that there are ten operators which mix under renormalisation, the presence of QED contributions to the scale evolution makes this analysis very complicated. The first step is

[5] $Q_{9,10}$ are in the (27,1) representation. Therefore, equation (2.97) predicts that their matrix elements should vanish in the chiral limit too. Also, as we shall see in the next section, the $(V-A)\times(V+A)$ structure of $Q_{7,8}$ enhances their matrix elements.

to calculate the Wilson coefficients at the scale M_W where we match the low-energy effective theory describing $\Delta S = 1$ transitions to the full Standard Model (*c.f.*, equation (1.21)). In NLLA, this matching has to be done at $\mathcal{O}(\alpha_s)$ and $\mathcal{O}(\alpha_{\rm em})$. At this order, top-quark contributions dominate the loops in the penguin diagrams (from the argument of CKM factors and the asymptotic behaviours of the relevant Inami-Lim functions). Here we just list the Wilson coefficients of Q_7 and Q_8 at the the scale M_W [100]

$$C_7(M_W) = \frac{\alpha_{\rm em}}{6\pi}\left[4C_0(x_t) + \tilde{D}_0(x_t)\right], \tag{4.62}$$

$$C_8(M_W) = 0, \tag{4.63}$$

where C_0 and $\tilde{D}_0$ are the relevant Inami-Lim functions. Because of the complication arising from the inclusion of QED effects, the scale-evolution function for the Wilson coefficients is more complicated than the one introduced in equation (1.60). In this case, it is [100]

$$\hat{U}_c(\mu_1,\mu_2;\alpha_{\rm em}) = T_g \exp \int_{g(\mu_2)}^{g(\mu_1)} dg' \frac{\hat{\gamma}^T(g',\alpha_{\rm em})}{\beta(g')}, \tag{4.64}$$

where $\hat{\gamma}(g',\alpha_{\rm em})$ is the 10×10 anomalous dimension matrix including QCD and QED contributions, it can be expanded as

$$\hat{\gamma}(g',\alpha_{\rm em}) = \frac{\alpha_s}{4\pi}\hat{\gamma}_s^{(0)} + \frac{\alpha_s^2}{16\pi^2}\hat{\gamma}_s^{(1)} + \cdots + \frac{\alpha_{\rm em}}{4\pi}\left[\hat{\gamma}_{\rm em}^{(0)} + \frac{\alpha_s}{4\pi}\hat{\gamma}_{\rm sem}^{(1)} + \cdots\right]. \tag{4.65}$$

$\hat{\gamma}_s^{(0)}$ and $\hat{\gamma}_s^{(1)}$ are one- and two-loop anomalous dimension matrices arising purely from QCD effects, while $\hat{\gamma}_{\rm em}^{(0)}$ and $\hat{\gamma}_{\rm sem}^{(1)}$ are from the presence of QED corrections. Numerical values of the matrix elements of these four 10×10 matrices have been calculated by the authors of [95], [99] and [100]. On the other hand, the scale-evolution function for the operators $Q_1,\cdots,Q_{10}$ is also slightly complicated than the one introduced in equation (1.70). In this case, it is

$$\hat{U}(\mu_1,\mu_2;\alpha_{\rm em}) = T_g \exp \int_{g(\mu_2)}^{g(\mu_1)} dg' \frac{-\hat{\gamma}(g',\alpha_{\rm em})}{\beta(g')}. \tag{4.66}$$

This scale-evolution function can be decomposed as

$$\hat{U}(\mu_1,\mu_2;\alpha_{\rm em}) = \hat{U}^s(\mu_1,\mu_2) + \frac{\alpha_{\rm em}}{4\pi}\hat{R}(\mu_1,\mu_2), \tag{4.67}$$

where $\hat{U}^s(\mu_1, \mu_2)$ is from the pure QCD contributions, and $\hat{R}(\mu_1, \mu_2)$ arises from the QED corrections. In NLLA, $\hat{U}^s(\mu_1, \mu_2)$ sums the leading logarithms $\alpha_s^n \ln^n(\mu_2^2/\mu_1^2)$ and the next-to-leading logarithms $\alpha_s^{n+1} \ln^n(\mu_2^2/\mu_1^2)$, while $\hat{R}(\mu_1, \mu_2)$ sums the logarithms $[\ln(\mu_2^2/\mu_1^2)\alpha_s^n \ln^n(\mu_2^2/\mu_1^2)]$ and $\alpha_s^n \ln^n(\mu_2^2/\mu_1^2)$. In this work, we need to evolve the scale in a range of a few GeV, where α_s is between 0.1 and 0.2. Therefore, the contributions from the logarithms summed by $\hat{R}(\mu_1, \mu_2)$ are much smaller than the ones summed by $\hat{U}^s(\mu_1, \mu_2)$, as they are suppressed by the factor $\alpha_{\mathrm{em}}/\alpha_s$. Hence we drop $\hat{R}(\mu_1, \mu_2)$ in performing the two-loop running of $B_7^{3/2}$ and $B_8^{3/2}$. As we will see in the next section, we are performing lattice calculations of $B_7^{3/2}$ and $B_8^{3/2}$ in the chiral limit. In this case, Q_7 and Q_8 mix with each other under renormalisation, but not with the other eight operators. Under these circumstances, we have the one- and two-loop anomalous dimension matrices

$$\hat{\gamma}_{78}^{(0)} = \begin{pmatrix} 2 & -6 \\ 0 & -16 \end{pmatrix}, \tag{4.68}$$

$$\hat{\gamma}_{78}^{(1)} = \begin{pmatrix} \frac{71}{3} - \frac{22n_f}{9} & -99 + \frac{22n_f}{3} \\ \frac{-225}{2} + 4n_f & \frac{-1343}{6} + \frac{68n_f}{9} \end{pmatrix}, \tag{4.69}$$

where n_f is the number of active flavours. We then use these two matrices and equation (1.72) to perform two-loop running[6] for $B_7^{3/2}$ and $B_8^{3/2}$.

4.2 Lattice Calculation

Our goal is to non-perturbatively calculate the matrix elements

$$\langle \bar{K}^0 | \mathcal{O}_{LL}^{\Delta S=2}(\mu) | K^0 \rangle, \tag{4.70}$$

$$\langle \pi\pi | \mathcal{O}_7^{3/2}(\mu) | K \rangle, \tag{4.71}$$

$$\langle \pi\pi | \mathcal{O}_8^{3/2}(\mu) | K \rangle, \tag{4.72}$$

[6] As we shall see in the next section, in order to perform two-loop running for $B_7^{3/2}$ and $B_8^{3/2}$ we still need to know the one- and two-loop anomalous dimensions for the pseudo-scalar density quark bilinear. We will present this anomalous dimension then.

using Lattice QCD. μ is the renormalisation scale. However, in calculating the $K \to \pi\pi$ transition matrix elements, we have to deal with the two-pion final state. In the limit of large Euclidean time, the final state with two rest pions dominates. However, this state is not the one we need in calculating the matrix elements of $K \to \pi\pi$ decays. This makes the lattice calculation of these matrix elements difficult. A remedy [101, 102, 103] of this problem is to use Chiral Perturbation Theory prediction to relate the matrix elements $\langle\pi\pi|\mathcal{O}^{3/2}(\mu)|K\rangle$ to the matrix elements $\langle\pi|\mathcal{O}^{3/2}(\mu)|K^+\rangle$

$$\langle\pi^+\pi^0|\mathcal{O}^{3/2}|K^+\rangle = \frac{-i}{f_\pi}\langle\pi^+|\mathcal{O}^{3/2}|K^+\rangle. \tag{4.73}$$

However, this is just a result from the lowest-order Chiral Perturbation Theory. Therefore, throughout this work, we study (the B parameters of) the matrix elements $\langle\pi^+|\mathcal{O}^{3/2}(\mu)|K^+\rangle$ *in the chiral limit*, where u, d and s are massless[7]. These matrix elements can be related to $\Delta I = 3/2$ $K \to \pi\pi$ decay matrix elements through equation (4.73). In the end, we are investigating

$$\langle\bar{K}^0|\mathcal{O}_{LL}^{\Delta S=2}(\mu)|K^0\rangle, \tag{4.74}$$

$$\langle\pi^+|\mathcal{O}_7^{3/2}(\mu)|K^+\rangle, \tag{4.75}$$

$$\langle\pi^+|\mathcal{O}_8^{3/2}(\mu)|K^+\rangle. \tag{4.76}$$

As addressed in section 3.2, these matrix elements are of dimension four. That means they have a strong dependence upon the lattice spacing. Therefore, we study their B parameters (subsection 3.1.4), which are dimensionless and are expected to have much smaller dependence upon the lattice spacing than the matrix elements themselves. The vacuum-saturation approximation of the above matrix elements and their B parameters will be discussed in subsection 4.2.2.

[7]Since the typical scale for chiral symmetry breaking is 1 GeV, one would expect that this approximation has a $\left(M_K^2/(1GeV)^2\right) \sim 20\%$ error.

4.2.1 Simulation Details

The simulation details are the same as those presented in subsection 3.2.1 (table 3.1). We use the three κ_l values in table 3.2 for light-quark masses. In the investigation of the chiral behaviour of the $\Delta S = 2$ operator, we need the recoil variable $(p \cdot q)$, where p is the four-momentum carried by K^0 and q is the four-momentum carried by $\bar{K}^0$. Bearing in mind that the energies of the pseudo-scalar mesons can be determined from fitting the large-time behaviour of the correlator in equation (3.63), we only need to implement the spatial components of the momenta at simulation time. We use spatial momenta $(2\pi/L, 0, 0)$, $(0, 2\pi/L, 0)$ and $(0, 0, 2\pi/L)$ for K^0 and $\bar{K}^0$. Here L is the number of lattice points in the spatial directions, therefore $L = 16$ at $\beta = 6.0$ and $L = 24$ at $\beta = 6.2$.

4.2.2 Bag Parameters: B_K, $B_7^{3/2}$ and $B_8^{3/2}$

Let's start with the left-left $\Delta S = 2$ operator which accounts for the K^0–$\bar{K}^0$ oscillations. This operator has the same left-left structure as the $\Delta B = 2$ operator studied in the last chapter. Therefore, following the discussion in subsection 3.1.4, especially equations (3.37), (3.38) and (3.39), the B parameter of this matrix element (called B_K) at the renormalisation scale μ is defined as

$$B_K(\mu) = \frac{\langle \bar{K}^0(q)|\mathcal{O}_{LL}^{\Delta S=2}(\mu)|K^0(p)\rangle}{\langle \bar{K}^0(q)|\mathcal{O}_{LL}^{\Delta S=2}(\mu)|K^0(p)\rangle_{\mathrm{VS}}} = \frac{\langle \bar{K}^0(q)|\mathcal{O}_{LL}^{\Delta S=2}(\mu)|K^0(p)\rangle}{\frac{8}{3} f_K^2 (p \cdot q)}, \tag{4.77}$$

where p and q are the momenta carried by K^0 and $\bar{K}^0$ respectively. The renormalisation-scale independent B_K is defined as

$$\hat{B}_K = b^{\Delta S=2}(\mu) B_K(\mu). \tag{4.78}$$

Now we turn to the B parameters of $\mathcal{O}_7^{3/2}$ and $\mathcal{O}_8^{3/2}$. We first look at $\mathcal{O}_7^{3/2}$, which has the structure

$$\left(\bar{q}_\alpha^1 \gamma_\mu^{\mathrm{L}} q_\alpha^2\right) \left(\bar{q}_\beta^3 \gamma_{\mathrm{R}}^\mu q_\beta^4\right), \tag{4.79}$$

where $\gamma_\mu^{\mathrm{L}} = \gamma_\mu(1 - \gamma_5)$ and $\gamma_\mu^{\mathrm{R}} = \gamma_\mu(1 + \gamma_5)$. Its parity-conserving part is

$$\left(\bar{q}_\alpha^1 \gamma_\mu q_\alpha^2\right) \left(\bar{q}_\beta^3 \gamma^\mu q_\beta^4\right) - \left(\bar{q}_\alpha^1 \gamma_\mu \gamma_5 q_\alpha^2\right) \left(\bar{q}_\beta^3 \gamma^\mu \gamma_5 q_\beta^4\right), \tag{4.80}$$

which has the same structure as $\mathcal{O}_2$ in equation (3.77). Now we insert the vacuum state in all possible ways in the matrix element $\langle\pi^+|\mathcal{O}_2|K^+\rangle$. There are two different ways to insert the vacuum state. One is equivalent to leaving all the quark fields in their original positions in equation (4.80), the other one is equivalent to exchanging the flavours of q^2 and q^4 with their colours unchanged. The former one simply results in a term

$$\langle\pi^+|V^1_\mu|0\rangle\langle 0|V^\mu_2|K^+\rangle - \langle\pi^+|A^1_\mu|0\rangle\langle 0|A^\mu_2|K^+\rangle, \tag{4.81}$$

where V^i_μ are the local vector currents and A^i_μ are the local axial-vector currents with the correct flavour content. The latter one results in a term

$$\frac{2}{3}\left(\langle\pi^+|P^1|0\rangle\langle 0|P^2|K^+\rangle - \langle\pi^+|S^1|0\rangle\langle 0|S^2|K^+\rangle\right), \tag{4.82}$$

where S^i are the scalar-density local quark bilinears and P^i are the pseudo-scalar-density local quark bilinears with the correct flavour content. The factor 1/3 is from the arrangement of colour indices. Here we have used the Fierz identity

$$\begin{aligned} & (\bar{q}^1\gamma_\mu q^4)(\bar{q}^3\gamma^\mu q^2) - (\bar{q}^1\gamma_\mu\gamma_5 q^4)(\bar{q}^3\gamma^\mu\gamma_5 q^2) \\ = \;& 2\times\left[(\bar{q}^1\gamma_5 q^2)(\bar{q}^3\gamma_5 q^4) - (\bar{q}^1 q^2)(\bar{q}^3 q^4)\right] \end{aligned} \tag{4.83}$$

to bring the spinors to the positions which results in the transition between the kaon and the vacuum, and the transition between the pion and the vacuum. Because of parity and Lorentz symmetry, the vector current and the scalar density do not contribute to the matrix elements when sandwiched by the vacuum and a pseudo-scalar-meson state. Therefore, vacuum saturation of the matrix element $\langle\pi^+|\mathcal{O}^{3/2}_7|K^+\rangle$ leads to the result

$$\langle\pi^+|\mathcal{O}^{3/2}_7|K^+\rangle_{\rm VS} = \frac{2}{3}\langle\pi^+|P^1|0\rangle\langle 0|P^2|K^+\rangle - \langle\pi^+|A^1_\mu|0\rangle\langle 0|A^\mu_2|K^+\rangle. \tag{4.84}$$

However, the second term on the right hand side vanishes in the chiral limit, where we are performing the lattice calculation for $B^{3/2}_7$. In this limit, the vacuum-saturation approximation of the above matrix element becomes

$$\langle\pi^+|\mathcal{O}^{3/2}_7|K^+\rangle_{\rm VS} = \frac{2}{3}\langle\pi^+|P^1|0\rangle\langle 0|P^2|K^+\rangle. \tag{4.85}$$

A similar procedure leads to the result

$$\langle\pi^+|\mathcal{O}^{3/2}_8|K^+\rangle_{\rm VS} = 2\langle\pi^+|P^1|0\rangle\langle 0|P^2|K^+\rangle. \tag{4.86}$$

There are two important observations here:

1. The pseudo-scalar densities P^i have larger overlaps with pseudo-scalar-meson states than other quark bilinears. Hence we can expect that the contributions to the term $(\mathrm{Im}A_2/2\mathrm{Re}A_2)$ in ϵ' form $\mathcal{O}_7^{3/2}$ and $\mathcal{O}_8^{3/2}$ should be bigger than the contributions from $\mathcal{O}_9^{3/2}$ and $\mathcal{O}_{10}^{3/2}$ [8], especially $\mathcal{O}_8^{3/2}$ should have the biggest contribution amongst the EM-penguin operators. This is actually an important reason for why the contribution of the QCD-penguin operator $\mathcal{O}_6$ dominates the term $(\mathrm{Im}A_0/2\mathrm{Re}A_0)$ in ϵ'.

2. The vacuum-saturated matrix elements $\langle\pi^+|\mathcal{O}_7^{3/2}|K^+\rangle_{\mathrm{VS}}$ and $\langle\pi^+|\mathcal{O}_8^{3/2}|K^+\rangle_{\mathrm{VS}}$ depend upon the renormalisation scale μ, as the pseudo-scalar density P is not a symmetry current.

The B parameters $B_7^{3/2}$ and $B_8^{3/2}$ in the chiral limit are then defined as

$$B_7^{3/2}(\mu) = \frac{\langle\pi^+|\mathcal{O}_7^{3/2}(\mu)|K^+\rangle}{\frac{2}{3}\langle\pi^+|P(\mu)|0\rangle\langle 0|P(\mu)|K^+\rangle}, \tag{4.87}$$

$$B_8^{3/2}(\mu) = \frac{\langle\pi^+|\mathcal{O}_8^{3/2}(\mu)|K^+\rangle}{2\langle\pi^+|P(\mu)|0\rangle\langle 0|P(\mu)|K^+\rangle}, \tag{4.88}$$

where we do not distinguish the pseudo-scalar-density quark bilinears in $\langle\pi^+|P(\mu)|0\rangle$ and $\langle 0|P(\mu)|K^+\rangle$ any more.

4.2.3 Correlation Functions

In order to study B_K, it is obvious that the correlation function we need is similar to the one in equation (3.47). However, as we shall see later, we want to investigate the dependence of B_K upon the recoil variable in performing chiral extrapolation. Therefore, we need the correlation function

$$C^3_{\Delta S=2}(t_1, t_2; \vec{p}, \vec{q}) = \sum_{\vec{x},\vec{y}} \mathrm{e}^{-i\vec{p}\cdot\vec{x}}\mathrm{e}^{i\vec{q}\cdot\vec{y}}\langle P_{\mathrm{F}}^\dagger(\vec{y}, t_2)\mathcal{O}_{\mathrm{L}}^{\Delta S=2}(\vec{0}, 0)P_{\mathrm{F}}^\dagger(\vec{x}, t_1)\rangle, \tag{4.89}$$

where the notation follows the one introduced in subsection 3.2.2. Once again, we fix the operator $\mathcal{O}_{\mathrm{L}}^{\Delta S=2}$ at the space-time point $(\vec{0}, 0)$ and let t_1 and t_2 move

[8] $\mathcal{O}_9^{3/2}$ and $\mathcal{O}_{10}^{3/2}$ have left-left structure. Therefore, we only have axial-vector-current contributions in the vacuum saturation of the matrix elements $\langle\pi^+|\mathcal{O}_{9,10}^{3/2}|K^+\rangle$

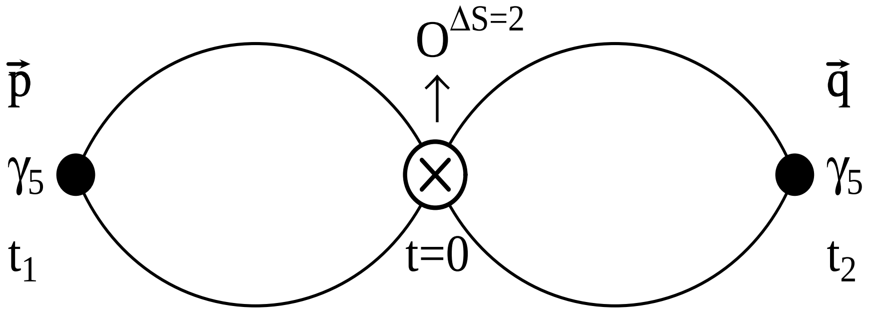

Figure 4.5: Three-point function for the $K^0-\bar{K}^0$ mixing

in the range

$$\frac{T}{2} < \quad t_1 \quad < T, \tag{4.90}$$

$$0 < \quad t_2 \quad < \frac{T}{2}. \tag{4.91}$$

This correlation function is depicted in figure 4.5. This diagram is known as the 'eight diagram'. The backward contaminations of this correlation function are similar to the ones in equations (3.53) and (3.54), with M_P replaced by the energy $E(M_P, \vec{p})$.

Notice that there is more than one lattice $\mathcal{O}^{\Delta S=2}$ which contributes to $K^0-\bar{K}^0$ mixing, because of explicit chiral symmetry breaking. This is also true for $\mathcal{O}_7^{3/2}$ and $\mathcal{O}_8^{3/2}$ in $K \to \pi\pi$ decays. As we shall see in the next section, all these operators have structures listed in equation (3.77). This offers a convenient way to obtain matrix elements of $\mathcal{O}_7^{3/2}$ and $\mathcal{O}_8^{3/2}$ from correlation functions similar to $C^3_{\Delta S=2}$. If we work out the Wick contraction of matrix elements of $\mathcal{O}_7^{3/2}$ and $\mathcal{O}_8^{3/2}$ in equations (4.60) and (4.61) with an initial one-kaon state and a final one-pion state, there are eye-diagram (penguin) contractions depicted in figure 4.6. These contractions will result in the mixing with lower dimensional operators, which makes the lattice calculations very difficult. However, these contributions will cancel amongst each other in the limit where isospin symmetry is exact. This means we do not have to take them into account, since we are investigating $\langle\pi^+|\mathcal{O}_7^{3/2}(\mu)|K^+\rangle$ and $\langle\pi^+|\mathcal{O}_8^{3/2}(\mu)|K^+\rangle$ in the chiral limit[9]. Therefore, we only

[9]Of course, lattice simulations are not done in this limit. We have to resort to Chiral Perturbation Theory to study these matrix elements in the chiral regime.

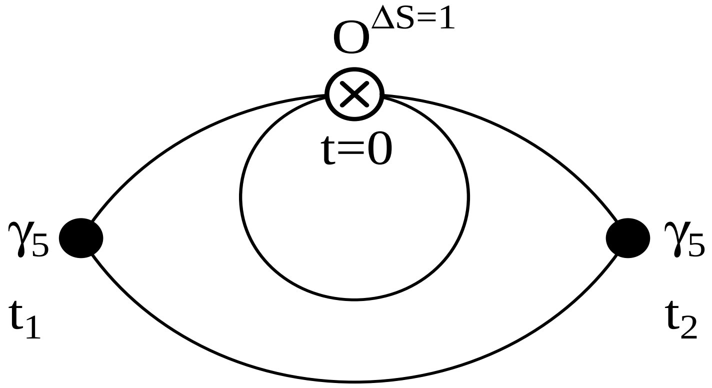

Figure 4.6: The eye-diagram (penguin) contraction for $\langle\pi^+|\mathcal{O}_7^{3/2}|K^+\rangle$ and $\langle\pi^+|\mathcal{O}_8^{3/2}|K^+\rangle$.

have the eight-diagram contributions which are the same as the contraction shown in figure 4.5, with $\mathcal{O}^{\Delta S=2}$ replaced by $\mathcal{O}^{\Delta S=1}$. Moreover, we do not need the dependence of $B_{7,8}^{3/2}$ upon the recoil variable to investigate their chiral behaviours. We then resort to the correlation function

$$C^3_{7,8}(t_1,t_2) = \sum_{\vec{x},\vec{y}} \langle P_{\rm F}^\dagger(\vec{y},t_2)(\mathcal{O}_{7,8}^{3/2})_{\rm L}(\vec{0},0)P_{\rm F}^\dagger(\vec{x},t_1)\rangle, \tag{4.92}$$

in the calculations of $B_{7,8}^{3/2}$. Note that this correlation function has the feature that the initial- and final-state mesons have the same mass. This will give matrix elements $\langle\bar{P}|\mathcal{O}_{7,8}^{3/2}|P\rangle$, with the quark content of $\mathcal{O}_{7,8}^{3/2}$ different from the operators in equations (4.60) and (4.61). However, the above matrix elements are equivalent to $\langle\pi^+|\mathcal{O}_{7,8}^{3/2}|K^+\rangle$ in the chiral limit.

In order to complete the calculations of B_K, $B_{7,8}^{3/2}$, we also need the correlators

$$\begin{aligned} C_{PP}^{FL}(t,\vec{p}) &= \sum_{\vec{x}} {\rm e}^{-i\vec{p}\cdot\vec{x}}\langle P_{\rm F}(x)P_{\rm L}^\dagger(0)\rangle, && (4.93)\\ C_{PP}^{LF}(t) &= \sum_{\vec{x}}\langle P_{\rm L}(x)P_{\rm F}^\dagger(0)\rangle, && (4.94)\\ C_{AP}^{LF}(t) &= \sum_{\vec{x}}\langle A_{\rm L}^4(x)P_{\rm F}^\dagger(0)\rangle, && (4.95)\end{aligned}$$

where P is the pseudo-scalar-density, and A^4 is the fourth component of the axial-vector-current quark bilinears.

The authors of [104], [105] have proposed a way of examining the chiral behaviour of B_K and $B_{78}^{3/2}$. Evidence shows this reduces systematic errors arising from the exclusion of higher-order terms in Chiral Perturbation Theory in the calculations of B_K. In this work, we follow this convention. We will discuss it more in section 4.4. Here we just list the ratios between the correlation functions we need in this convention. To look at the chiral behaviour of B_K, we need the ratio in the limit where t_1 and $T-t_2$ are large enough

$$R_{\Delta S=2}(\vec{p},\vec{q}) = \frac{1}{Z_A^2}\frac{C^3_{\Delta S=2}(t_1,t_2;\vec{p},\vec{q})}{C^{FL}_{PP}(t_1,\vec{p})C^{FL}_{PP}(t_2,\vec{q})} \longrightarrow \frac{\langle \bar{P}^0(\vec{q})|\mathcal{O}^{\Delta S=2}|P^0(\vec{p})\rangle}{Z_A^2\langle \bar{P}^0(\vec{q})|P|0\rangle\langle 0|P|P^0(\vec{p})\rangle}, \quad (4.96)$$

where Z_A is the renormalisation constant for the lattice axial-vector current. The reason why we have Z_A^2 in the denominator in the above ratio will become clear later on. K^0 and $\bar{K}^0$ carry momenta $\vec{p}$ and $\vec{q}$ respectively. $R_{\Delta S=2}(\vec{p},\vec{q})$ can be quite noisy when $\vec{p}$ and $\vec{q}$ are both non-zero, *c.f.*, the signal-to-noise-ratio problem discussed in subsection 2.1.4. Figure 4.7 shows extreme examples of the best plateaus and worst plateaus of $R_{\Delta S=2}(\vec{p},\vec{q})$ in this work.

For $B_{7,8}^{3/2}$, we need the ratios in the well-separated time and chiral limit

$$R_7^{3/2} = -\frac{3}{2}\frac{C_7^3(t_1,t_2)}{C^{FL}_{PP}(t_1,\vec{0})C^{FL}_{PP}(t_2,\vec{0})} \longrightarrow \frac{3}{2}\frac{\langle \bar{P}|\mathcal{O}_7^{3/2}|P\rangle}{\langle \bar{P}|P|0\rangle\langle 0|P|P\rangle}, \quad (4.97)$$

$$R_8^{3/2} = -\frac{1}{2}\frac{C_8^3(t_1,t_2)}{C^{FL}_{PP}(t_1,\vec{0})C^{FL}_{PP}(t_2,\vec{0})} \longrightarrow \frac{1}{2}\frac{\langle \bar{P}|\mathcal{O}_8^{3/2}|P\rangle}{\langle \bar{P}|P|0\rangle\langle 0|P|P\rangle}. \quad (4.98)$$

Examples of the plateaus of $R_{7,8}^{3/2}$ are shown in figure 4.8.

To study the chiral behaviour of the above ratios, we define the mass and recoil variable (when t is large enough)

$$X = \frac{8}{3}\frac{C^{LF}_{AP}(t)C^{LF}_{AP}(t)}{C^{LF}_{PP}(t)C^{LF}_{PP}(t)} \longrightarrow \frac{8}{3}\frac{f_P^2 M_P^2}{Z_A^2|\langle 0|P|P\rangle|^2}, \quad (4.99)$$

$$Y = \frac{p\cdot q}{M_P^2}X, \quad (4.100)$$

where X is a fitted quantity and is proportional to the mass of the pseudo-scalar meson mass. Y is obtained from X and is proportional to the recoil variable $(p\cdot q)$.

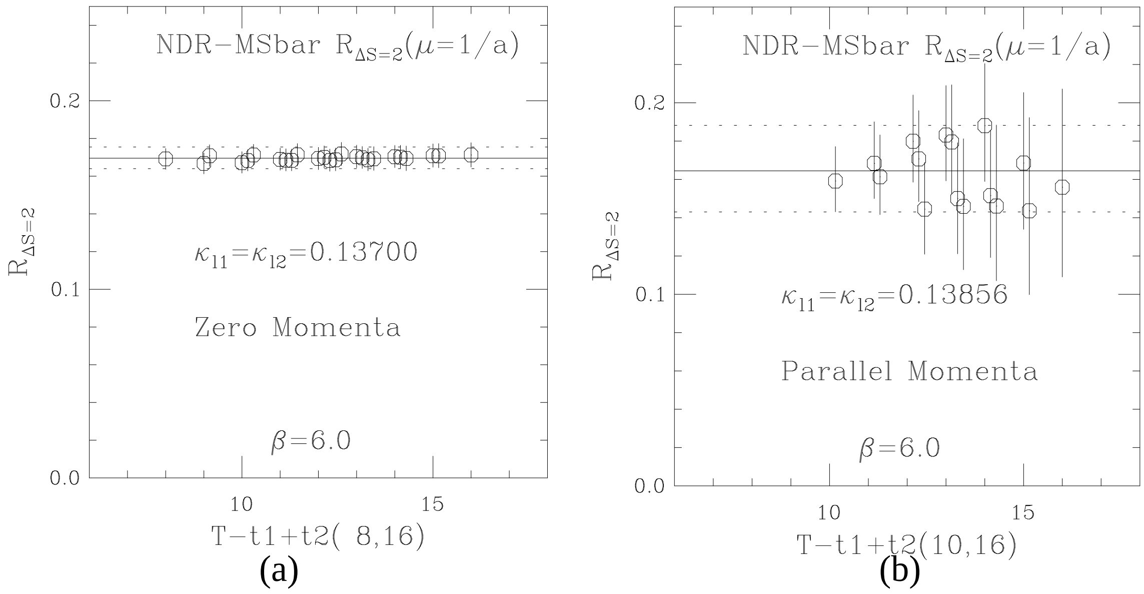

Figure 4.7: Plateaus of $R_{\Delta S=2}$ (matched to NDR-$\overline{\text{MS}}$ at the matching scale $\mu = 1/a$) at $\beta = 6.0$. (a) is the plateau of $R_{\Delta S=2}$ with the heaviest light meson and light anti-meson in this work. The meson and the anti-meson do not carry momentum in this case. The fitting time-slice range is $4 \leq t_2 \leq 8$ and $4 \leq T - t_1 \leq 8$. (b) is the plateau of $R_{\Delta S=2}$ with the lightest light meson and light anti-meson in this work. The meson carries momentum $\vec{p}$ and the anti meson carries momentum $\vec{q}$, with $|\vec{p}| = |\vec{q}| = 2\pi/L$ (L is the number of lattice points in each spatial direction), and $\vec{p}$ parallel to $\vec{q}$. The fitting time-slice range is $5 \leq t_2 \leq 8$ and $5 \leq T - t_1 \leq 8$.

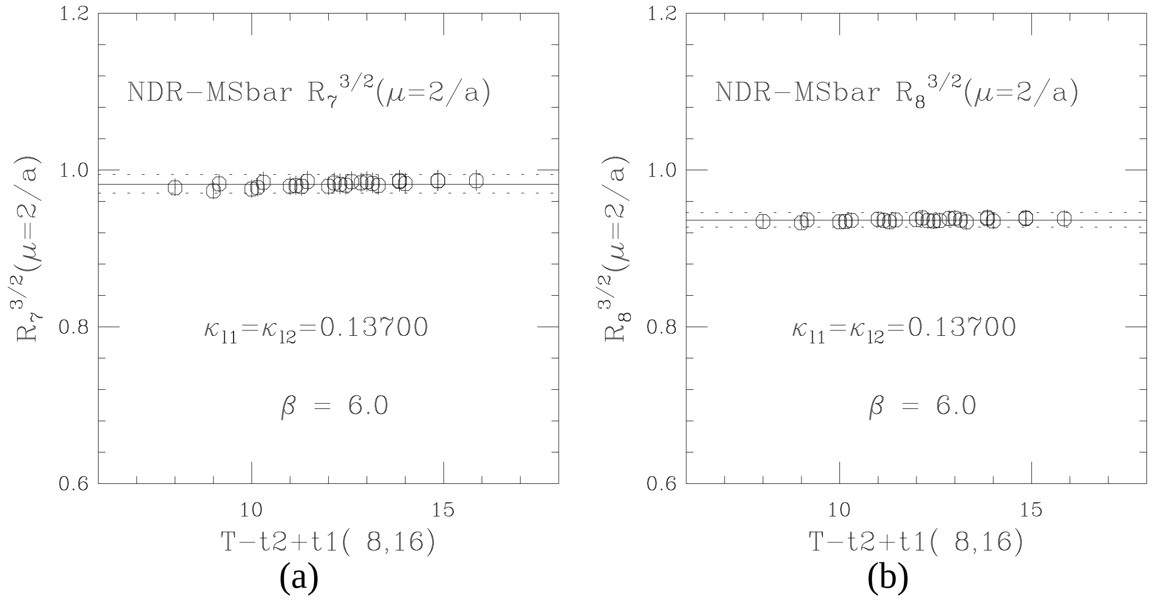

Figure 4.8: Plateaus of NDR-$\overline{\mathrm{MS}}$ $R^{3/2}_{7,8}$ at $\beta = 6.0$. The fitting time-slice range are $4 \leq t_2 \leq 8$ and $4 \leq T - t_1 \leq 8$ in both plots. The matching scale μ is $2/a$.

4.3 Operator Matching

From what we have seen in subsection 4.2.2, we know the study of B_K and $B^{3/2}_{7,8}$ requires the matching of the lattice four-fermion operators $\mathcal{O}^{\Delta S=2}$, $\mathcal{O}^{3/2}_{7,8}$ and quark bilinears $\bar{q}_1\gamma_4\gamma_5 q_2$, $\bar{q}_1\gamma_5 q_2$ to the corresponding continuum operators. Because of explicit chiral symmetry breaking on the lattice, we have operator mixing amongst the four-fermion operators. In this section, we use the basis introduced in equation (3.77). Once again, we use the one-loop-perturbation-theory results from the tree-level clover action with appropriate modifications for the KLM normalisation and mean-field improvement to perform the matching. However, we will not discuss the mean-field improvement in details here, since it is implemented in the same way described in subsection 3.3.

4.3.1 From Lattice to NDR-$\overline{\rm MS}$

The matching of B_K between the lattice and the NDR-$\overline{\rm MS}$ scheme is the same as the one of B_B in equation (3.85)

$$B_K^{\rm NDR-\overline{MS}}(\mu) = \frac{Z_1(\alpha_s, a\mu; c_{\rm SW})}{Z_A^2(\alpha_s; c_{\rm SW})}\left(B_1^{\rm latt}(a) + \sum_{i=2}^{5} Z_i(\alpha_s; c_{\rm SW}) B_i^{\rm latt}(a)\right), \quad (4.101)$$

with Z_j $(j = 1, \cdots, 5)$ the renormalisation constants in equations (3.82), (3.83) and (3.84). Here we treat $Z_A^2(\alpha_s; c_{\rm SW})$ as an overall factor (*i.e.*, not combine its one-loop correction with the one in Z_1). Again, we find taking and not taking Z_A as an overall factor produces compatible results of B_K.

We now turn to the matching of $B_{7,8}^{3/2}$. This can also be done by relating the renormalisation constants of four-fermion operators to the ones of quark bilinears in the DRED-$\overline{\rm MS}$, then match to the NDR-$\overline{\rm MS}$ scheme [76]. First, we have the relations between $O_{7,8}^{3/2}$ and the basis operators in equation (3.77)

$$\mathcal{O}_7^{3/2} \longrightarrow \mathcal{O}_2, \quad (4.102)$$

$$\mathcal{O}_8^{3/2} \longrightarrow -2\mathcal{O}_4. \quad (4.103)$$

The matching of these two operators between the lattice and any continuum scheme can be split into two steps, as $\mathcal{O}_7^{3/2}$ and $\mathcal{O}_8^{3/2}$ mix with each other under renormalisation in any scheme.

The first step is the 'chiral subtraction' introduced in subsection 2.1.6. Define $\hat{\mathcal{O}}_j^{\rm latt}$ $(j = 1, \ldots, 5)$ to be the operators after chiral subtraction, then we want to perform the one-loop chiral subtraction

$$\begin{pmatrix} \hat{\mathcal{O}}_2^{\rm latt}(a) \\ \hat{\mathcal{O}}_4^{\rm latt}(a) \end{pmatrix} = \begin{pmatrix} \mathcal{O}_2^{\rm latt}(a) \\ \mathcal{O}_4^{\rm latt}(a) \end{pmatrix} + \frac{\alpha_s}{4\pi} \hat{Z}_{24}^{\rm chiral} \begin{pmatrix} \mathcal{O}_1^{\rm latt}(a) \\ \mathcal{O}_3^{\rm latt}(a) \\ \mathcal{O}_5^{\rm latt}(a) \end{pmatrix}, \quad (4.104)$$

where $\hat{Z}_{24}^{\rm chiral}$ is a 2×3 matrix. The values of the elements of this matrix have been calculated by the authors of [76]

$$\hat{Z}_{24}^{\rm chiral} = \frac{\Delta_I - \Delta_{\gamma_5}}{24} \begin{pmatrix} -16 & -28 & 2 \\ 2 & 32 & 0 \end{pmatrix}, \quad (4.105)$$

where Δ_I and Δ_{γ_5} arise from the matching of scalar- and pseudo-scalar-density quark bilinears between the lattice and the NDR-$\overline{\rm MS}$ scheme, their values [46] are already listed in table 3.3.

The second step is to match the chirally subtracted $\hat{\mathcal{O}}_2^{\rm latt}(a)$ and $\hat{\mathcal{O}}_4^{\rm latt}(a)$ to their NDR-$\overline{\rm MS}$ counterparts using one-loop perturbation theory

$$\begin{pmatrix} \mathcal{O}_2^{\rm NDR-\overline{MS}} \\ \mathcal{O}_4^{\rm NDR-\overline{MS}} \end{pmatrix} = \begin{pmatrix} Z_{22}(\alpha_s, a\mu; {\rm tad}) & Z_{24}(\alpha_s, a\mu; {\rm tad}) \\ Z_{42}(\alpha_s, a\mu; {\rm tad}) & Z_{44}(\alpha_s, a\mu; {\rm tad}) \end{pmatrix} \begin{pmatrix} \hat{\mathcal{O}}_2^{\rm latt} \\ \hat{\mathcal{O}}_4^{\rm latt} \end{pmatrix}. \qquad (4.106)$$

The mixing of $\mathcal{O}_2$ and $\mathcal{O}_4$ is a 'universal' phenomena, *i.e.*, it happens in any scheme. In principle, the renormalisation constants in equation (4.106) should all depend upon the renormalisation scale μ. At one-loop level, they can be related to the one-loop quark-bilinear renormalisation constants through [76]

$$\begin{aligned} Z_{22}(\alpha_s, a\mu; {\rm tad}) &= 1 + \frac{\alpha_s}{4\pi} \times \\ \Big\{ -2\ln(a\mu) &+ \frac{1}{12}\left[18\left(\Delta_{\gamma_\mu} + \Delta_{\gamma_5\gamma_\mu}\right) - 5\Delta_I + \Delta_{\gamma_5} + 32\Delta_{\Sigma_1}\right] + 1 - 2X\Big\}, \end{aligned} \qquad (4.107)$$

$$Z_{24}(\alpha_s, a\mu; {\rm tad}) = \frac{\alpha_s}{4\pi} \times \Big\{ -12\ln(a\mu) + \frac{1}{6}\left[6\left(\Delta_{\gamma_\mu} + \Delta_{\gamma_5\gamma_\mu}\right) - 7\Delta_I - 5\Delta_{\gamma_5}\right] + 6\Big\}, \qquad (4.108)$$

$$Z_{42}(\alpha_s, a\mu; {\rm tad}) = \frac{\alpha_s}{4\pi} \times \Big\{ \frac{-1}{24}\left(\Delta_I - \Delta_{\gamma_5}\right) + \frac{3}{2}\Big\}, \qquad (4.109)$$

$$Z_{44}(\alpha_s, a\mu; {\rm tad}) = 1 + \frac{\alpha_s}{4\pi} \times \Big\{ 16\ln(a\mu) + \frac{1}{12}\Big[13\Delta_I + 19\Delta_{\gamma_5} + 32\Delta_{\Sigma_1}\Big] + 1 - 2X\Big\}, \qquad (4.110)$$

where X is the one-loop coefficient of the perturbative expansion of u_0 in equation (3.69). All the Δ_i are the same as those listed in table 3.3. The term $(-2X)$ appears in Z_{22} and Z_{44} through the implementation of mean-field improvement. Note that X and Δ_{Σ_1} only show up in Z_{22} and Z_{44} because other two renormalisation constants start at $\mathcal{O}(\alpha_s)$. Another feature worth-noting is that the one-loop anomalous dimension matrix in this matching (renormalisation) procedure is

$$\hat{\gamma}_{24}^{(0)} = \begin{pmatrix} -2 & -12 \\ 0 & 16 \end{pmatrix}, \qquad (4.111)$$

which shows the universality of the one-loop anomalous dimensions when compared with equation (4.68).

From equations (4.87) and (4.88), we also have to perform the matching

$$(\bar{q}_1\gamma_5 q_2)^{\mathrm{NDR-\overline{MS}}}(\mu) = Z_P(\alpha_s, a\mu; \mathrm{tad})\,(\bar{q}_1\gamma_5 q_2)^{\mathrm{latt}}(a), \tag{4.112}$$

in order to obtain $B_{7,8}^{3/2}$ in the NDR-$\overline{\mathrm{MS}}$ scheme. Here we use the one-loop Z_P from [46] and [76], with mean-field improvement

$$Z_P(\alpha_s, a\mu; \mathrm{tad}) = 1 + \frac{\alpha_s}{4\pi}\left[6\ln(a\mu) + \frac{4}{3}\left(\Delta_{\gamma_5} + \Delta_{\Sigma_1}\right) - X\right], \tag{4.113}$$

and treat it as an overall factor in the calculations of $B_{7,8}^{3/2}$.

In order to estimate the systematic errors arising from the truncation of the perturbative series in this one-loop-matching procedure, we match the lattice B parameters to the NDR-$\overline{\mathrm{MS}}$ scheme at three renormalisation scales $\mu = 1/a, 2/a, \pi/a$. In this matching procedure, we use the $\overline{\mathrm{MS}}$ coupling constants listed in table 3.4, *i.e.*, the ones obtained from the procedure described in subsection 3.3.1.

4.3.2 Running in the $\overline{\mathrm{MS}}$ Scheme

As mentioned in the last subsection, we perform operator matching between the lattice and the NDR-$\overline{\mathrm{MS}}$ scheme at the scales $1/a$, $2/a$ and π/a. In order to compare our results with other calculations and to estimate systematic errors, we have to perform the scale evolution in the NDR-$\overline{\mathrm{MS}}$ scheme. Unlike what we do in the study of the B^0–$\bar{B}^0$ mixing, here we perform the two-loop running in the NDR-$\overline{\mathrm{MS}}$ scheme with $n_f = 0$. Our procedure is equivalent to the 'horizontal matching' introduced in [76]. Here we stress again that it is also valid to perform scale evolution with particle threshold taken into account. We favour the NDR-$\overline{\mathrm{MS}}$ running with $n_f = 0$ in the calculations of B_K and $B_{7,8}^{3/2}$ because most previous calculations of these quantities were done in this way, and we want to compare our results with these previous work. A point in the two-loop running of $B_{7,8}^{3/2}$ is that we use $(-\gamma_m)$ to evolve pseudo-scalar density quark bilinear which appears in the vacuum-saturation approximations of the matrix elements $\langle\pi^+|\mathcal{O}_{7,8}^{3/2}|K^+\rangle$, where γ_m is the QCD γ function for the running quark mass. To summarise the two-loop running in NDR-$\overline{\mathrm{MS}}$ scheme:

1. For B_K, we use $U^{\Delta S=2}_{\mathrm{NLLA}}(\mu_1, \mu_2)$ which is the same as $U^{\Delta B=2}_{\mathrm{NLLA}}$ in equation (3.35).

2. For $\mathcal{O}^{3/2}_{7,8}$, we use the 2×2 scale-evolution matrix $\hat{U}^{78}_{\mathrm{NLLA}}(\mu_1, \mu_2)$ constructed from the procedure explained in the end of subsection 1.2.3, with one- and two-loop anomalous dimension matrices in equations (4.68) and (4.69) (with $n_f = 0$).

3. For pseudo-scalar density, use $(-\gamma_m)$.

4.4 Analysis and Results

We have arrived at the stage where we can extract B_K and $B^{3/2}_{7,8}$ by studying the chiral behaviour of the ratios $R_{\Delta S=2}$ and $R^{3/2}_{7,8}$. As stated in subsection 4.2.3, There is more than one lattice operator which contribute to each ratio. In this subsection, we present the analysis in which we form $R_{\Delta S=2}$ and $R^{3/2}_{7,8}$ in the NDR-$\overline{\mathrm{MS}}$ scheme using the renormalisation constants in equations (4.101) and (4.107),...,(4.110), and then fit the plateaus of these NDR-$\overline{\mathrm{MS}}$ ratios. As we did in the analysis of B^0–$\bar{B}^0$ mixing, we also tried to fit $R_{\Delta S=2}$ and $R^{3/2}_{7,8}$ formed by using lattice operator $\mathcal{O}^{\mathrm{latt}}_i$ $(i = 1, \ldots, 5)$, and and then obtain NDR-$\overline{\mathrm{MS}}$ ratios using these fitted 'lattice ratios'. This procedure gives results that are almost indistinguishable from the ones we present here.

An issue in the study of the chiral behaviour of $R_{\Delta S=2}$ is its dependence upon the recoil variable $(p \cdot q)$, where p and q are the momenta carried by K^0 and $\bar{K}^0$ respectively. For each pseudo-scalar meson (we have six in total), we form the following four combinations of $\vec{p}$ and $\vec{q}$:

1. $|\vec{p}| = |\vec{q}| = 0$.

2. Average over all cases in which one of the momenta has absolute value $2\pi/L$, while the other one is zero.

3. Average over all cases in which $|\vec{p}| = |\vec{q}| = 2\pi/L$, with $\vec{p}$ perpendicular to $\vec{q}$.

4. Average over all cases in which $|\vec{p}| = |\vec{q}| = 2\pi/L$, with $\vec{p}$ parallel to $\vec{q}$.

Therefore, we have twenty-four data points for $R_{\Delta S=2}$ in total.

4.4.1 B_K and Chiral Behaviour of $\mathcal{O}_{LL}^{\Delta S=2}$

In terms of the notation introduced in subsection 2.3.3, $\mathcal{O}_{LL}^{\Delta S=2}$ is a pure (27,1) operator. According to equation (2.97), its matrix element $\langle \bar{P}|\mathcal{O}_{LL}^{\Delta S=2}|P\rangle$ is proportional to $(p \cdot q)$ in Chiral Perturbation Theory, where p and q the momenta carried by the initial- and final-state mesons. However, because we are using a clover fermion action to calculate this matrix element, chiral symmetry is explicitly broken, the scaling of $\langle \bar{P}|\mathcal{O}_{LL}^{\Delta S=2}|P\rangle$ should take the form

$$\langle \bar{P}|\mathcal{O}_{LL}^{\Delta S=2}|P\rangle = a_{00} + a_{10}M_P^2 + a_{01}(p \cdot q), \tag{4.114}$$

if the chiral subtraction is not performed exactly. M_P is the pseudo-scalar-meson mass, a_{00} and a_{10} are lattice artifacts. We can also parameterise the above ChPT expansion in terms of $R_{\Delta S=2}$, X (proportional to M_P^2) and Y (proportional to $(p \cdot q)$) introduced in equations (4.96), (4.99) and (4.100). This leads to

$$R_{\Delta S=2} = \alpha_K + \beta_K X + \gamma_K Y, \tag{4.115}$$

where α_K and β_K are lattice artifacts. There could be contributions from higher-order terms in Chiral Perturbation Theory. For instance, including the $\mathcal{O}(p^4)$ terms gives the expansion

$$R_{\Delta S=2} = \alpha_K + \beta_K X + \gamma_K Y + \delta_K X^2 + \epsilon_K XY + \xi_K Y^2, \tag{4.116}$$

where α_K, β_K, δ_K are lattice artifacts. We have used both equations (4.115) and (4.116) to perform chiral extrapolations and have found

1. These two extrapolations give consistent α_K, β_K and γ_K.

2. δ_K and ϵ_K in equation (4.116) are always consistent with zero. ξ_K does contribute in some cases, but the contribution is always very small.

This means the contributions from higher-order ChPT expansion are insignificant in the parameterisation we use. Therefore, we can safely perform chiral extrapolations with equation (4.115). From the definitions of $R_{\Delta S=2}$, X and Y, we conclude

$$B_K = \gamma_K. \tag{4.117}$$

The lattice artifacts α_K and β_K arise from the *explicit chiral symmetry breaking in Wilson-type fermion actions*[10] and have been observed to give large systematic errors on B_K because:

1. In equation (4.115), we can see that γ_K is a $\mathcal{O}(p^2)$ term, while α_K is a $\mathcal{O}(p^0)$ term, in Chiral Perturbation Theory. This means even a small lattice artifact α_K might give a large systematic error on B_K, as α_K is not small compared with $\gamma_K Y$, at the scale M_K (*i.e.*, $(p \cdot q) \sim M_K^2$).

2. β_K has been observed to be quite large in comparison with γ_K in the calculations of B_K. For instance, a calculation of B_K using the tree-level clover action [105] shows β_K is not consistent with zero, and might give a 30% systematic error on B_K (assuming $X \sim Y$). Another calculation[11] using the Wilson fermion action [76] shows β_K is not zero and could give 10% systematic errors on B_K.

Therefore, *B_K is very sensitive to chiral symmetry breaking, and its chiral behaviour should be analysed carefully, especially when calculating it using lattice actions which explicitly break chiral symmetry.* Figures 4.9 and 4.10 show the Y dependence in the chiral extrapolations of NDR-$\overline{\text{MS}}$ $R_{\Delta S=2}$ at the renormalisation scale $\mu = 1/a$, according to equation (4.115), at two values of lattice spacing we have[12]. In these two plots, we draw a Y-dependence curve for each fixed X (meson mass) we have, so there are six curves in each plot. To make it more

[10] α_K and β_K do not appear in the calculations using lattice fermion actions which have continuous-like chiral symmetry.

[11] This calculation is done using a different parameterisation of the ratio between matrix elements and the mass and recoil variables.

[12] Chiral extrapolations of $R_{\Delta S=2}$ at the renormalisation scales $2/a$ and π/a exhibit very similar features such that they do not change the discussion in this subsection at all.

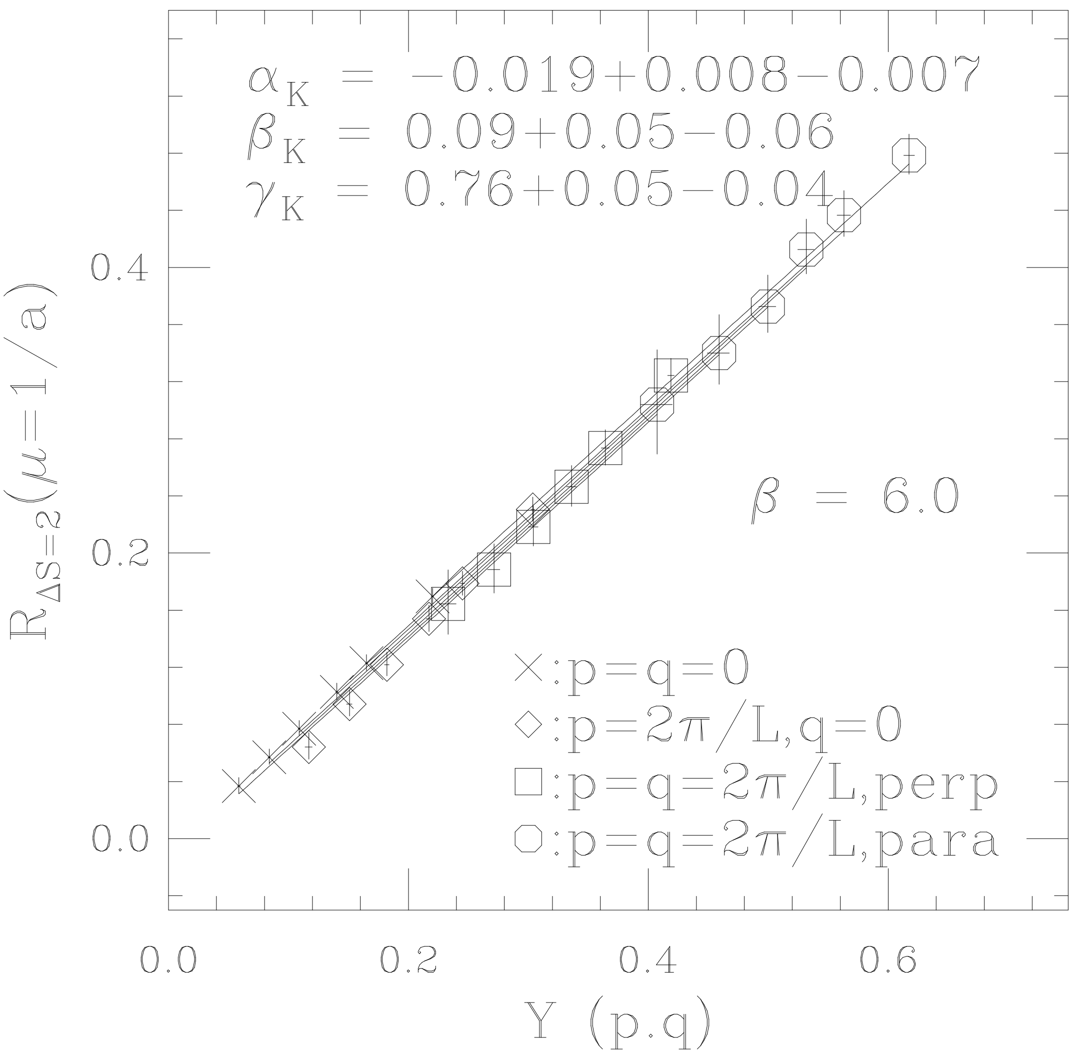

Figure 4.9: Y dependence of $R_{\Delta S=2}(1/a)$ in the chiral extrapolation according to equation (4.115) at $\beta = 6.0$. We use four different symbols to indicate different combinations of momenta carried by K^0 and $\bar{K}^0$ explained in the text. There are six points for each symbol, since we have six pseudo-scalar mesons in the simulation.

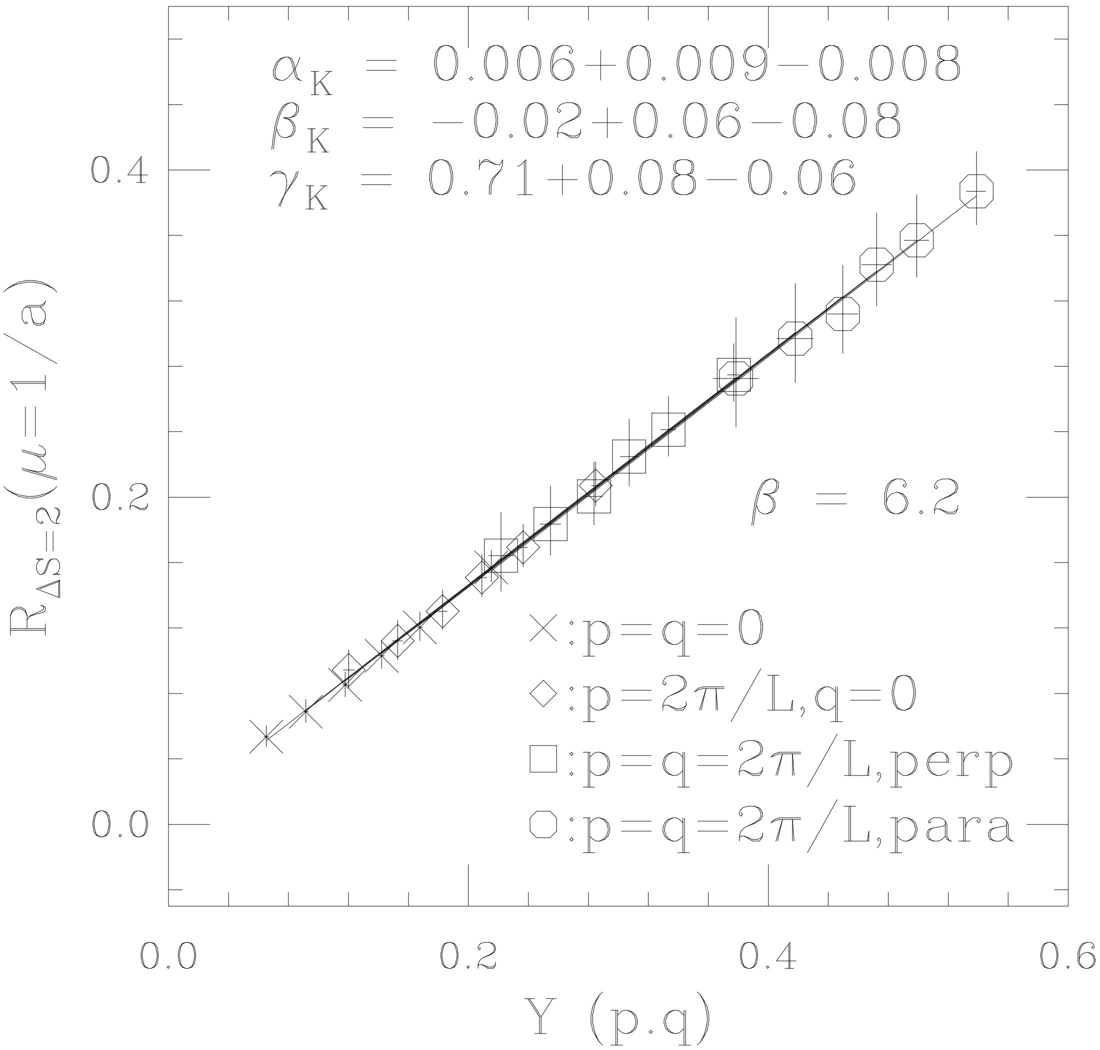

Figure 4.10: Y dependence of $R_{\Delta S=2}(1/a)$ in the chiral extrapolation according to equation (4.115) at $\beta = 6.2$. Other details are the same as the ones in figure 4.9

clear, these curves are drawn according to the relation

$$R_{\Delta S=2} = \alpha_K + \beta_K X_{\text{fixed}} + \gamma_K Y, \tag{4.118}$$

where X_{fixed} are from the meson masses we use in the simulations. Therefore, these curves will become closer to each other as β_K gets smaller. We also list the resultant α_K, β_K and γ_K in these figures.

There are two factors which can cause the presence of the lattice artifacts α_K and β_K in using Wilson-type fermion actions:

1. $\mathcal{O}(a\alpha_s^n)$ discretisation errors. For instance, in the Wilson fermion action, chiral Ward identities are violated by the presence of a $\mathcal{O}(a)$ term [27], which arise from the irrelevant operator Wilson suggested to add to the naive fermion action.

2. Operator matching. As discussed in subsection 2.1.6, explicit chiral symmetry breaking causes further operator mixing on the lattice, in addition to the mixing which happens in every regularisation/renormalisation procedure. Ideally, this operator mixing is subtracting the effects of chiral-symmetry violations on the lattice, and reproducing the chiral behaviour of the operator to be the one as expected in the continuum scheme. Figure 4.11 shows the effect of chiral subtraction at $\beta = 6.2$ in our calculation of B_K. In this plot, we draw separately the contributions from the diagonal operator ($\mathcal{O}_1^{\text{latt}}$) and the off-diagonal operators ($Z_i\mathcal{O}_i$, $i = 2, \ldots, 5$) for all the twenty-four data points we have. However, in using the one-loop perturbative matching, there are $\mathcal{O}(\alpha_s^2)$ systematic errors due to the truncation of the series. Therefore, there are residual chiral-symmetry-breaking effects.

It has been suggested [76, 104, 105, 106] that the errors in perturbative matching contribute mainly to the lattice artifact α_K and result in larger systematic errors than the discretisation errors do. There are methods of performing non-perturbative matching between the lattice and the NDR-$\overline{\text{MS}}$ scheme using chiral Ward identities [107] or using an intermediate scheme[13][47, 108]. It also has been

[13] This scheme is called the Regularisation Independent (RI) scheme, which can be defined both perturbatively and non-perturbatively. Using this scheme, one can non-perturbatively

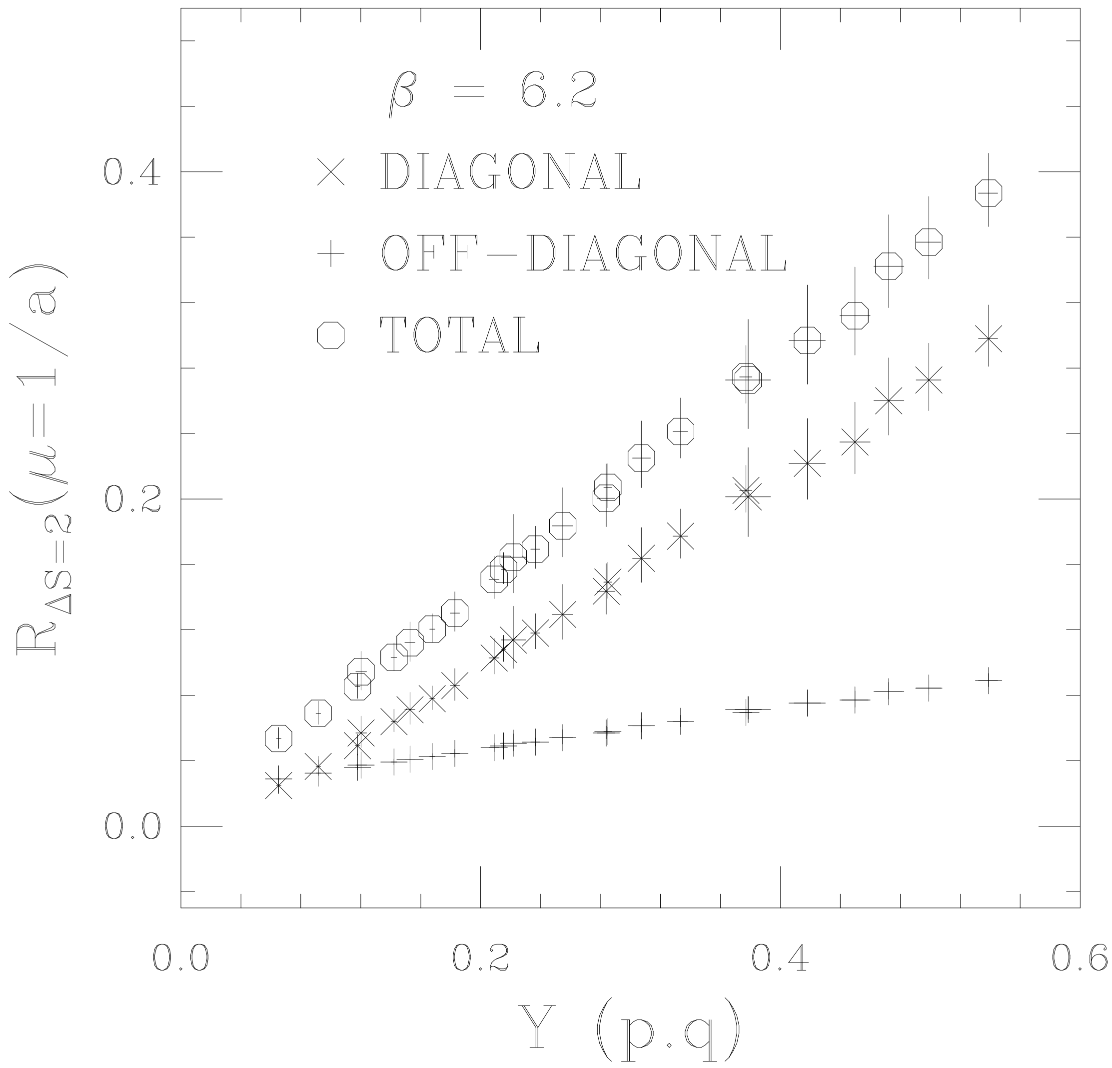

Figure 4.11: Y dependence of $R_{\Delta S=2}$, with diagonal- and off-diagonal-operator contributions drawn separately. The sum of these two contributions are also shown explicitly. See the text for further explanations.

shown that non-perturbative renormalisation in lattice calculations does reduce the systematic errors in B_K [104, 105]. However, our findings seem not to totally agree with the suggestion that perturbative matching is the main source of systematic errors in the lattice calculations of B_K. As observed in figures 4.9 and 4.10, the lattice artifact β_K is consistent with zero at $\beta = 6.2$, and it is about 2σ away from zero at $\beta = 6.0$. Also, α_K is consistent with zero at $\beta = 6.2$, and is about 3σ away from zero at $\beta = 6.0$. Comparing this feature with calculations using less improved Wilson-type fermion actions and one-loop perturbative matching with $\bar{g}$ in equation (2.63) [76, 104, 105], our results suggest

1. Discretisation errors play an important role in the presence of both α_K and β_K [14].
2. From the action we use (mean-field improved clover action), one-loop perturbative matching works well at small lattice spacing.

4.4.2 Chiral Extrapolations of $B_7^{3/2}$ and $B_8^{3/2}$

As already discussed in subsection 4.1.2, $\mathcal{O}_7^{3/2}$ and $\mathcal{O}_8^{3/2}$ are in the (8,8) representation. According to equation (2.98), their matrix elements should approach constants in the chiral limit. Therefore, we perform the chiral extrapolations for $B_{7,8}^{3/2}$ using the relation

$$R_7^{3/2} = \alpha_7 + \beta_7 X + \delta_7 X^2, \tag{4.119}$$

$$R_8^{3/2} = \alpha_8 + \beta_8 X + \delta_8 X^2, \tag{4.120}$$

such that

$$B_7^{3/2} = \alpha_7, \tag{4.121}$$

$$B_8^{3/2} = \alpha_8. \tag{4.122}$$

Figure 4.12 shows examples of chiral behaviour of $R_{7,8}^{3/2}$. Note that we find quadratic terms contribute significantly in the chiral extrapolations of $B_{7,8}^{3/2}$.

perform the matching between the lattice and the RI scheme, then perturbatively match the RI results to the NDR-$\overline{\mathrm{MS}}$ scheme.

[14] Other recent calculations of B_K [109, 110] also suggest this.

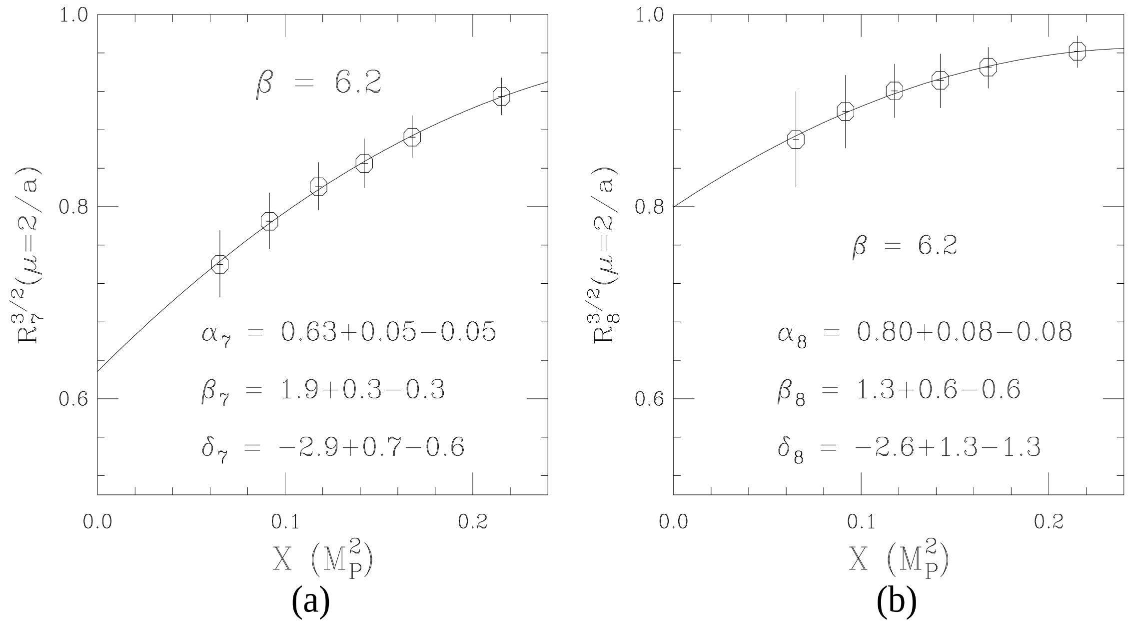

Figure 4.12: Chiral behaviour of (a) $R_7^{3/2}$ and (b) $R_7^{3/2}$ at $\beta = 6.2$, with renormalisation scale $2/a$.

4.4.3 Results and Systematic Errors

To evaluate matching uncertainties and to compare our results with the ones from other calculations, we run our NDR-$\overline{\mathrm{MS}}$ B_K and $B_{7,8}^{3/2}$ to 2 GeV using the procedure described in subsection 4.3.2. The coupling constant used in this running is the same as the one we use for the matching (between the lattice and the NDR-$\overline{\mathrm{MS}}$ scheme), run to the appropriate scales at two loops. We first look at table 4.1 which lists the results of B_K and $B_{7,8}^{3/2}$ matched at three different matching scales and two different lattice spacing. We find that B_K at 2 GeV is almost independent of the matching scale μ between the range $1/a \sim \pi/a$. Bearing in mind that the lattice artifacts α_K and β_K are always consistent with zero at $\beta = 6.2$ and are small at $\beta = 6.0$, we conclude that the systematic errors arising from operator matching (chiral subtraction) are small in our calculations of B_K, especially at $\beta = 6.2$. Since we only have two values of the lattice spacing, it is not possible for us to perform a continuum extrapolation. However, from table 4.1, we find our results for B_K have a small dependence on lattice spacing,

Table 4.1: NDR-$\overline{\mathrm{MS}}$ B parameters at the renormalisation scale 2 GeV. The error bars quoted here are statistical.

β	μ	B_K	$B_7^{3/2}$	$B_8^{3/2}$
	π/a	0.75^{+4}_{-4}	0.55^{+3}_{-3}	0.74^{+3}_{-3}
6.0	$2/a$	0.75^{+4}_{-4}	0.53^{+3}_{-3}	0.73^{+3}_{-3}
	$1/a$	0.76^{+5}_{-4}	0.43^{+3}_{-2}	0.68^{+3}_{-3}
	π/a	0.71^{+8}_{-6}	0.60^{+5}_{-4}	0.81^{+8}_{-8}
6.2	$2/a$	0.71^{+8}_{-6}	0.58^{+5}_{-4}	0.80^{+8}_{-8}
	$1/a$	0.72^{+8}_{-6}	0.50^{+4}_{-4}	0.76^{+8}_{-8}

although we cannot exclude discretisation errors at $\beta = 6.0$. We then quote the $\mu = 1/a$ result at $\beta = 6.2$ as our best estimate of B_K

$$B_K(2\text{ GeV}) \quad = \quad 0.72^{+8}_{-6},$$

with the comment that discretisation errors might be small, and we only quote statistical errors here.

We also observe that $B_{7,8}^{3/2}$, especially $B_7^{3/2}$, have a stronger $\mu-$dependence than B_K. This is a consequence of the large scheme-dependent terms and anomalous dimensions. In order to see this point clearly, let's write the numerical values of the one-loop matching coefficients in equations (4.107), (4.108), (4.109) and (4.110) in the form $Z_{ij} = 1 + \frac{\alpha_s}{4\pi}\left[\gamma_{ij}\ln(a\mu) + d_{ij}\right]$, with $i, j = 2, 4$

$$Z_{22}(\alpha_s, a\mu; \mathrm{tad}) \quad = \quad 1 + \frac{\alpha_s}{4\pi}\left[-2\ln(a\mu) - 10.08\right], \tag{4.123}$$

$$Z_{24}(\alpha_s, a\mu; \mathrm{tad}) \quad = \quad \frac{\alpha_s}{4\pi}\left[-12\ln(a\mu) + 18.53\right], \tag{4.124}$$

$$Z_{42}(\alpha_s, a\mu; \mathrm{tad}) \quad = \quad \frac{\alpha_s}{4\pi}\left[1.37\right], \tag{4.125}$$

$$Z_{44}(\alpha_s, a\mu; \mathrm{tad}) \quad = \quad 1 + \frac{\alpha_s}{4\pi}\left[16\ln(a\mu) - 29.64\right]. \tag{4.126}$$

Also, the numerical value of Z_P is

$$\begin{aligned} Z_P(\alpha_s, a\mu; \mathrm{tad}) &= 1 + \frac{\alpha_s}{4\pi}\left[\gamma_P \ln(a\mu) - d_P\right] \\ &= 1 + \frac{\alpha_s}{4\pi}\left[6\ln(a\mu) - 16.99\right], \end{aligned} \tag{4.127}$$

from equation (4.113). Let's look at the matching and running of $B_7^{3/2}$ first. We observe that $d_{22} + d_P^2 = 23.9$ and $d_{24} + d_P^2 = 52.51$. This means the scheme-dependent terms are big in the one-loop perturbative matching of $B_7^{3/2}$ between the lattice and the NDR-$\overline{\mathrm{MS}}$ scheme. What is worse is that a large $d_{24} + d_P^2$ in the one-loop matching of $B_7^{3/2}$ can induce a strong mixing with $B_8^{3/2}$, which is bigger according to the discussion in subsection 4.2.2. These big scheme-dependent terms $d_{22} + d_P^2$ and $d_{24} + d_P^2$ can be cancelled by tuning the matching scale μ in equations (4.123), (4.124) and (4.127). However, here we stress that tuning the matching scale μ might introduce large contributions from the logarithms at higher orders, which we do not know how to deal with. In this work, we only vary μ between $1/a$ and π/a, such that these higher-order logarithms are numerically small. As we can see, $\gamma_{22} - \gamma_P^2 = -14$ and $\gamma_{24} - \gamma_P^2 = -24$, are both quite large. This means we do not have to go to a very high matching scale in order to cancel the scheme-dependent terms $d_{22} + d_P^2$ and $d_{24} + d_P^2$. However, this means $B_7^{3/2}$ is unstable with respect to the matching scale.

The same argument applies to $B_8^{3/2}$. However, $B_8^{3/2}$ is more stable with respect to the variation of the matching scale than $B_7^{3/2}$ is, because

1. $d_{44} + 2d_P = 4.34$ and $\gamma_{44} - 2\gamma_P = 4$ are small numbers in comparison with $d_{22} + 2d_P$ and $\gamma_{22} - 2\gamma_P$.

2. $d_{42} + 2d_P = 35.35$ is quite big, which means the one-loop matching of $B_8^{3/2}$ can induce a strong mixing with $B_7^{3/2}$. However, $B_7^{3/2}$ is smaller than $B_8^{3/2}$. This reduces the effect of a large $d_{42} + 2d_P$.

In quoting our best estimates of $B_{7,8}^{3/2}$, we favour the results at larger values of μ because the matching times running is better behaved. Again, we cannot perform continuum extrapolations for $B_{7,8}^{3/2}$, and we stress that discretisation errors are difficult to quantify because of the large μ dependence (systematic errors due to one-loop perturbative matching). Therefore, we quote the $\mu = 2/a$ results at $\beta = 6.2$ as our best estimates of $B_{7,8}^{3/2}$, and add systematic errors to take into account the μ dependence we have observed

$$B_7^{3/2}(2\ \mathrm{GeV}) = 0.58^{+5+2}_{-4-8},$$

$$B_8^{3/2}(2\ \mathrm{GeV}) = 0.80^{+8+1}_{-8-4},$$

where the first error bars are statistical, and the second ones are systematic.

4.4.4 Comparison with Other Calculations

We now compare our results for B_K and $B_{7,8}^{3/2}$ with other recent lattice calculations. In table 4.2, we can see that our result for B_K is compatible with other calculations except for the results from JLQCD-W and Gupta. A word of caution about the JLQCD result using the staggered fermion action is that significant systematic errors from the truncation of perturbative series in the matching procedure have been observed [111], and it is difficult to quantify these errors. We show the $\mathcal{O}(p^0)$ and $\mathcal{O}(p^2)$ lattice artifacts (which we call α_K and β_K in equation (4.115)) in the table. Note that Gupta and GBS use different parameterisations for the mass and the recoil variables from what Roma and we use, in analysing the chiral behaviour of $\langle \bar{P}^0|\mathcal{O}^{\Delta S=2}|P^0\rangle$. However, we still call them α_K and β_K for simplicity. The analysis of the chiral behaviour of $\langle \bar{P}^0|\mathcal{O}^{\Delta S=2}|P^0\rangle$ in the JLQCD result from the Wilson fermion action is somewhat different from other calculations using Wilson-type fermion actions. These authors only analyse the mixing processes in which initial- and final-state mesons do not carry spatial momentum. Therefore, they cannot quantify the systematic error equivalent to β_K in equation (4.115). In the result from GBS, there are two error bars. The first one is the statistical error, and the second one is the systematic error arising from one-loop perturbative matching between the lattice and the NDR-$\overline{\mathrm{MS}}$ scheme. This error is estimated by the method proposed by the authors of [106]. As we can see in table 4.2, our result for B_K is not compatible with the one from Gupta, while we have used the same action and the same matching procedure. Here we stress that the result from Gupta is obtained using different parameterisations for the mass

Table 4.2: Comparison of our result of B_K with other recent lattice calculations, at the renormalisation scale $\mu = 2$ GeV in the NDR-$\overline{\mathrm{MS}}$ scheme. All the results, except for the one from JLQCD-S, are obtained using Wilson-type fermion actions. 'PT' means 'One-loop Perturbation Theory', 'RI' means 'Non-perturbative Matching via Regularisation-Independent scheme' and 'WI' means 'Non-perturbative Matching via Ward Identities'. The results from JLQCD-W and JLQCD-S are already extrapolated to the continuum limit. α_K and β_K are $\mathcal{O}(p^0)$ and $\mathcal{O}(p^2)$ lattice artifacts (see text).

Authors	Fermion action	β	Matching	α_K	β_K	B_K
This Work	$c_{\rm SW} = 1/u_0^3$	6.2	PT	0	0	0.72^{+8}_{-6}
Gupta[110]	$c_{\rm SW} = 1/u_0^3$	6.0	PT	$\neq 0$	0	0.58(7)
Roma[105]	$c_{\rm SW} = 1$	6.0	RI	0	$\neq 0$	0.66(11)
JLQCD-W[107]	Wilson	∞	WI	0	N.A.	0.562(64)
GBS[76]	Wilson	6.0	PT	$\neq 0$	$\neq 0$	0.74(4)(5)
JLQCD-S[111]	Staggered	∞	PT	N.A.	N.A.	0.628(42)

and the recoil variables in investigating the chiral behaviour of $\langle \bar{P}^0 | \mathcal{O}^{\Delta S=2} | P^0 \rangle$, and this is a result at $\beta = 6.0$. We have tried to use the same parameterisations for the mass and the recoil variables as Gupta has used to perform the analysis of B_K. In this way, we find:

1. At $\beta = 6.0$, our result is compatible with the one from Gupta.

2. At $\beta = 6.2$, the result is almost indistinguishable from the one we obtain by using X and Y to parameterise the mass and the recoil variables, *i.e.*, the one presented in table 4.2.

Therefore, we conclude that the result of B_K at $\beta = 6.0$ depends on how we parameterise the mass and the recoil variables, while the one at $\beta = 6.2$ does not.

We compare our results for $B_{7,8}^{3/2}$ with other recent lattice calculations in table 4.3. Our results seem to be compatible with the ones from GBS. However, a word of caution must be added that GBS do not seem to present the results for $B_{7,8}^{3/2}$

in the chiral limit[15]. As can be seen in table 4.3, our results for $B_{7,8}^{3/2}$ are lower than the ones from Roma. A possible reason for this is that Roma investigate the chiral behaviour of $B_{7,8}^{3/2}$ using the relations

$$R_7^{3/2} = \alpha_7 + \beta_7 X + \gamma_7 Y, \tag{4.128}$$

$$R_8^{3/2} = \alpha_8 + \beta_8 X + \gamma_8 Y, \tag{4.129}$$

where $R_7^{3/2}$, $R_8^{3/2}$, X and Y are the same as those defined in equations (4.97), (4.98), (4.99) and (4.100). They then identify $\alpha_{7,8}$ as $B_{7,8}^{3/2}$. This analysis is different from what we do, as we drop Y but include X^2 in studying the chiral behaviour of $B_{7,8}^{3/2}$ (*c.f.*, equations (4.119) (4.120)), and we observe that the $\mathcal{O}(p^4)$ term X^2 results in significant negative curvatures in the chiral extrapolations for $R_{7,8}^{3/2}$ (figure 4.12)[16].

Table 4.3: Comparison of our results of $B_{7,8}^{3/2}$ with other recent lattice calculations at the renormalisation scale $\mu = 2$ GeV, in the NDR-$\overline{\rm MS}$ scheme. The results from Roma and GBS are calculated at $\beta = 6.0$.

Authors	$c_{\rm SW}$	β	Matching	$B_7^{3/2}$	$B_8^{3/2}$
This Work	$1/u_0^3$	6.2	PT	0.58^{+5+2}_{-4-8}	0.80^{+8+1}_{-8-4}
Roma[105]	1	6.0	RI	0.72(5)	1.03(3)
GBS[76]	0	6.0	PT	$0.58(2)^{+7}_{-3}$	$0.81(3)^{+3}_{-2}$

[15] These authors do not write clearly how they obtain their results for $B_{7,8}^{3/2}$ in their paper [76].

[16] Roma do not show the plots of the chiral extrapolations for $R_{7,8}^{3/2}$ in their paper [105].

Chapter 5

Conclusion and Outlook

In this work, we have investigated long-distance strong-interaction effects in some FCNC weak-interaction processes which can be described by four-quark operators when energy is much smaller than M_W. We have looked at the matrix elements for B^0–$\bar{B}^0$ mixing, K^0–$\bar{K}^0$ mixing and the $\Delta I = 3/2$ part of the EM-penguin-operator contributions to $K \to \pi\pi$ decays. Apart from quenching, the main sources of systematic errors we have observed are:

1. Large discretisation errors in Lattice calculations of systems with heavy quarks involved. This causes especially large systematic errors in our results of heavy-light pseudo-scalar decay constants.

2. The matching between the lattice and the NDR-$\overline{\mathrm{MS}}$ scheme using one-loop perturbation theory. This results in significant uncertainties of $B_{7,8}^{3/2}$ due to the strong dependence on the matching scale.

Discretisation errors might be greatly reduced in the end, by the increasing computing power lattice theorists have access to and by more and more efficient algorithms used in the simulations. It might also be systematically controlled through the investigations of more-improved actions. The errors in the one-loop matching forbids us from performing high-precision calculations for some matrix elements (*e.g.*, $B_{7,8}^{3/2}$)[1], although they seem to be quite well controlled for certain matrix elements (*e.g.*, B_B and B_K), at least when the lattice spacing is small enough. Methods for performing non-perturbative renormalisation have been proposed [47, 107] and some studies of weak hadronic matrix elements using these methods have been performed over the last few years. This might allow us to extract more reliable information from lattice calculations, although there might be large discretisation errors in the renormalisation constants determined by these methods.

Apart from the processes we have examined in this work, there are many other interesting weak-interaction processes described by four-quark operators which deserve extensive investigations. For instance:

1. Hadronic B-meson decays, which are contributions from penguin operators involving b quarks. These processes also allow us to search for signals of direct CP violation.
2. $\Delta I = 1/2$ amplitudes of $K \to \pi\pi$ decays. This is essential in the theoretical calculation of ϵ'.
3. FCNC processes in supersymmetry-extended Standard Models.

Since the earliest attempts of calculating the four-quark-operator matrix elements in the Standard Model using lattice QCD [112, 113], there have been problems of subtracting divergences arising from mixing with lower-dimension operators. 'The classical example' is the attempt of understanding the $\Delta I = 1/2$ rule. Recently, a new approach [88, 114] to resolving this difficulty has been proposed. This proposal is based upon the observation that the amplitudes of the decay or mixing processes with four quarks involved are finite in the full Standard Model. One obtains divergences only after integrating out the W boson to obtain the four-quark operators. That is, these divergences only arise from the contact terms. For instance, in dealing with the amplitude of a lowest-order weak-interaction process:

---

[1] $B_{7,8}^{3/2}$ also have a 20% uncertainty in this work, because we perform the calculations in the chiral limit.

1. First of all, the amplitude in the full Standard Model has the expression

$$A \sim \frac{g_2^2}{2} \int d^4x D(x, M_W) \langle F|T \left[J_L^\mu(x) J_\mu^L(0) \right] |I\rangle, \tag{5.1}$$

where $D(x, M_W)$ is the W-boson propagator, J_L^μ is the left-handed hadronic weak current and T is time ordering. $\langle F|$ and $|I\rangle$ are final and initial states.

2. After performing the OPE, the two split hadronic currents can be represented as a series of local operators. Therefore, the matrix element in equation (5.1) can be written as

$$\langle F|T \left[J_L^\mu(x) J_\mu^L(0) \right] |I\rangle = \sum_i c_i(x, \mu) \langle F|\mathcal{O}^i(\mu)|I\rangle, \tag{5.2}$$

where $\mathcal{O}^i$ are operators of dimension six or higher, with i labels a series of operators arranged in terms of their dimensions. $c_i(x, \mu)$ are the Wilson coefficients which can be calculated perturbatively when renormalisation scale μ is large enough that perturbation theory works for QCD. The operators $\mathcal{O}^i(\mu)$ could be divergent, hence they depend upon the renormalisation scale μ. The μ dependence in $c_i(x, \mu)$ must cancel the one in $\mathcal{O}^i(\mu)$. As we can see, the divergences in the contact terms arise at this step.

3. Define

$$C_i(\mu, M_W) = M_W^{d_i - 6} \int d^4x D^W(x, M_W) c_i(x, \mu), \tag{5.3}$$

where d_i is the dimension of the operator $\mathcal{O}^i(\mu)$ in equation (5.2), then the amplitude in equation (5.1) can be written as

$$A \sim \frac{G_F}{2} \sum_i C_i(\mu, M_W) M_W^{6-d_i} \langle F|\mathcal{O}^i(\mu)|I\rangle, \tag{5.4}$$

which is what is usually written in the literature.

Traditionally, one keeps the contribution from the lowest-dimension operator ($i = 1$), calculates $C_1(\mu, M_W)$ perturbatively, and extract $\langle F|\mathcal{O}^1(\mu)|I\rangle$ from some non-perturbative calculation (*e.g.*, Lattice QCD). This is the strategy we have been using in this work. However, instead of calculating the amplitude after the OPE is performed, one could also calculate the hadronic matrix elements $\langle F|T \left[J_L^\mu(x) J_\mu^L(0) \right] |I\rangle$ on the lattice with respect to different values of x restricted in the range $a \ll |x| \ll \Lambda_{\mathrm{QCD}}^{-1}$. One can then fit the matrix elements $\langle F|\mathcal{O}^i(\mu)|I\rangle$ using equation (5.2) and the functional form of $c_i(x,\mu)$ obtained from perturbation theory. In this way, the matrix elements of four-quark operators can be extracted without performing large subtractions in the renormalisation procedure, hence one does not have to be concerned with divergences arising on the lattice from mixing with lower-dimension operators at all. The μ dependence of $\langle F|\mathcal{O}^i(\mu)|I\rangle$ is simply obtained from the one of $c_i(x,\mu)$. Since this method deals directly with the matrix element of split hadronic currents on the left-hand side of equation (5.2), it is called 'OPE without OPE' [114].

Although this procedure contains systematic errors of $\mathcal{O}(|x|^2\Lambda_{\mathrm{QCD}}^2)$, which is the difference between the left-hand side and the right-hand side of equation (5.2) and might be big, it offers a possible way of avoiding large systematic errors arising from the operator matching between the lattice and the continuum scheme in calculating matrix elements of four-quark operators. Hopefully, with this newly developed technique and the improvement in other aspects of lattice calculations (including more powerful machines, more efficient algorithms and other advances in lattice field theory), we will be able to control the strong-interaction effects in the weak-interaction processes such that we can gain further understanding of the Standard Model and possible new physics beyond it.

Bibliography

[1] C.M. Maynard, PhD thesis, University of Edinburgh, 1998.

[2] B.Joó, private communications.

[3] C.-L. Wu, PhD thesis, University of Edinburgh, 1993.

[4] A.-L. Shiau, PhD thesis, University of Edinburgh, 1993.

[5] A.-L. Shiau, H.-M. Yang, P. Wu and C.-L. Wu, Gene Therapy **5**, 1571 (1998).

[6] A. Buras, lectures given at 1997 Les Houches summer school, to appear in 'Probing the Standard Model of Particle Interactions', F. David and R. Gupta, eds, Elsevier Science B.V., hep-ph/9806471.

[7] C.T. Sachrajda, lectures given at the 1997 European School of High-Energy Physics, Menstrup, Denmark, 15 May - 7 June 1997, to be published in the proceedings, hep-ph/9801343.

[8] J. F. Donoghue, E. Golowich, and B. R. Holstein, *Dynamics of the Standard Model* (Cambridge University Press, Cambridge, 1992).

[9] T.-P. Cheng and L.-F. Li, *Gauge Theory of Elementary Particle Physics* (Clarendon Press, Oxford, 1984).

[10] N. Cabibbo, Phys. Lett. **10**, 531 (1963).

[11] M. Kobayashi and K. Maskawa, Prog. Theor. Phys **49**, 652 (1973).

[12] L. Wolfenstein, Phys. Rev. Lett. **51**, 1945 (1983).

[13] A. Buras, M. Lautenbacher and G. Ostermaier, Phys. Rev. D **50**, 3433 (1994).

[14] M. Schmidtler and K. Schubert, Z. Phys. **C 53**, 347 (1992).

[15] S. Glashow, J. Iliopoulos and L. Maiani, Phys. Rev. D **2**, 1285 (1970).

[16] T. Inami and C. S. Lim, Prog. Theor. Phys **65**, 297 (1981), ibid **65** (1981) 1772.

[17] P. Gambino, A. Kwiatkowski and N. Pott, hep-ph/9810400.

[18] G. Buchalla and A. Buras, Phys. Rev. D **57**, 216 (1998).

[19] G. Buchalla, A. Buras and M. Lautenbacher, Rev. Mod. Phys. **68**, 1125 (1996).

[20] M. Lüscher, Commun. Math. Phys. **104**, 177 (1986).

[21] I. Montvay and G. Münster, *Quantum Fields on a Lattice* (Cambridge University Press, Cambridge, 1994).

[22] K. G. Wilson, Phys. Rev. D **10**, 2445 (1974).

[23] H. B. Nielsen and M. Ninomiya, Nucl. Phys. B **185**, 20 (1981).

[24] L. H. Karsten and J. Smit, Nucl. Phys. B **183**, 103 (1981).

[25] K. G. Wilson, in *New Phenomena in Subnuclear Physics*, edited by A. Zichichi (Plenum, New York, 1975).

[26] A. Gonzalez Arroyo, G. Martinelli and F.J. Yndurain, Phys. Lett. **B 117**, 437 (1982).

[27] M. Bochicchio, L. Maiani, G. Martinelli, G. Rossi and M. Testa, Nucl. Phys. B **262**, 331 (1985).

[28] J. Kogut and L. Susskind, Phys. Rev. D **11**, 395 (1975).

[29] D. Kaplan, Phys. Lett. **B288**, 342 (1992).

[30] T. Blum, Plenary talk at LATTICE98, hep-lat/9810017.

[31] M. Lüscher, Phys. Lett. **B 428**, 342 (1998).

[32] H. Neuberger, Phys. Lett. **B 417**, 141 (1998).

[33] H. Neuberger, Phys. Lett. **B 427**, 353 (1998).

[34] P.H. Ginsparg and K.G. Wilson, Phys. Rev. D **25**, 2649 (1982).

[35] B.Efron, *The Jacknife, the Bootstrap and other Resampling Plans* (Soc. for Industrial and Applied mathematics, 1982).

[36] S. Duane, A.D. Kennedy, B.J. Pendleton and D. Roweth, Phys. Lett. **195B**, 216 (1987).

[37] S. Gusken, Phys. Lett. B **227**, 266 (1989).

[38] P. Lacock, A. McKerrel, C. Michael, I.M. Stopher and P.W. Stephenson, Phys. Rev. D **51**, 5403 (1995).

[39] K. Symanzik, Nucl. Phys. B **226**, 187 (1983).

[40] M. Lüscher, S. Sint, R. Sommer, and P. Weisz, Nucl. Phys. B **478**, 365 (1996).

[41] S. Weinberg, Physica **96 A**, 327 (1979).

[42] A. Pich, lectures given at 1997 Les Houches summer school, to appear in 'Probing the Standard Model of Particle Interactions', F. David and R. Gupta, eds., Elsevier Science B.V., hep-ph/9806303.

[43] B. Sheikholeslami and R. Wohlert, Nucl. Phys. B **259**, 572 (1985).

[44] G. Heatlie *et al.*, Nucl. Phys. B **352**, 266 (1991).

[45] A. El-Khadra, A. Kronfeld and P. Mackenzie, Phys. Rev. D **55**, 3933 (1997).

[46] E. Gabrielli, G. Heatlie, G. Martinelli, C. Pittori and C.T. Sachrajda, Nucl. Phys. B **362**, 475 (1991).

[47] G. Martinelli, C. Pittori, C.T. Sachrajda, M. Testa and A. Vladikas, Nucl. Phys. B **445**, 81 (1995).

[48] G. Lepage and P. Mackenzie, Phys. Rev. D **48**, 2250 (1992).

[49] A.F. Falk, M. Neubert and M.E. Luke, Nucl. Phys. B **388**, 363 (1992).

[50] M. Luke, A.V. Manohar and M.J. Savage, Phys. Rev. D **51**, 4924 (1995).

[51] M. Neubert and C.T.Sachrajda, Nucl. Phys. B **438**, 235 (1995).

[52] G. Martinelli and C.T.Sachrajda, Phys. Lett. **B354**, 423 (1995).

[53] G. Martinelli, M. Neubert and C.T.Sachrajda, Nucl. Phys. B **461**, 238 (1996).

[54] J. Gasser and H. Leutwyler, Nucl. Phys. B **250**, 465 (1985).

[55] M. Knecht and J. Stern, Contribution to the second edition of the DaΦne Physics Handbook, L. Maiani, G. Pancheri and N. Paver, eds., INFN, Frascati.

[56] M. Gell-Mann, R.J. Oakes and B. Renner, Phys. Rev. **175**, 2195 (1968).

[57] E. Witten, Nucl. Phys. B **223**, 422 (1983).

[58] C. Bernard, T. Draper, H.D. Politzer, A. Soni and M.B. Wise, Phys. Rev. D **32**, 2343 (1985).

[59] C. Bernard, T. Draper, G.Hockney and A. Soni, Phys. Rev. D **38**, 3540 (1988).

[60] A. Abada *et al.*, ELC Collaboration, Nucl. Phys. B **376**, 172 (1992).

[61] S. Aoki *et al.*, JLQCD Collaboration, Nucl. Phys. B (Proc. Suppl.) **47**, 433 (1996).

[62] C. Bernard, T. Blum and A. Soni, Phys. Rev. D **58**, 014501 (1998).

[63] A.K. Ewing *et al.*, UKQCD Collaboration, Phys. Rev. D **54**, 3526 (1996).

[64] V. Giménez and G. Martinelli, Phys. Lett. **B 398**, 135 (1997).

[65] J. Christensen, T. Draper and C. McNeile, Phys. Rev. D **56**, 6993 (1997).

[66] J.M. Flynn and C.T. Sachrajda, To appear in Heavy Flavours (2nd edition) edited by A J Buras and M Lindner (World Scientific, Singapore), hep-lat/9710057.

[67] J.M. Flynn, O.F. Hernández and B.R. Hill, Phys. Rev. D **43**, 3709 (1991).

[68] A. J. Buras, M. Jamin, and P. H. Weisz, Nucl. Phys. B **347**, 491 (1990).

[69] M.K. Gaillard and B.W. Lee, Phys. Rev. D **10**, 897 (1974).

[70] M. Creutz, Phys. Rev. D **36**, 2394 (1987).

[71] F.R. Brown and T.J. Woch, Phys. Rev. Lett. **58**, 163 (1987).

[72] N. Cabibbo and E. Marinari, Phys. Lett. **B 119**, 387 (1982).

[73] S. Pickles, PhD thesis, University of Edinburgh, 1998.

[74] G. Martinelli, Phys. Lett. **141B**, 395 (1984).

[75] R. Frezzotti, E. Gabrielli, C. Pittori and G.C. Rossi, Nucl. Phys. B **373**, 781 (1991).

[76] R. Gupta, T. Bhattacharya and S.R. Sharpe, Phys. Rev. D **55**, 4036 (1997).

[77] A. Billoire, Phys. Lett. **104B**, 472 (1981).

[78] W. Fischler, Nucl. Phys. B **129**, 157 (1977).

[79] A. Morel, J. Phys. **48**, 1111 (1987).

[80] C. Bernard and M. Golterman, Phys. Rev. D **46**, 853 (1992).

[81] P.A. Rowland, PhD thesis, University of Edinburgh, 1997.

[82] E. Jenkins, A.V. Manohar and M.B. Wisse, Phys. Rev. Lett. **75**, 2272 (1995).

[83] Particle Data Group, C. Caso *et al.*, The European Physical Journal **C3**, (1998).

[84] M. Lüscher and P. Weisz, Nucl. Phys. B **479**, 429 (1996).

[85] T. Draper, Plenary talk at LATTICE98, hep-lat/9810065.

[86] C. Bernard, J. Labrenz and A. Soni, Phys. Rev. D **49**, 2536 (1994).

[87] G.P. Lepage, Nucl. Phys. B (Proc. Suppl.) **26**, 45 (1992).

[88] C. Dawson, G. Martinelli, G.C. Rossi, C.T. Sachrajda, S. Sharpe, M. Talevi and M. Testa, Nucl. Phys. B **514**, 313 (1998).

[89] J.H. Christenson, J.W. Cronin, V.L. Fitch and R. Turlay, Phys. Rev. Lett. **13**, 128 (1964).

[90] G.D. Barr *et al.*, Phys. Lett. **B317**, 233 (1993).

[91] L.K. Gibbons *et al.*, Phys. Rev. Lett. **70**, 1203 (1993).

[92] S. Herrlich and U. Nierste, Nucl. Phys. B **419**, 292 (1994).

[93] S. Herrlich and U. Nierste, Nucl. Phys. B **476**, 27 (1996).

[94] A.J. Buras, M. Jamin and M.E. Lautenbacher, Nucl. Phys. B **408**, 209 (1993).

[95] M. Ciuchini, E. Franco, G. Martinelli, L. Reina and L. Silvestrini, Z. Phys. **C68**, 239 (1995).

[96] M. Shifman, A. Vainshtein and V. Zakharov, Nucl. Phys. B **120**, 316 (1977).

[97] J. Donoghue, E. Golowich, B. Holstein and N. Ponce, Phys. Rev. D **23**, 1213 (1981).

[98] J. Bijnens and M.B. Wise, Phys. Lett. **B 137**, 245 (1984).

[99] A.J. Buras, M. Jamin, M.E. Lautenbacher and P.H. Weisz, Nucl. Phys. B **400**, 37 (1993).

[100] A.J. Buras, M. Jamin and M.E. Lautenbacher, Nucl. Phys. B **400**, 75 (1993).

[101] C. Bernard, T. Draper, A. Soni, H.D. Politzer and M.B. Wise, Phys. Rev. D **23**, 2343 (1985).

[102] M.B. Gavela *et al.*, Nucl. Phys. B **306**, 677 (1988).

[103] E. Franco, L. Maiani, G. Martinelli and A. Morelli, Nucl. Phys. B **317**, 63 (1989).

[104] M. Crisafulli *et al.*, Phys. Lett. **B369**, 325 (1996).

[105] L. Conti *et al.*, Phys. Lett. **B421**, 273 (1998).

[106] C. Bernard and A. Soni, Nucl. Phys. B (Proc. Suppl.) **17**, 495 (1990).

[107] JLQCD Collaboration, S. Aoki *et. al*, Phys. Rev. Lett. **81**, 1778 (1998).

[108] A. Donini, G. Martinelli, C.T. Sachrajda, M. Talevi and A. Vladikas, Phys. Lett. **B360**, 83 (1995).

[109] JLQCD Collaboration, S. Aoki *et al.*, Nucl. Phys. B (Proc. Suppl.) **60A**, 67 (1998).

[110] R. Gupta, Parallel talk presented at LATTICE98.

[111] JLQCD Collaboration, S. Aoki *et al.*, Phys. Rev. Lett. **80**, 5271 (1998).

[112] N. Cabibbo, G. Martinelli and R. Pentronzio, Nucl. Phys. B **244**, 381 (1984).

[113] R.C. Brower, M.B. Gavela, R. Gupta and G. Maturana, Phys. Rev. Lett. **53**, 1318 (1984).

[114] G. Martinelli, Plenary talk at LATTICE98, hep-lat/9810013.